POLITECNICO
MILANO 1863

SCUOLA DI INGEGNERIA INDUSTRIALE
E DELL'INFORMAZIONE

Integration of Galileo High Accuracy Service within ARAIM for enhanced navigation performance

Tesi di Laurea Magistrale in
Space Engineering - Ingegneria Spaziale

Author: **Joaquín González López-Cepero**

Student ID: 10769923
Advisor: Lorenzo Luini
Co-advisors: Omar García Crespillo
Academic Year: 2024-25

Abstract

Currently, Advanced Receiver Autonomous Integrity Monitoring (ARAIM) only plans to support air navigation up to LPV-200, mainly due to limitations imposed by the signal-in-space (SIS) errors. This work proposes a novel approach where the Galileo High Accuracy Service (HAS) is integrated within ARAIM, analyzing the potential benefits of using a more precise continuity Signal-In-Space error model. First, a sensitivity analysis is performed on ARAIM world-wide availability with respect to the main Integrity Support Message (ISM) parameters and HAS corrections accuracy. Secondly, using precise products from the International GNSS Service (IGS) as a reference, orbit and clock errors of broadcast and HAS-corrected ephemeris are characterized for GPS and Galileo constellations, obtaining an independent analysis of the expected performance for HAS in terms of ranging errors. From this analysis, a continuity error model is derived.

Finally, the proposed algorithm is tested with observation data from an experimental flight campaign, using ionospheric-free dual-frequency dual-constellation observations. The positioning error is analyzed as well as the key performance indicators of ARAIM, such as protection levels improvements. Results suggest that a reduction of vertical and horizontal protection levels between 5 and 10 % can be expected.

Additionally, a reduction of unavailability for LPV-200 navigation requirements of more than 50 % was found for the validation dataset. This indicates that the integration of Galileo HAS with ARAIM could be able to deliver an enhancement of performance for operations with strict requirements such as urban air mobility or civil aviation.

Keywords: GNSS, ARAIM, Galileo HAS, Signal-In-Space error, Air Navigation.

Abstract in lingua italiana

Attualmente, l'Advanced Receiver Autonomous Integrity Monitoring (ARAIM) prevede di supportare la navigazione aerea solo fino a LPV-200, principalmente a causa delle limitazioni imposte per gli errori Signal-In-Space (SIS). Questo lavoro propone un approccio innovativo che prevede l'integrazione del servizio di alta precisione (HAS) di Galileo in ARAIM, al fine di analizzare i potenziali benefici derivanti dall'utilizzo di un modello di continuità degli errori Signal-In-Space di maggiore precisione. In primo luogo, viene eseguita un'analisi di sensibilità sulla disponibilità mondiale di ARAIM rispetto ai principali parametri dell'Integrity Support Message (ISM) e all'accuratezza delle correzioni HAS. In seguito, utilizzando come riferimento i prodotti precisi dell'International GNSS Service (IGS), sono stati caratterizzati gli errori di orbita e di orologio delle effemeridi trasmesse e corrette dall'HAS per le costellazioni GPS e Galileo, al fine di ottenere un'analisi indipendente delle prestazioni previste per l'HAS in termini di errori di ranging. A partire da tale analisi è stato ricavato un modello di continuità.

Infine, l'algoritmo proposto è stato testato con i dati di osservazione di una campagna di volo sperimentale, utilizzando osservazioni Iono-Free a doppia frequenza e doppia costellazione. Vengono analizzati l'errore di posizionamento e gli indicatori di prestazione chiave di ARAIM, come i miglioramenti dei livelli di protezione. I risultati suggeriscono che ci si può aspettare una riduzione dei livelli di protezione verticale e orizzontale compresa tra il 5 e il 10%. Inoltre, per il set di dati di convalida è stata riscontrata una riduzione dell'indisponibilità per i requisiti di navigazione LPV-200 di oltre il 50%. Ciò indica che l'integrazione di Galileo HAS con ARAIM potrebbe migliorare le prestazioni per operazioni con requisiti rigorosi, come la mobilità aerea urbana o l'aviazione civile.

Parole chiave: GNSS, ARAIM, Galileo HAS, errore Signal-In-Space, Navigazione Aerea

This Master's Thesis has been developed by its author as a student at the Institute of Communications and Navigation of the German Aerospace Center (DLR).

A Pablo Sampalo Estrade.

Contents

1 | Introduction

1.1. Background

Global Navigation Satellite Systems (GNSS) have been used for air navigation for decades. In particular, the US Global Positioning System (GPS) has been used in commercial aviation since the 1990s, complementing radio navigation systems on the ground.

With the development of new GNSS constellations such as the European Galileo, as well as the improvement of GPS, there has been an enhancement on the performance of GNSS-based systems.

In particular, there is a special interest on the ability of GNSS systems to support civil aviation navigation requirements for global users that would reduce the need of ground infrastructures such as Instrumental Landing Systems (ILS) [1].

The main challenge that GNSS systems have to face is to assure the integrity of the positioning solutions in order to support safety critical operations in accordance to current operational requirements provided by entities such as the International Civil Aviation Administration (ICAO). In this context, several augmentation systems have been developed that enhance baseline GNSS performance to support such operations. An example of these systems are the Space Based Augmentation System (SBAS), Ground Based Augmentation System (GBAS) and Aircraft Based Augmentation System (ABAS).

While SBAS and GBAS both require additional infrastructure either on the ground or in space, ABAS is fully handled by the user by either including additional measurements (barometric, intertial, etc...) or the use of redundant GNSS information. Among ABAS, Receiver Autonomous Integrity Monitoring (RAIM) is widely used in aviation. This system is able to detect potential faults in the pseudorange measurements performed by users in order to guarantee the integrity of the positioning solution. Currently, RAIM is only used for lateral guidance [2].

In order to support vertical precision navigation, the Advanced RAIM (ARAIM) concept is currently being developed by the Working Group C of the EU-US cooperation of

Satellite Navigation [3]. This new system proposes a set of improvements to the legacy RAIM algorithm in order to support operations requiring vertical precision guidance. In particular, these include the use of dual-frequency dual-constellation measurements, as well as information from an Integrity Support Message (ISM).

On the other hand, Galileo High Accuracy Service (HAS) recently entered into service on 2023 [4], offering live code biases and orbit and satellite clock bias corrections globally, which aims to reduce the signal-in-space errors of the open service (OS) broadcast navigation messages for GPS and Galileo users.

Beyond its performance enhancements, Galileo HAS stands out due to its open and free accessibility. This commitment to open access encourages the development of a wider range of applications across various sectors such as aviation. Moreover, the dual-frequency nature of the HAS signals enables robust performance even in challenging environments and its interoperability between global navigation satellite systems (GPS + Galileo) provides more resilient and accurate positioning solutions worldwide.

1.2. Motivation and problem statement

ARAIM currently plans to support operations up to Localizer Performance for Vertical Guidance (LPV) 200 [3], mainly due to limitations imposed by the Signal-In-Space error of Galileo and GPS broadcast ephemeris and satellite clock corrections. In this context, it is interesting to explore whether Galileo High Accuracy Service could be integrated within the current baseline algorithm for ARAIM in order to improve the system performance, potentially enhancing current performance and enabling operations under more strict navigation requirements.

As a consequence, the following research questions arise

1. *Is it possible to integrate Galileo HAS into the baseline ARAIM algorithm?*
2. *What are the potential improvements provided by this novel approach?*

1.3. Objectives

In order to answer the research question proposed in Section 1.2, the following objectives are set for this work:

- Develop a modified ARAIM algorithm that integrates Galileo HAS corrections into the positioning solution.

- Investigate the potential performance improvements of the proposed system based on simulations of ARAIM with different continuity and integrity performances of the system.
- Perform an independent analysis of the performance of Galileo HAS in terms of orbit and satellite clock errors.
- Test the performance of the proposed algorithm in a real scenario using data collected from a experimental flight campaign.

1.4. Thesis outline

The thesis is organized as follows. Chapter 2 lays the fundamentals on GNSS navigation, error sources and the computation of a navigation solution. Chapter 3 offers an overview of current navigation requirements in the context of civil aviation, as well as a general description of ARAIM and its baseline algorithm. Chapter 4 provides a general description of Galileo High Accuracy Service, with special focus on its implementation from the point of view of the user and its expected performance.

Chapter 5 defines the proposed integration of Galileo HAS into ARAIM, with a description of the modified algorithm and its implementation. On Chapter 6 a sensibility analysis is performed based on ARAIM simulations, that provide information on the dependencies of the main performance indicators of ARAIM with the continuity and integrity error models that characterize GPS and Galileo constellations.

An assessment of the performance of Galileo and GPS open services (OSs) and HAS for 337 days of data is developed in Chapter 7. This aims to provide an independent characterization of the signal-in-space errors for both constellations, quantifying the performance of each spacecraft separately and estimating the parameters that characterize the updated continuity error model for Galileo HAS.

Finally, Chapter 8 provides a real scenario application of the proposed algorithm using observations obtained during a flight test. The results are compared against the baseline ARAIM solution in order to quantify the enhancements delivered and the potential viability of its future implementation.

2 | GNSS Navigation Fundamentals

2.1. General GNSS concepts

Global Navigation Satellite Systems (GNSS) provide positioning, navigation and timing capabilities (PNT) to its users with worldwide coverage. Since their establishment, GNSS have proven to be a strategic asset, as they have become essential across multiple sectors such as transportation, agriculture, defense, telecommunications, finances, etc. [5]

Currently, 4 different GNSS constellations are active including Galileo, GPS, Glonass and BeiDou. In spite of their particularities, all GNSS share certain characteristics in terms of system architecture and principle of operation. In this section, a general description of such characteristics is given.

2.1.1. High level GNSS architecture

At a system level, current Global Navigation Satellite Systems consist of three main elements: [6]

1. **Space segment**: It is composed of a constellation of satellites. Depending on the system, these are located on different orbital regimes: Medium Earth Orbit (MEO), Inclined Geo-Synchronous Orbit (IGSO) or Geostationary Orbit (GEO).

   Each satellite is associated with a certain orbital plane and slot inside the constellation. Satellites are the responsible for disseminating the navigation signal across different frequencies. This signal contains information about the satellite's position and time. The time is kept by onboard high precision atomic clocks, which are simultaneously monitored by the ground segment.

2. **Ground Segment**: It is the responsible for the operation of the system. The ground segment covers tasks ranging from mission control, constellation maintenance and navigation system control. It also generates the navigation messages and

monitors the health status of the satellites composing the constellation.

3. **User segment**: It is composed by the receivers that, based on the broadcast signals, compute Position, Navigation and Timing (PNT) solutions for a specific purpose.

Currently, four GNSS constellations are operational, whose characteristics are summarized on table 2.1.

	Galileo	GPS	GLONASS	BeiDou
Nominal #SV	30 (MEO)	24 (MEO)	24 (MEO)	27 (MEO), 5 (GEO), 3 (IGSO)
Origin	Europe	USA	Russia	China

Table 2.1: Summary of current operational Global Navigation Satellite Systems. [6]

2.1.2. Principle of operation

GNSS are based on the principle of trilateration for estimating the position of the user. They exploit ranging measurements with respect to a set of space vehicles (SVs) from one or more constellations, based on the Time of Arrival (ToA). [6]

In particular, GNSS signals are transmitted by the Spacecraft Vehicles (SVs) using specific carrier frequencies in the range of 1.1 to 1.6 GHz. The use of these frequencies minimizes atmospheric attenuation under regular weather conditions [6]. Additionally, the carrier is modulated with specific pseudorandom noise (PRN). This signal consists of a pseudorandom binary sequence of 1s and 0s that is repeated with a specific period. The objective of this modulation is two-fold:

1. It allows the receiver to uniquely identify each SV by storing local copies of the PRN associated to each one.
2. It is possible to compute an estimate of the travel time of the signal by means of the cross-correlation between the received signal and the locally-stored PRN.

2.1.3. Basic GNSS observables

Three main types of measurements can be obtained from GNSS signals that allow for the computation of the navigation solution

- **Pseudorange**: As indicated on Figure 2.1, the time delay Δt can be extracted from the received signal, exploiting the properties of the PRNs used in the carrier signal modulation. In particular, PRN codes are designed to be as orthogonal to each

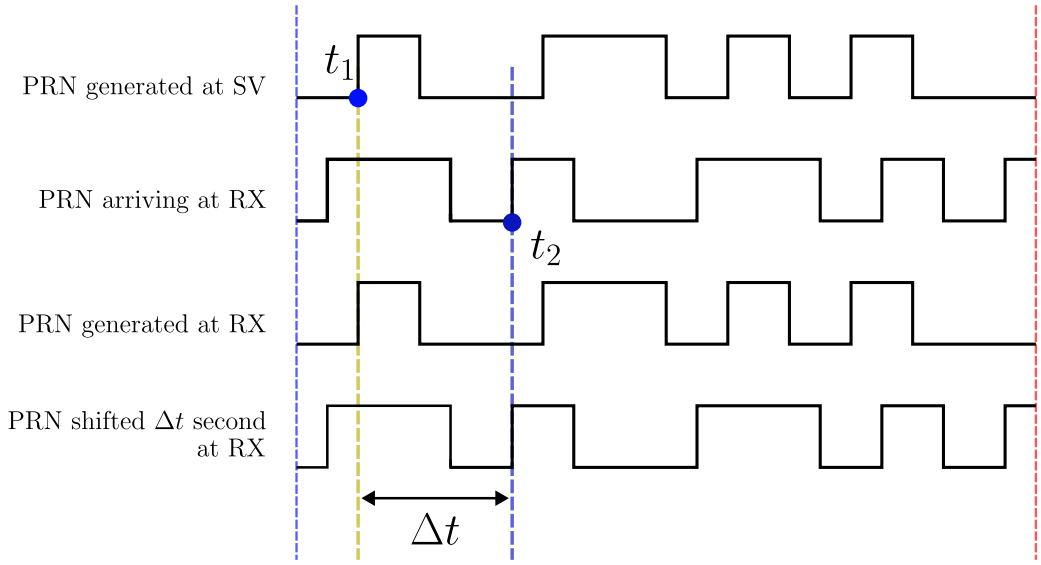

Figure 2.1: Schematic representation of the use of PRN code for estimating the travel time.

other as possible. As a consequence, a correlation peak is only found if a copy of the PRN code associated to the emitting SV is used with a delay equal to Δt. When multiplying this results by the speed of light, an "apparent" range (or pseudorange) is obtained $\rho = c\Delta t$.

This value contains the actual distance between the SV and the user, as well as other terms related with atmospheric delays, time system offsets, clock biases, instrumental and relativistic effects and multipath. The user should compensate for these effect to obtain an estimate of the actual range to the transmitting SV, in order to obtain an accurate positioning solution.

- **Carrier Phase**: It is possible to obtain measurements of the apparent distance between the user and the SV by tracking the phase of the carrier signal. Carrier phase measurements are about two order of magnitude more precise than pseudorange. However, they suffer from ambiguity. In general, they are ambiguous by an integer number of wavelengths ($N\lambda$, $\lambda \simeq 20$cm). Cycle slip occurs when there are unaccounted cycles without loss of track of a SV. Moreover, whenever the receiver loses lock on a satellite, the ambiguity changes arbitrarily once lock is recovered. [7]
- **Doppler shift:** By measuring the change in the receiving frequency, it is possible to estimate the time derivative of the range (i.e. range rate). In order to receive the GNSS signal, the receivers must properly estimate the Doppler shift. [7]

2.2. GNSS error sources

Ideally, by knowing with perfect accuracy the position of 4 given satellites and their clock bias with respect to a common time reference frame, it would be possible to compute the exact position of the user. However, as it was discussed in the previous section, there are a set of additional effects of different nature that modify the apparent range. For the purpose of this work, the following code ρ and carrier phase Φ measurement models are used

$$\rho = L + c(\delta t - \delta t^{SV}) + T + I + M_\rho + \delta_{rel} + \delta_{sagnac} + K^\rho_{RX} + K^\rho_{SV} + \epsilon_\rho \tag{2.1}$$

$$\Phi = L + c(\delta t - \delta t^{SV}) + T - I + M_\Phi + \delta_{rel} + \delta_{sagnac} + K^\Phi_{RX} - K^\Phi_{SV} + \epsilon_\Phi \tag{2.2}$$

where

- L is the range between RX and SV.
- δt, δt^{SV} are the receiver and satellite clock biases.
- T is the tropospheric delay.
- I is the ionospheric delay.
- M represents the effect of multipath.
- δ_{rel} represents the relativistic clock effect.
- K_{RX}, K_{SV} are the user and satellite instrumental delays.
- ϵ represents the receiver's noise, as well as the rest of unmodeled errors including solid tides, ocean loading, shapiro effect, etc.

Some of the aforementioned unmodeled errors are included only on Precise Point Positioning (PPP) algorithms, where centimeter-level accuracy is required in the position domain. In the following, a brief description is given regarding each of the terms.

SV and receiver clock biases

In general, the pseudorange ρ_i between the user and the i-th SV is estimated as

$$\rho_i = c(t_2^{RX} - t_1^{SV}) \tag{2.3}$$

where $c = 299792458$ m/s is the speed of light in vacuum, t_2^{RX} is the time of arrival of the signal to the receiver according to the receiver clock, and t_1^{SV} is the time of transmission according to the SV's atomic clock. This expression can be written as

$$\rho_i = c(t_2 - t_1) + c(\delta t - \delta t^{SV}) \tag{2.4}$$

where $t_2^{ST} - t_1^{ST}$ represents the actual travel time for the signal, and $\delta t - \delta t^{SV}$ represents the difference on time biases with respect to a common Time Reference System (e.g. Galileo System Time, GPS System Time, etc.) of the receiver and satellite clocks. δt^{SV} is generally monitored by the Control Segment, and clock corrections are periodically disseminated that allows the user to correct for the specific bias of each satellite. On the other hand, δt is a priori unknown. As a consequence, it is estimated together with the user position when computing the navigation solution. This means that users working with a single constellation require at least 4 satellites in view to obtain a PNT solution (3 position unknowns plus the receivers' clock bias).

Tropospheric delay

The troposphere is a non-dispersive media for typical GNSS signals. As a consequence, its effect on the propagation delay is not frequency dependent. In general, this effect depends on temperature, pressure and humidity along the travel path of the signal. It can be modeled as the integral of the refractivity N_{atm} along the path [6]

$$T = 10^{-6} \int_s N_{atm}\, ds \tag{2.5}$$

where the refractivity is defined as a function of air's refractive index n

$$N = 10^6(n - 1). \tag{2.6}$$

In general, refractivity is composed by a dry (i.e. due to *dry* gases) and wet (i.e. due to water vapor) components. The former is characterized by a more predictable behavior and errors of up to 2.5 meters in the zenithal direction. On the other hand, the wet component is much more complex to model and unpredictable. However, the error associated is in the order of a few decimeters.

Ionospheric delay

Ionospheric delay is a frequency-dependent delay caused by the electron content of the ionosphere. In particular, the total delay can be approximated as

$$I = \frac{81}{2f^2} \int_s N(s)\, ds \tag{2.7}$$

where f is the carrier frequency, and N is the electron content (e^-/m^3) along the propagation path. Without any corrections, it can take values of up to 5 meters [6].

As indicated by Eq. (2.7), this effect is frequency dependent. As a consequence, it is possible to compensate for this delay by exploiting measurements from different carrier frequencies. For instance, let ρ_1, ρ_2, Φ_1, Φ_2 be the code and phase measurements taken from frequencies f_1 and f_2 of a GNSS constellation, respectively. Then, the ionospheric-free combination of measurements for code and phase are given by

$$\rho_{IF} = \frac{f_1^2}{f_1^2 - f_2^2}\rho_1 - \frac{f_2^2}{f_1^2 - f_2^2}\rho_2, \tag{2.8}$$

$$\Phi_{IF} = \frac{f_1^2}{f_1^2 - f_2^2}\Phi_1 - \frac{f_2^2}{f_1^2 - f_2^2}\Phi_2. \tag{2.9}$$

These combinations mitigate up to 99% of the ionospheric error present on the original measurements. However, the noise level is magnified due to the combination of both signals and the frequency-dependent proportional factors. For mitigating this issue, a Hatch Filter [8] can be used, that smooths code measurements exploiting the information provided by the carrier phase.

Multipath

Multipath error is caused by the arrival of the very same signal to the receiver's antenna by following different paths. It is mainly caused due to reflections on structures in the neighborhood of the receiver. In general, multipath affects both phase and code measurements.

This effect has a high dependency on the satellite elevation. Additionally, it is generally complex to model, specially in applications such as railway positioning and urban navigation where it is common to have nearby structures producing multipath.

Many solutions have been proposed for dealing with multipath, such as map-based models

for railway applications [9] and the use of convolutional neural networks for multipath detection [10].

Relativistic clock correction

Due to the effect of gravitational potential and relative speed (general and special relativity, respectively), two identical clocks would measure a different rate of advance when one of them is placed in orbit around Earth while the other stays on land. This difference generates two effects

- A constant component that is compensated by an adjustment of the real SV's clock oscillating frequency.
- A periodic component due to orbital eccentricity. This correction must be accounted for by the user as

$$\delta_{rel} = -2\frac{(\mathbf{r}^{sat})^T \mathbf{v}^{sat}}{c^2}, \tag{2.10}$$

  where $\mathbf{r}^{sat}$ and $\mathbf{v}^{sat}$ are the SV's position and velocity in an inertial system.

Instrumental delays and receiver noise

Instrumental delays are introduced by the processing that takes place on the satellite and user sides. For the dual-frequency ionospheric free combination of codes, SV's instrumental delays are cancelled out. For single-frequency users, appropiate correction terms are broadcasted in the navigation message (Time Group Delay - TGD for GPS, and Broadcast Group Delays - BGD for Galileo) [11]. On the other hand, receiver instrumental delays are generally absorbed by the receiver clock bias obtained from the navigation solution (as it is common to all measurements). Finally, receiver noise can be modeled as a white Gaussian noise, that can be smoothed by means of a low pass filter.

2.3. Single Point Positioning Navigation Solution

In order to estimate the navigation solution at a given epoch based on a set of measurements obtained at that very same epoch, a Single Point Positioning (SPP) algorithm can be implemented. SPP relies on the instantaneous measurements retrieved by the receiver, without using any previous information about the state of the user.

The use of a receiver capable of obtaining measurements from two (or, more) constellations greatly improves the number of measurements available at any given epoch, generally improving the geometry. Additionally, certain techniques, such as Advance Receiver Au-

tonomous Integrity Monitoring (ARAIM), rely on dual constellation measurements to guarantee a better integrity performance.

By applying Eq. (2.8) to single frequency measurements, the ionospheric free pseudorange measurement from satellite i of constellation j are obtained

$$\rho_i^j = L^{i,j} + c(\delta t^j - \delta t_{SV,i}^j) + T + M + \delta_{rel,i}^j + \boldsymbol{\epsilon}. \tag{2.11}$$

Let $\mathbf{x}$ be a vector of N_j ionospheric free pseudorange measurements corresponding to constellation j, $\tilde{\rho}_i^j$,

$$\tilde{\rho}_i^j = \rho_i^j - (-c\delta t_{SV,i}^j + T + I + \delta_{rel}) = \rho_i^j - D_i^j, \tag{2.12}$$

which can be written as

$$\tilde{\rho}_i^j = \rho_i^j - D_i^j \simeq \left((\mathbf{x}_u - \mathbf{x}_{sat,i})^T(\mathbf{x}_u - \mathbf{x}_{sat,i})\right)^{1/2} + c\delta t^j + \epsilon_i^j \quad i = 1, \ldots, N_j. \tag{2.13}$$

Where ϵ_i^j represents the receiver noise, as well as all other error sources affecting the pseudorange measurement from SV i of constellation j. This expression already includes corrections for satellite clock bias $c\delta t_j^{SV,i}$, relativistic effects $\delta_{rel,i}^j$ and tropospheric delay T. Let $\mathbf{x}_u = [x_u, y_u, z_u]^T$ and $\mathbf{x}_{s,j}^i = [x_{s,j}^i, y_{s,j}^i, z_{s,j}^i]^T$ be the coordinates of the user and the i-th satellite of constellation j referred to the Earth-Centered Earth-Fixed (ECEF) frame of reference, respectively. The equation that relates the range measurements of each constellation j with $\mathbf{x}_{s,i}^j$ and $\mathbf{x}_u$ is given by

$$\tilde{\rho}_i = \rho_i - D_i \simeq \left((\mathbf{X} - \mathbf{x}_{s,i}^j)^T(\mathbf{X} - \mathbf{x}_{s,i}^j)\right)^{1/2} + c\delta t^j + \epsilon_i^j \quad i = 1, \ldots, N_j. \tag{2.14}$$

It is important to notice that, as there are two constellations, it is necessary to take into account the clock bias of the receiver with respect to the system time reference associated to each of them, δt^1 and δt^2.

This constitutes a system of $N_1 + N_2$ non-linear equations on the variables $\{x_u, y_u, z_u,$ $c\delta t^1$,$c\delta t^2\}$. By linearizing the system around a point $\mathbf{x}_0 = [x_0, y_0, z_0]$, characterized by a distance to the i-th SV of constellation j, $L_0^{i,j}$, the system can be written as a linear system of equations

$$\begin{bmatrix} \tilde{\rho}_1^1 - L_0^{1,1} \\ \vdots \\ \tilde{\rho}_{N_1}^1 - L_0^{N_1,1} \\ \vdots \\ \tilde{\rho}_1^2 - L_0^{1,2} \\ \vdots \\ \tilde{\rho}_{N_2}^2 - L_0^{N_2,2} \end{bmatrix} = \begin{bmatrix} \frac{x_0 - x_1^{s,1}}{L_0^{1,1}} & \frac{y_0 - y_1^{s,1}}{L_0^{1,1}} & \frac{z_0 - z_{s,1}^1}{L_0^{1,1}} & 1 & 0 \\ \vdots & \vdots & \vdots & \vdots & \vdots \\ \frac{x_0 - x_{s,1}^{N_1}}{L_0^{N_1,1}} & \frac{y_0 - y_{s,1}^{N_1}}{L_0^{N_1,1}} & \frac{z_0 - z_{s,1}^{N_1}}{L_0^{N_1,1}} & 1 & 0 \\ \frac{x_0 - x_{s,2}^1}{L_0^{1,2}} & \frac{y_0 - y_{s,2}^1}{L_0^{1,2}} & \frac{z_0 - z_{s,2}^1}{L_0^{1,2}} & 0 & 1 \\ \vdots & \vdots & \vdots & \vdots & \vdots \\ \frac{x_0 - x_{s,2}^{N_2}}{L_0^{N_2,2}} & \frac{y_0 - y_{s,2}^{N_2}}{L_0^{N_2,2}} & \frac{z_0 - z_{s,2}^{N_2}}{L_0^{N_2,2}} & 0 & 1 \end{bmatrix} \begin{bmatrix} dx \\ dy \\ dz \\ c\delta t^1 \\ c\delta t^2 \end{bmatrix} + \boldsymbol{\epsilon}, \tag{2.15}$$

which is an over-determined system for $N > 5$. The vector of receiver noise and unmodelled effects is normally assumed to have a certain mean and covariance matrix

$$\boldsymbol{\mu} = E\left[\boldsymbol{\epsilon}\right], \quad \boldsymbol{R} = E\left[\boldsymbol{\epsilon}^T \boldsymbol{\epsilon}\right]. \tag{2.16}$$

The error term $\boldsymbol{\epsilon}$ on Eq. (2.15) leads to an inconsistent system. An appropriate solution strategy would be to compute a Weighted Least Squares (WLS) solution, as discussed on Section 2.3. However, other approaches might be used. Once a solution is obtained, the user position is estimated as

$$\mathbf{x}_u = \mathbf{x}_0 + \begin{bmatrix} dx \\ dy \\ dz \end{bmatrix}. \tag{2.17}$$

The problem described by Eq. (2.15) can be written in compact form as

$$\mathbf{y} = \mathbf{G}\mathbf{x} + \boldsymbol{\epsilon}, \tag{2.18}$$

where $\mathbf{G}$ is generally known as the Geometry Matrix, as it only depends on the constellation(s) geometry with respect to the user. Due to the error term $\boldsymbol{\epsilon}$, Eq. (2.18) is an inconsistent system. As a consequence, the problem reduces to finding $\hat{\mathbf{x}}$ that minimizes the discrepancy between the measurements and $\mathbf{G}\hat{\mathbf{x}}$ (i.e. provides the "best fit" to the measurements based on a given geometry $\mathbf{G}$).

In particular, since in general not all satellites or constellations are affected by the same error (due to geometry, characteristics, faults, etc.), its interesting to add a symmetric semi-positive definite weighting matrix $\mathbf{W}$ that penalizes those measurements character-

ized by larger errors.

Equation (2.18) transforms in a minimization problem on the variable $\hat{\mathbf{x}}$,

$$\min_{\hat{\mathbf{y}}} ||\mathbf{y} - \hat{\mathbf{y}}||_W^2 = \min_{\hat{\mathbf{y}}} (\mathbf{y} - \hat{\mathbf{y}})^T \mathbf{W} (\mathbf{y} - \hat{\mathbf{y}}) \quad \text{with } \hat{\mathbf{y}} = \mathbf{G}\hat{\mathbf{x}}. \tag{2.19}$$

In the case where $\mathbf{W} = \mathbf{I}_{N_1+N_2}$, the problem would be reduced to

$$\min_{\hat{\mathbf{y}}} ||\mathbf{y} - \hat{\mathbf{y}}||^2 = \min_{\hat{\mathbf{y}}} \left[\sum_{j=1}^{j=2} \sum_{i=1}^{i=N_j} \left(y^{i,j} - \hat{y}^{i,j} \right)^2 \right]. \tag{2.20}$$

The solution of Eq. (2.19) is given by [11]

$$\hat{\mathbf{x}} = \left(\mathbf{G}^T \mathbf{W} \mathbf{G} \right)^{-1} \mathbf{G}^T \mathbf{W} \mathbf{y}. \tag{2.21}$$

By using Eq. (2.18) and Eq. (2.21), an estimate on the error is obtained [11]

$$\hat{\mathbf{x}} - \mathbf{x} = \left(\mathbf{G}^T \mathbf{W} \mathbf{G} \right)^{-1} \mathbf{G}^T \mathbf{W} \boldsymbol{\epsilon}. \tag{2.22}$$

Furthermore, assuming that $\boldsymbol{\epsilon}$ is characterized by a mean $\boldsymbol{\mu}_\epsilon = 0$ and covariance $\mathbf{R}_\epsilon$, the mean $\boldsymbol{\mu}$ and covariance matrix $\mathbf{P}$ characterizing the solution are given by

$$\begin{aligned} \boldsymbol{\mu} &= E\left[\hat{\mathbf{x}} - \mathbf{x}\right] = \left(\mathbf{G}^T \mathbf{W} \mathbf{G} \right)^{-1} \mathbf{G}^T \mathbf{W} \boldsymbol{\mu}_\epsilon = \mathbf{0}, \\ \boldsymbol{P} &= E\left[(\hat{\mathbf{x}} - \mathbf{x}) (\hat{\mathbf{x}} - \mathbf{x})^T \right] = \left(\mathbf{G}^T \mathbf{W} \mathbf{G} \right) \mathbf{G}^T \mathbf{W} \mathbf{R} \mathbf{W} \mathbf{G} \left(\mathbf{G}^T \mathbf{W} \mathbf{G} \right)^{-1}. \end{aligned} \tag{2.23}$$

If we assume uncorrelated errors with equal variance, $\mathbf{R} = \sigma^2 \mathbf{I}$, $\mathbf{P}$ is reduced to

$$\mathbf{P} = \sigma^2 \left(\mathbf{G}^T \mathbf{W} \mathbf{G} \right). \tag{2.24}$$

It can be proven that, by taking $\mathbf{W} = \mathbf{R}^{-1}$, the best Linear Unbiased Minimum Variance Estimator is obtained [12]. In general, the characterization of $\mathbf{R}$ is not trivial. As a consequence, it is normally assumed that the errors are uncorrelated across satellites and constellations, where $\mathbf{R}$ is a diagonal matrix whose diagonal elements are $\mathbf{R}_{kk} = \sigma_{ij}^2$, $k = 1 \ldots N_1 + N_2$. Each term represents the uncertainty associated to the different error sources affecting the range measurement from the i-th SV of constellation j.

3 | Navigation System Requirements and ARAIM fundamentals

When implementing GNSS-based navigation on safety-critical applications (i.e. Aircraft and railway positioning, urban air mobility, etc...) it is necessary to fulfill a series of navigation requirements in terms of accuracy, integrity, continuity and availability. For this purpose, several augmentation systems exist that provide a certain performance level according to its characteristics. These augmentation systems may rely on ground infrastructure, on space infrastructure or on additional logic on the receiver side. The latter is particularly interesting as it does not require any additional equipment as it solely relies on the information readily available for the user. The main example of this technique is the so-called (Advanced) Receiver Autonomous Integrity Monitoring - (A)RAIM.

On this chapter, a formal definition of each requirement is provided in the context of safety critical operations. Additionally, the ARAIM concept is defined, discussing its principle of operation and implementation on dual-frequency dual-constellation GNSS receivers.

3.1. Navigation Requirements

A definition for each of the aforementioned requirements is provided by the International Civil Aviation Organization (ICAO) on its Standards and Recommended Practices (SARPs) [13] and the 2008 US Federal Radionavigation Plan [14]:

- **Integrity:** *A measure of the trust that can be placed in the correctness of the information supplied by the total system. Integrity includes the ability of a system to provide timely and valid warnings to the user (alert).*
- **Continuity:** *The continuity of a system is the ability of the total system (comprising all elements necessary to maintain aircraft position within the defined airspace) to perform its function without interruption during the intended operation. More*

specifically, continuity is the probability that the specified system performance will be maintained for the duration of a phase of operation, presuming that the system was available at the beginning of that phase of operation.

- **Availability:** *The availability of a navigation system is the percentage of time that the services of the system are usable by the navigator. Availability is an indication of the ability of the system to provide usable service within the specified coverage area. Signal availability is the percentage of time that navigation signals transmitted from external sources are available for use. It is a function of both the physical characteristics of the environment and the technical capabilities of the transmitter facilities.*
- **Accuracy:** *the accuracy of an estimated or measured position of a craft (vehicle, aircraft, or vessel) at a given time is the degree of conformance of that position with the true position of the craft at that time. Since accuracy is a statistical measure of performance, a statement of navigation system accuracy is meaningless unless it includes a statement of the uncertainty in position that applies.*
- **Time-to-alert:** *The maximum allowable time elapsed from the onset of the navigation system being out of tolerance until the equipment enunciates the alert.*

3.1.1. Integrity risk and protection level definition

Depending on the type of operation, a determined alert limit (horizontal, HAL; or vertical, VAL) is provided with an associated integrity risk. The integrity risk (or probability of hazardous misleading information, P_{HMI}) is defined as the probability that, at any given instant, the positioning error along one dimension exceeds a certain alert limit [2]

$$P_{HMI} = P(|e| \geq AL), \tag{3.1}$$

where e is the error in a given dimension (horizontal, vertical) and AL is its associated alert limit (HAL, VAL). Given a certain integrity budget (i.e. the required maximum P_{HMI}), the user computes a set of protection levels (PLs) along each dimension. In particular, vertical and horizontal protection levels (VPL, HPL) define a cylinder centered at the real user position. The probability for the estimated position to be outside the volume defined by this cylinder is the associated integrity risk. Figure 3.1 shows a schematic representation of the concepts of alert limits and protection levels.

By definition, the protection levels are only a function of satellite and user geometry as

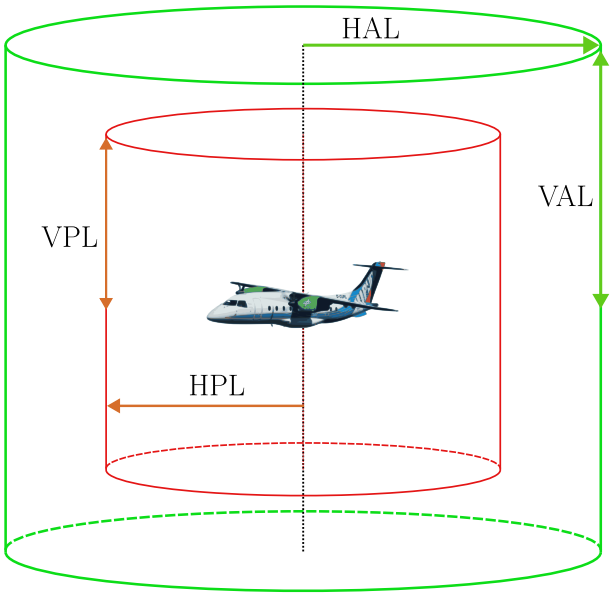

Figure 3.1: Concepts of Alert Limit (HAL, VAL) and Protection Level (HPL, VPL).

well as expected error characteristics. In principle, they do not depend directly on the value of specific measurements. However, PL can rely on the performance of a monitor that creates an indirect dependence with the measurements.

3.1.2. Navigation performance requirements for civil aviation

For civil aviation, navigation requirements are defined in terms of integrity (integrity risk and alert limits), accuracy, time to alert, continuity and availability. Table 3.1 provides a summary of the requirements organized per operation. It can be seen that there is no vertical requirement for cruise operations (Oceanic en-route, Continental en-route) nor Terminal and non-precission approach (NPA).

The minimum horizontal alert limit is 40 m, while the vertical alert limit is reduced down to 10 meters for autoland operations. Additionally, note that on final approach procedures, the integrity risk is provided per operation (and not per flight hour). For this purpose, on LPV-200 and CAT I (Autoland), a standardized operation time is provided of 150 seconds.

Operation	Accuracy (Horizontal, Vertical) (Equiv. 1-σ)	Integrity Risk	HAL, VAL	Time to Alert	Continuity Risk	Availability
Oceanic en-route	3.7 km, N/A	10^{-7}/h	7.4 km, N/A	5 min	10^{-4}/h to 10^{-8}/h	0.99 to 0.99999
Continental en-route	1.85 km, N/A	10^{-7}/h	3.7 km, N/A	5 min	10^{-4}/h to 10^{-8}/h	0.99 to 0.99999
Terminal	370 m, N/A	10^{-7}/h	1.85 km, N/A	15 s	10^{-4}/h to 10^{-8}/h	0.99 to 0.99999
NPA	110 m, N/A	10^{-7}/h	556 m, N/A	10 s	10^{-4}/h to 10^{-8}/h	0.99 to 0.99999
APV-I	8 m, 10 m	2×10^{-7}/ approach	40 m, 50 m	10 s	8×10^{-6}/ 15 s	0.99 to 0.99999
LPV-250	8 m, 2 m (1.87 m fault-free)	2×10^{-7}/ 150 s	40 m, 50 m	6 s	8×10^{-6}/ 15 s	0.99 to 0.99999
LPV-200	8 m, 2 m (1.87 m fault-free)	2×10^{-7}/ 150 s	40 m, 35 m	6 s	8×10^{-6}/ 15 s	0.99 to 0.99999
CAT I Autoland	8 m, 2 m	2×10^{-7}/ 150 s	40 m, 10 m	6 s	8×10^{-6}/ 15 s	0.99 to 0.99999

Table 3.1: Summary of current navigation performance requirements for aviation. Extracted from [2], based on [13, 15–17].

3.2. Advanced Receiver Autonomous Integrity Monitoring (ARAIM)

In order to guarantee the integrity requirements necessary for Safety-of-Life (SoL) applications (e.g. Table 3.1), GNSS require the implementation of so-called GNSS augmentation systems. These systems provide an enhancement of the positioning solution by exploiting redundant or additional information available to the user. In this way, it is possible to provide a guarantee of integrity together with the navigation solution.

There are 3 GNSS augmentation systems according to ICAO [13]

- Ground Based Augmentation System (GBAS),
- Satellite Based Augmentation System (SBAS),
- Aircraft Based Augmentation System (ABAS).

SBAS guarantees GNSS signal integrity using data broadcasted by geostationary satellites. On the other hand, GBAS exploits information provided by a network of ground stations in the vicinity of the airport location, allowing operations down to CAT I precision approach procedures (see table 3.1). Both systems provide differential corrections and integrity monitoring.[2].

Finally, ABAS exploit additional information onboard, without relying on any external infrastructure. In particular, Receiver Autonomous Integrity Monitoring (RAIM) provides an integrity layer by exploiting the redundancy of GNSS measurements.

Due to the requirement of additional infrastructure and its local and regional nature, GBAS and SBAS systems are not always ideal neither economically or operationally. In this context, RAIM evolved as a versatile technique that allows the computation of an integrity solution onboard anywhere around the globe.

RAIM algorithms perform two main tasks in order to provide integrity monitoring capabilities to the user

- **Fault detection and exclusion (FDE):** By exploiting redundant GNSS measurements, it aims to detect potential faults by performing statistical tests on the residuals of the least squares navigation solution. Additionally, it is possible to try to mitigate or avoid potential faults by excluding certain measurements from the navigation solution.
- **Protection Levels Computation:** RAIM computes, based on the satellite ge-

ometry and error characteristics, the Horizontal Protection Level (HPL) associated with the navigation solution.

Currently, RAIM is certified for its use on civil aviation for horizontal guidance [17]. With the commissioning of new GNSS constellations (e.g. Galileo), as well as the broadcast of navigation signals on multiple frequencies (e.g. L1/L5, E1/E5a), multiple-constellation users will benefit of better geometry and the ability of mitigating first order ionosphere error (see Section 2.2). [3]

In this context, Advanced RAIM (ARAIM) aims to exploit these improvements on GNSS systems. The objective of ARAIM is to provide, in a first phase, support down to RNP 0.1 non-precission approach based on Horizontal ARAIM (H-ARAIM) (see Table 3.1). In the future, ARAIM aims to support down to LPV-200 with Vertical ARAIM (V-ARAIM). [3]

ARAIM relies on information regarding the error and error model provided by an Integrity Support Message (ISM). This message will be broadcast using GNSS satellites. In particular, GPS will broadcast the integrity message via de CNAV Navigation Message (L2C & L5) and the CNAV2 message through L1C [18]. On the other hand, Galileo will broadcast the integrity data through the I/NAV navigation message via E5b-1 and E1-b signals. [19]

Additionally, the integrity data can be stored in the receivers' non-volatile memories or transmitted through existing aviation databases. [3]

3.2.1. ARAIM user algorithm

This section provides a brief description of the ARAIM user algorithm proposed by [3, 17]. ARAIM requires a set of input parameters in order to solve the navigation problem with FDE and PL computation. First, a set of standard deviations that characterize the Signal-In-Space error (SISE) error of each SV for integrity (User Range Accuracy, URA) and continuity (User Range Error, URE) purposes are provided by the ISM, which are obtained by analyzing historical system performance. The ISM also provides a nominal bias b_{nom} for each SV that characterizes its Signal-In-Space Range error (SISRE) distribution, together with the URA for integrity purposes. Finally, the a priori probabilities of satellite and constellation-wide fault, P_{sat} and P_{const}, are also provided by the ISM.

On the receiver side, ARAIM requires a set of iono-free pseudorange observations for each SV (after performing smoothing and implementing tropospheric corrections), as well as the number of satellites and constellations that are in view. ARAIM requires that any SV

used for the positioning solution must not have been flagged as unhealthy for a certain period T_{recov}. [3]

A summary of these parameters and their source can be found on Table 3.2. Currently, according to [3], there are only plans to support GPS+Galileo measurements within ARAIM. On the other hand, Table 3.3 provides a brief description of the constants used by the algorithm.

Inputs to the ARAIM user algorithm. [3, 17]

Name	Definition	Source
PR_i	Iono-Free pseudorange for SV i, after smoothing and tropospheric correction is performed.	RX
$\sigma_{URA,i}$	Standard deviation of Signal-In-Space error of SV i, used for integrity.	ISM
$\sigma_{URE,i}$	Standard deviation of Signal-In-Space error of SV i, used for continuity.	ISM
$b_{nom,i}$	Maximum nominal bias for satellite i used for integrity.	ISM
$P_{sat,i}$	Prior probability of fault in satellite i per approach.	ISM
$P_{const,j}$	Prior probability of a fault affecting more than one satellite in constellation j per approach.	ISM
$I_{const,j}$	Index of satellites belonging to constellation j.	RX
N_{sat}	Number of satellites.	RX
N_{const}	Number of constellations.	RX

Table 3.2: Input to the ARAIM user algorithm for receiver (RX) and Integrity Support Message (ISM) parameters.

ARAIM applies a FDE mechanism by implementing a Multiple Hypothesis Solution Separation (MHSS) test [20] that allows the user to detect potential faults in the measurements and attempt to exclude them. Then, if the FDE is passed,it estimates a set of Protection Levels (PLs). In particular, a set of fault modes is monitored (the number of monitored fault modes depend on the value of P_{TRESH} chosen). Each fault mode (k) corresponds to the failure of 1 or more measurements. As a consequence, a subset of non-faulty measurements is generated per fault-mode and tested against the all in view solution (0). The navigation problem is solved using a Weighted Least Square (see section 2.3) with weight matrix $\mathbf{W}$ equal to the inverse of the integrity covariance matrix $\mathbf{C}_{int}$

$$\mathbf{W} = \mathbf{C}_{int}^{-1} \tag{3.2}$$

where

Name	Definition
$PHMI$	Total integrity budget.
$PHMI_{VERT}$	Integrity budget for the vertical component.
$PHMI_{HOR}$	Integrity budget for the horizontal component.
P_{THRES}	Threshold for integrity risk coming from unmonitored faults.
P_{FA}	Continuity budget allocated to disruptions because of false alert.
$P_{FA,VERT}$	Continuity budget allocated to the vertical solution.
$P_{FA,HOR}$	Continuity budget allocated to the horizontal solution.
P_{FA,χ^2}	Continuity budget associated to the chi-squared test.
TOL_{PL}	Tolerance for solving protection levels equation.
K_{acc}	Inflation factor for accuracy.
K_{FF}	Inflation factor for the 1E-7 fault-free vertical position error.
P_{EMT}	Probability used for computing the EMT[1].
T_{RECOV}	Minimum time a previously excluded satellite remains out of the all-in-view solution.

[1] Effective Monitor Threshold.

Table 3.3: Definition of the constant parameters used on ARAIM. [3, 17]

$$\mathbf{C}_{int}(i,i) = \sigma^2_{URA,i} + \sigma^2_{tropo,i} + \sigma^2_{user,i}, \tag{3.3}$$

being $\sigma_{tropo,i}$ the residual tropospheric error, and $\sigma_{user,i}$ the nominal noise and multipath error. The error models used in ARAIM are discussed on Section 3.2.2. The estimator $\mathbf{S}$ for subset k is given by

$$\mathbf{S}^{(k)} = \left(\mathbf{G}^T_{ENU}\mathbf{W}^{(k)}\mathbf{G}_{ENU}\right)^{-1}\mathbf{G}^T_{ENU}\mathbf{W}^{(k)}. \tag{3.4}$$

where $\mathbf{G}_{ENU}$ is the geometry matrix in East, North, Up (ENU) coordinates.

Let $q = 1, 2, 3$ refer to East, North and Up components, respectively. The variances of the position solution for each subset k is given by [3]

$$\left(\sigma^{(k)}_q\right)^2 = \left(\mathbf{G}^T_{ENU}\mathbf{W}^{(k)}\mathbf{G}_{ENU}\right)^{-1}_{(q,q)}, \tag{3.5}$$

where the subindex denotes the element in position (q, q) of the matrix.

The nominal bias of the SiS error for each SV, $b_{nom,i}$, will affect the user depending on its projection into the positioning domain through the corresponding projection matrix

$\mathbf{S}^{(k)}$. It can be proven that the worse case impact on the position solution of the bias is provided by [17]

$$b_q^{(k)} = \sum_{i=1}^{N_{sat}} \left| \mathbf{S}_{q,i}^{(k)} \right| b_{nom,i}. \tag{3.6}$$

On the other hand, the variance of the difference between the fault-tolerant position $\hat{\mathbf{x}}^{(k)}$ and the all-in-view position $\hat{\mathbf{x}}^{(0)}$ is provided by

$$\left(\sigma_{ss,q}^{(k)}\right)^2 = \mathbf{e}_q^T \left(\mathbf{S}^{(k)} - \mathbf{S}^0\right) \mathbf{C}_{acc} \left(\mathbf{S}^{(k)} - \mathbf{S}^0\right)^T \mathbf{e}_q. \tag{3.7}$$

where the covariance matrix for accuracy purposes is given by

$$\mathbf{C}_{acc}(i,i) = \sigma_{URE,i}^2 + \sigma_{tropo,i}^2 + \sigma_{user,i}^2. \tag{3.8}$$

and $\mathbf{e}_q$ is the unit vector along direction q (North, East, Up).

Based on $\sigma_{ss,q}$, a threshold T is defined per coordinate q of each subset k as

$$T_{k,q} = K_{fa,q}\sigma_{ss,q}^{(k)}, \tag{3.9}$$

where

$$K_{fa,1} = K_{fa,2} = Q^{-1}\left(\frac{P_{FA,HOR}}{4N_{faultmodes}}\right), \quad K_{fa,3} = Q^{-1}\left(\frac{P_{FA,VERT}}{2N_{faultmodes}}\right), \tag{3.10}$$

and $Q^{-1}(p)$ is the $(1-p)$ quantile of a standard normal distribution. This threshold is used for evaluating each of the statistical tests, that depend on the difference between the q-th component of the fault-tolerant position $\hat{x}_q^{(k)}$ and the correspondant component of the all-in-view solution

$$|\hat{x}_q^{(k)} - \hat{x}_q^{(0)}| \leq T_{k,q}. \tag{3.11}$$

If any of these tests fail exclusion must be attempted based on the measurements excluded on subset (k).

Once the test is passed, ARAIM computes the horizontal and vertical protection levels. Let $p_{fault,k}$ be the a priori probability associated to each fault mode k based on the information of the ISM (see Table 3.2). Then, the horizontal and vertical protection

levels (HPL, VPL) can be computed by solving the following equations

$$2Q\left(\frac{VPL-b_3^{(0)}}{\sigma_3^{(0)}}\right)+\sum_{k=1}^{N_{Faultmodes}} p_{fault,k}Q\left(\frac{VPL-T_{k,3}-b_3^{(k)}}{\sigma_3^{(k)}}\right)= \\ =PHMI_{VERT}\left(1-\frac{P_{sat,not\ monitored}+P_{const,not\ monitored}}{PHMI_{VERT}+PHMI_{HOR}}\right), \tag{3.12}$$

$$2Q\left(\frac{HPL_q-b_q^{(0)}}{\sigma_q^{(0)}}\right)+\sum_{k=1}^{N_{Faultmodes}} p_{fault,k}Q\left(\frac{HPL_q-T_{k,q}-b_q^{(k)}}{\sigma_q^{(k)}}\right)= \\ =\frac{1}{2}PHMI_{HOR}\left(1-\frac{P_{sat,not\ monitored}+P_{const,not\ monitored}}{PHMI_{VERT}+PHMI_{HOR}}\right). \tag{3.13}$$

with $HPL=\sqrt{HPL_1^2+HPL_2^2}$. Note that in these expressions there is an indirect dependency on σ_{URE} through the threshold $T_{k,q}$. Additionally, $p_{sat,not\ monitored}$ and $p_{const,not\ monitored}$ correspond to the a priori probability associated to the fault modes that have not been included on any subset because the associated probability was below P_{THRES}.

In the navigation requirements of Table 3.1 there is also a limit in terms of accuracy of the navigation solution. For this purpose, the 95th percentile vertical accuracy measure is obtained as

$$\sigma_{acc,95\%}=K_{acc}\sqrt{\mathbf{e}_3^T\mathbf{S}^{(0)}\mathbf{C}_{acc}\left(\mathbf{S}^{(0)}\right)^T\mathbf{e}_3}, \tag{3.14}$$

where K_{acc} is an inflation factor equal to 1.96. Finally, the Effective Monitoring Threshold (EMT) is defined as the largest $T_{k,3}$ such that the a priori probability associated with its fault mode is above P_{EMT}:

$$EMT=\max_{p_k\geq P_{EMT}} T_{k,3}. \tag{3.15}$$

3.2.2. ARAIM error models

For computing the nominal values for σ_{tropo} and σ_{user}, specific error models are proposed on [17]. These models are the ones that ARAIM uses to account for residual tropospheric errors (after tropospheric corrections have been applied to the pseudorange measurements), as well as other effects such as receiver noise and multipath. These models are elevation-dependent, thus providing larger errors to those SV with lower elevation angles.

Galileo error model for σ_{user} is provided on Table 3.4. On the other hand, the GPS model

Elevation [°]	$\sigma^{Gal}_{n,user}$ $[m]$		Elevation [°]	$\sigma^{Gal}_{n,user}$ $[m]$
5°	0.4529		50°	0.2359
10°	0.3553		55°	0.2339
15°	0.3063		60°	0.2302
20°	0.2638		65°	0.2295
25°	0.2593		70°	0.2278
30°	0.2555		75°	0.2297
35°	0.2504		80°	0.2310
40°	0.2438		85°	0.2274
45°	0.2396		90°	0.2277

Table 3.4: Galileo Elevation-Dependent Signal-In-Space User Error for ARAIM. [17]

corresponds to the Airborne Accuracy Designator - Model A [21]

$$\begin{aligned} \sigma^{GPS}_{n,user} &= \sqrt{\frac{f_{L1}^4 + f_{L5}^4}{(f_{L1}^2 - f_{L5}^2)^2}} \sqrt{(\sigma_{MP})^2 + (\sigma_{Noise})^2} \\ \sigma_{MP}(\theta) &= 0.13 + 0.53 \exp\left(-\theta/10\right) \quad [m] \\ \sigma_{Noise}(\theta) &= 0.15 + 0.43 \exp\left(-\theta/6.9\right) \quad [m] \end{aligned} \tag{3.16}$$

where θ is the elevation angle in degrees. Finally, the nominal troposphere error is provided by

$$\sigma_{n,tropo}(\theta) = 0.12 \frac{1.001}{\sqrt{0.002001 + \left(\sin\left(\frac{\pi\theta}{180}\right)\right)}} \quad [m]. \tag{3.17}$$

For the default ISM input parameters, a value consistent with those used on the ARAIM Milestone Report 3 [3] are used, and can be found on Table 6.1. Note that the probability of a fault affecting more than one satellite for Galileo is four orders of magnitude larger than that of GPS as there is more historical data available for the latter.

3.2.3. Gaussian overbounding

In safety-critical applications, it is necessary to rigorously quantify the errors so the integrity requirements can be satisfied. For GNSS Navigation systems this means characterizing ranging errors. In general, empirical distributions are unknown and complex. In this context, [22] proposes a methodology that is able to substitute the real distribution with an *overbounding* Gaussian distribution. This distribution has many advantages which, while ensuring safety, greatly simplify the calculation of integrity risk. In particular, this

distribution is characterized by predicting a higher integrity risk than that predicted by the empirical distribution.

Given a sample distribution f_s, it is replaced by a unimodal, symmetric distribution f_{su}. Then, f_{su} is bounded following the procedure proposed by [22] obtaining a left-side Gaussian overbound $f_{ob}^{L} \sim N(\mu_L, \sigma_L)$. Analogously, one can obtain the right-hand overbound, $f_{ob}^{R} \sim N(\mu_R, \sigma_R)$. The CDF for the left and right overboundings are provided by

$$F_{ob}^{L}(x) = (1+\epsilon) \int_{-\infty}^{x} N(-\mu_L, \sigma_L)\, dx, \tag{3.18}$$

$$F_{ob}^{R}(x) = (1+\epsilon) \int_{-\infty}^{x} N(\mu_R, \sigma_R)\, dx, \tag{3.19}$$

where ϵ is a relaxation factor, known as excess mass [22]. Lastly, the final overbounding distribution is given by

$$f_{ob} \sim N\left(\max(\mu_L, \mu_R), \max(\sigma_L, \sigma_R)\right). \tag{3.20}$$

The final CDF overbound is provided by

$$F(x) \leq F_{OB}(x) = \begin{cases} F_{ob,L}(x), & x \leq 0 \\ F_{ob,R}(x), & x > 0 \end{cases} \tag{3.21}$$

As Gaussian distributions remain stable through convolution, the resulting positioning error based on the over bounding distribution of the range error will also be bounded thus becoming a crucial tool for integrity assessment.

4 | Galileo High Accuracy Service (HAS)

The Galileo High Accuracy Service (HAS) provides free-of-charge precise orbits, clock corrections and code biases that allows Precise Point Positioning (PPP) capabilities globally. This is achieved by broadcasting satellite clock and orbit corrections for the broadcast ephemeris, as well as biases for single frequency users [4]. In this chapter, a general description is provided regarding HAS architecture and capabilities. Additionally, an overview of the HAS user algorithm used for applying the corrections is given.

4.1. HAS Architecture

Currently, Galileo HAS provides multi-constellation multi-frequency corrections that support the following signals:

- **GPS** L1/L2C,
- **Galileo** E1/E5a/E5b/E6.

Galileo HAS relies on several Galileo system elements for the generation, dissemination and exploitation of correction messages. The High Accuracy Data Generator (HADG) processes data from Galileo Sensor Stations (GSS) to generate corrections for both Galileo and GPS. These high-accuracy (HA) corrections are transmitted in real-time to the Galileo core infrastructure.

The infrastructure then compiles this information into a single message (448 bps per connected satellite) and uploads it to the Galileo constellation via Uplink Stations (ULS). HA data are broadcast by the satellites through the E6-B signal component (see the Galileo HAS SIS ICD [23] for details on E6 signal reception). Additionally, users can also access HA data through a terrestrial internet connection (see Galileo HAS Internet Data Distribution (IDD) Interface Control Document (ICD) [24]). Figure 4.1 shows a schematic representation of Galileo HAS high level architecture, with the interaction among its

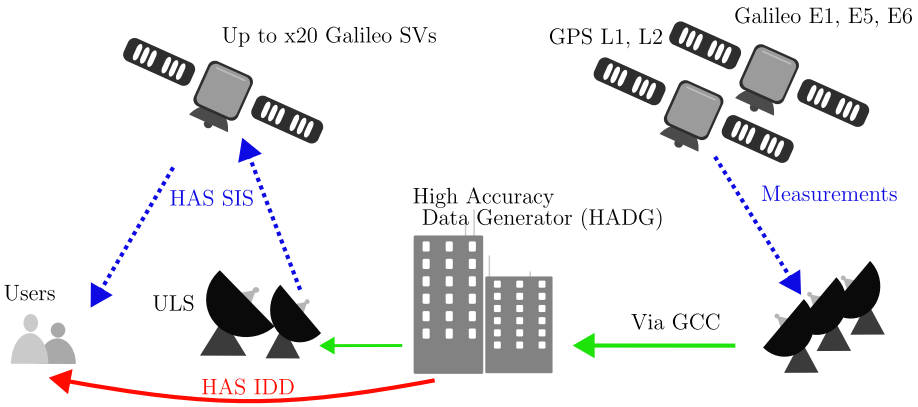

Figure 4.1: Schematic representation of Galileo HAS high level architecture.

	SL1	SL2
Coverage	Global	ECA[1]
Corrections	Orbit, clock, biases (code and phase)	Orbit, clock, biases (code and phase) + atmospheric corrections
Dissemination	Galileo E6b / Internet Data Distribution (IDD)	
Availability	99 %	99%

[1] European Coverage Area.

Table 4.1: Summary of Galileo HAS service levels. [24]

elements.

Compatible user receivers can apply these corrections to supported Galileo and GPS signals to achieve enhanced positioning performance.

HAS deployment is organized in three phases (0, 1 and 2). Currently Galileo HAS is on Phase 1, which ensures Service Level 1 capabilities with relaxed performance.

Two service levels (SL) are defined for Galileo HAS. SL1 provides global coverage and corrections for orbits, clocks and biases (codes and phase). On the other hand, SL2 will also include atmospheric corrections only for the European Coverage Area. See Table 4.1 for a summary on the characteristics of each service level.

4.2. HAS corrections

HAS corrections are disseminated either through Galileo Satellites on the E6b frequency, and through the Internet Data Distribution (IDD). On Phase 1, all corrections are provided in the same message type (Message Type 1). Each page is composed of 448 bits, 24 of which are used for the HAS page header, and 424 for the message itself. [25]

Galileo HAS IDD references per GNSS. [24]

System	Reference Nav. message	APC reference frequency
Galileo	I/NAV	E1
GPS	LNAV	L1

Table 4.2: Galileo HAS IDD references per GNSS.

In particular, for this work only HAS IDD corrections will be implemented. Even though both share the same Service Definition Document (SDD) [4], there are some particularities regarding the correction implementation. As a consequence, what follows is specifically valid for HAS IDD corrections. For information about the implementation with HAS SIS, refer to the correspondent Interface Control Document [23].

HAS provides orbit and clock corrections, as well as biases that substitute the Broadcast Group Delay (BGD) and Timing Group Delay (TGD) for single frequency users [24]. Both orbit and clock corrections are provided as a delta correction term that is added to the orbital position and SV clock bias computed from the broadcast navigation message. Only these corrections are implemented for the purpose of this work, as the ionospheric free L1/L2C E1/E5b combinations are used thus removing the need of single frequency code biases. Orbit and clock corrections are disseminated with a frequency of 10 seconds and have a period of validity of 40 seconds. [4]

4.2.1. Orbit corrections

Orbit corrections are provided as a set of delta and delta dot parameters

$$\delta\mathbf{r}_{HAS} = [\epsilon_n, \epsilon_t, \epsilon_w]^T \quad \delta\dot{\mathbf{r}}_{HAS} = [\dot{\epsilon}_n, \dot{\epsilon}_t, \dot{\epsilon}_w]^T. \tag{4.1}$$

These corrections are implemented on top of the broadcast ephemeris provided by the reference navigation message (I/NAV for Galileo and LNAV for GPS). In particular, the message indicates the associated Issue of Data (IOD), which might not correspond to the latest message available. Orbit corrections are referred to the NTW Satellite Coordinate System, which is defined by the radial (N), tangential (T) and cross-track

(W) components, that are defined as follows

$$\begin{aligned} \mathbf{e}_n &= \mathbf{e}_t \times \mathbf{e}_w, \\ \mathbf{e}_t &= \frac{\mathbf{v}_s}{|\mathbf{v}_s|}, \\ \mathbf{e}_w &= \frac{\mathbf{x}_s \times \mathbf{v}_s}{|\mathbf{x}_s \times \mathbf{v}_s|}, \end{aligned} \tag{4.2}$$

where $\mathbf{x}_s$ and $\mathbf{v}_s$ are the orbit position and velocity in ECEF frame, as provided by the reference navigation message. Figure 4.2 shows the definition of the NTW frame of reference with respect to ECEF frame.

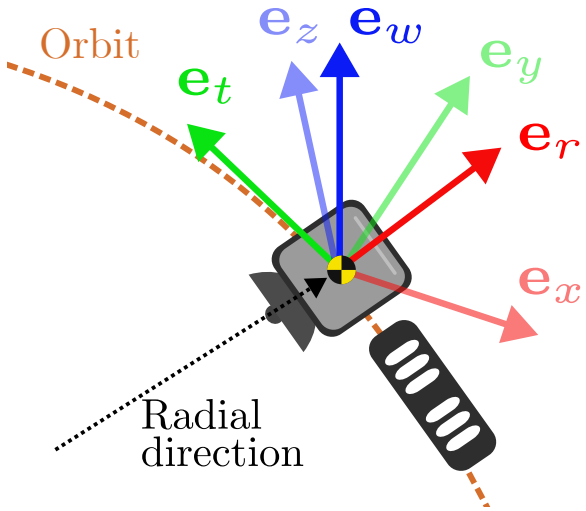

Figure 4.2: Definition of NTW frame of reference $\{\mathbf{e}_r, \mathbf{e}_t, \mathbf{e}_w\}$ with respect to ECEF frame $\{\mathbf{e}_x, \mathbf{e}_y, \mathbf{e}_z\}$.

Given the reference time of the HAS message $t_{ref,HAS}$, the orbit corrections at time t in the NTW frame are given by

$$\delta\mathbf{r}_{HAS}^{NTW}(t) = \delta\mathbf{r}_{HAS}(t_{ref,HAS}) + \delta\dot{\mathbf{r}}_{HAS}(t - t_{ref,HAS}). \tag{4.3}$$

These corrections can be rotated to ECEF frame as

$$\delta\mathbf{r}_{HAS}(t)^{ECEF} = \mathbf{R}_{NTW}^{ECEF}\,\delta\mathbf{r}_{HAS}(t)^{NTW} \tag{4.4}$$

where

$$\mathbf{R}_{NTW}^{ECEF} = [\mathbf{e}_n, \mathbf{e}_t, \mathbf{e}_w] \tag{4.5}$$

is the rotation matrix from NTW to ECEF frame of reference. Finally, HAS-corrected

position is provided by

$$\breve{\mathbf{x}}_s = \mathbf{x}_s - \delta \mathbf{r}_{HAS}^{ECEF}(t). \tag{4.6}$$

It is important to highlight that orbit corrections should be substracted from the position provided by the reference navigation message. This is not the case for HAS SIS corrections, which should be added instead according to its Interface Control Document [23]. The resulting orbital position corresponds to the L1/E1 Antenna Phase Center location, as indicated on Table 4.2. For dual frequency users, it is necessary to translate the solution using an appropriate attitude model and the Antenna Phase Center offsets provided by the IGS ANTEX files [6]. More information about how to perform this transformations is provided on Appendix A.

4.2.2. Clock corrections

HAS clock corrections δC_{HAS} are incremental corrections to be added to the ionosphere-free satellite clock error, provided by the reference broadcast navigation message. Each correction is composed of 3 coefficients for a second-order polynomial. The value of the correction is given by [24]

$$\delta C_{HAS} = C_0 + C_1 \left(t - t_{ref,HAS}\right) + C_2 \left(t - t_{ref,HAS}\right)^2. \tag{4.7}$$

This correction should be added to the SV clock bias broadcast in the navigation message, together with the relativistic correction δ_{rel}

$$\breve{\delta} t_{SV} = \delta t_{SV} + \frac{\delta C_{HAS}}{c} + \delta_{rel} \tag{4.8}$$

where $c = 299792458.0\ m/s$ is the speed of light in vacuum and δ_{rel} is provided by Eq. (2.10). The corrected clock error is referred to Galileo System Time (GST). A common offset per epoch has to be taken into account when working with GPS clock offsets. However, from the user side, this offset is absorbed by the receiver clock biases.

4.2.3. HAS IDD message reception

HAS IDD messages are distributed using the N-TRIP protocol [24]. In order to access the data, the user should apply on the European GNSS Service Center (GSC) website [1].

[1] https://www.gsc-europa.eu/galileo/services/galileo-high-accuracy-service-has/internet-data-distribution-registration-form

Then, several tools exist for retrieving the corrections live. In particular [24] proposes the use of the open-source tool BKG Ntrip Client.

4.3. Expected Signal-In-Space error performance

The Galileo HAS Service Definition Document (HAS SDD) defines and commits to a set of Minimun Performance Levels (MPLs) in terms of orbit and clock accuracy. Orbit accuracy is defined as the instantaneous 3D RMS of the residuals between the reference and the corrected orbital position. On the other hand, clock accuracy is defined as the instantaneous residual error between the HAS corrected clocks and the Galileo System Time reference. The values of the MPLs for each constellation are collected on Table 4.3. HAS MPLs are refereed to the accuracy computed over a period of 30 days. Galileo HAS commits to the MPL values shown on 4.3, according to its statistical characterization and assuming that the following assumptions are fulfilled [4]:

- Any of the following signal combinations are used:
  1. E1/E5a (+ L1/L2C)
  2. E1/E5b (+ L1/L2C)
  3. E1/E5a/E6-B (+ L1/L2C)
- User receivers are compliant with the technical requirements found in the corresponding ICD [23, 24].
- The user uses I/NAV (Galileo) and LNAV (GPS) navigation messages that have been declared healthy/marginal as per the correspondent interface document.
- Broadcast position and errors should be computed based on the correspondent ICD [19, 26].

SiS component	GPS	Galileo
Orbit MPL (95% RMS)	$\leq$ 33 cm	$\leq$ 20 cm
Clock MPL (95% RMS)	$\leq$ 15 cm	$\leq$ 12 cm

Table 4.3: Galileo HAS minimum performance levels (MPL) acording to HAS SDD. These values correspond to the 30 day average per constellation. [4]

4.3.1. HAS Service Area

HAS service Area is defined as the geographical region in which the users can expect a fulfillment of the Minimum Performance Levels (MPLs) defined in Table 4.3. This region is defined on Figure 4.3. [4]

Note that users outside the Service Area are able to use the service, however MPLs are not expected to be satisfied. This is a consequence of the geographical location of Galileo Sensor Stations, that are the responsible of performing measurements on Galileo and GPS SVs. [4]

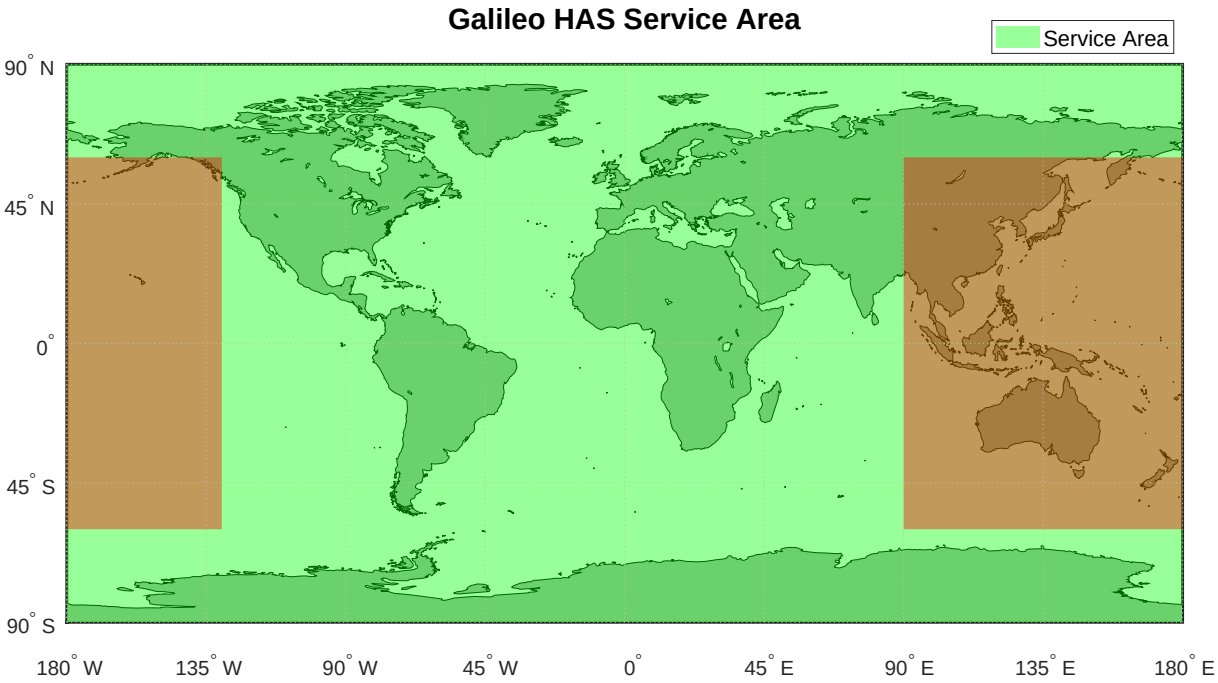

Figure 4.3: Definition of HAS Service Area (SA) (green) [4]. Users outside the SA, should not expect compliance with MPLs defined on table 4.3.

5 | Integration of Galileo HAS within ARAIM

In this chapter, a general discussion is provided on the methodology implemented for addressing the research questions proposed on Section 1.2. In particular, it aims to discuss the integration of Galileo HAS IDD into ARAIM.

From Eq. (3.12) and (3.13), it can be seen that ARAIM performance is driven both by the integrity (σ_{URE}) and continuity (σ_{URE}) error models, the latter having an indirect impact through the threshold $T_{k,q}$.

On the other hand, Galileo HAS IDD is a service that provides improvements in accuracy to the positioning solution based on a set of orbital and clock corrections that are transmitted in real time. In particular, HAS establishes a set of commitments commitment in terms of the 95th percentile of the constellation-wise RMS of the 3D orbit and clock errors computed over a period of 30 days, assuming that the user is inside the Service Area [4]. These MPLs are collected on Table 4.3.

As a consequence, it is proposed to integrate Galileo HAS into ARAIM, in such a way that the ISM's continuity model (σ_{URE}) is modified with values consistent with HAS performance, and HAS IDD is used for the computation of the positioning solution. In this chapter, a modified ARAIM algorithm is proposed that integrates Galileo HAS with the already existing ARAIM baseline algorithm described in [17].

5.1. Modified ARAIM user algorithm

The ARAIM algorithm described in Section 3.2 is modified in order to integrate HAS corrections into the processing pipeline. Since Galileo HAS is an accuracy service, only the continuity model is modified from the ISM.

By using HAS IDD, the corrected pseudorange measurements defined in Eq. (2.12) are

updated taking into account HAS satellite clock bias corrections

$$\breve{\rho}_i^j = \rho_i^j - \left(-c\breve{\delta t}_{SV,i}^{\,j} + T + \delta_{rel}\right) = \rho_i^j - \breve{D}_i^j, \tag{5.1}$$

where $\breve{(\cdot)}$ indicates that HAS corrections have been applied for the computation of that value. Additionally, let the refined satellite position of satellite j from constellation i, $\breve{\mathbf{x}}_{s,i}^j = [\breve{x}_{s,i}^j, \breve{y}_{s,i}^j, \breve{z}_{s,i}^j]^T$. Then, it is possible to compute a HAS-corrected measurements vector $\breve{\mathbf{y}}$ and geometry matrix $\breve{\mathbf{G}}$ based on Eq. (2.19) and using the HAS-corrected geometric distance $\breve{L}_0^{j,i}$, obtaining

$$\breve{\mathbf{y}} = \breve{\mathbf{G}}\breve{\mathbf{x}} + \breve{\boldsymbol{\epsilon}}, \tag{5.2}$$

for which an update of the WLS solution is provided as

$$\delta\breve{\hat{\mathbf{x}}} = \left(\breve{\mathbf{G}}^T\mathbf{W}\breve{\mathbf{G}}\right)^{-1}\breve{\mathbf{G}}^T\mathbf{W}\breve{\mathbf{y}}. \tag{5.3}$$

Solving iteratively, one obtains an estimate of the position in ECEF, $\breve{\hat{\mathbf{x}}}$.

As it is proposed that HAS only modifies the continuity model, the weight matrix is given by $\mathbf{W} = \mathbf{C}_{int}^{-1}$, where $\mathbf{C}_{int}$ is maintains its original definition provided by Eq. (3.3).

The HAS-corrected estimator for each subset k is given by

$$\breve{\mathbf{S}}^{(k)} = \left(\breve{\mathbf{G}}_{ENU}^T\mathbf{W}^{(k)}\breve{\mathbf{G}}_{ENU}\right)^{-1}\breve{\mathbf{G}}_{ENU}^T\mathbf{W}^{(k)}. \tag{5.4}$$

where $\breve{\mathbf{G}}_{ENU}$ is the HAS-corrected geometry matrix in ENU coordinates. The variances of the HAS-corrected position solution in ENU ($q = 1, 2, 3$) are given by

$$\left(\breve{\sigma}_q^{(k)}\right)^2 = \left(\breve{\mathbf{G}}_{ENU}^T\mathbf{W}^{(k)}\breve{\mathbf{G}}_{ENU}\right)_{(q,q)}^{-1} \tag{5.5}$$

where (q, q) indicates the q-th element in the diagonal of the matrix.

The nominal bias b_{nom} also remains unmodified after applying HAS corrections, as it corresponds to the integrity model. However, its projection do changes, obtaining

$$\breve{b}_q^{(k)} = \sum_{i=1}^{N_{sat}} \left|\breve{\mathbf{S}}_{q,i}\right| b_{nom,i}. \tag{5.6}$$

Additionally, the covariance matrix for accuracy is directly updated by using an appropiate continuity error model that characterizes HAS accuracy performance. This model is proposed to be defined by a set of σ_{URE}^{HAS} for each SV. This leads to

$$\breve{\mathbf{C}}_{acc}(i,i) = \left(\sigma_{URE,i}^{HAS}\right)^2 + \sigma_{tropo,i}^2 + \sigma_{user,i}^2. \tag{5.7}$$

Based on this definition, the value of $\sigma_{ss,q}^{(k)}$ is redefined as

$$\left(\breve{\sigma}_{ss,q}^{(k)}\right)^2 = \mathbf{e}_q^T \left(\breve{\mathbf{S}}^{(k)} - \breve{\mathbf{S}}\right) \breve{\mathbf{C}}_{acc} \left(\breve{\mathbf{S}}^{(k)} - \breve{\mathbf{S}}\right)^T \mathbf{e}_q. \tag{5.8}$$

The thresholds for the statistical tests are then updated as

$$\breve{T}_{k,q} = K_{fa,q}\breve{\sigma}_{ss,q}^{(k)}, \tag{5.9}$$

where $K_{fa,q}$ definition remains unchanged with respect to that provided on Eq. (3.10). Finally, an updated set of vertical and horizontal protection levels is obtained by applying the newly defined HAS-corrected parameters:

$$\begin{aligned} 2Q\left(\frac{V\breve{P}L - \breve{b}_3^{(0)}}{\breve{\sigma}_3^{(0)}}\right) + \sum_{k=1}^{N_{Faultmodes}} p_{fault,k} Q\left(\frac{V\breve{P}L - \breve{T}_{k,3} - \breve{b}_3^{(k)}}{\breve{\sigma}_3^{(k)}}\right) = \\ = PHMI_{VERT}\left(1 - \frac{P_{sat,notmonitored} + P_{const,notmonitored}}{PHMI_{VERT} + PHMI_{HOR}}\right), \end{aligned} \tag{5.10}$$

$$\begin{aligned} 2Q\left(\frac{H\breve{P}L_q - \breve{b}_q^{(0)}}{\breve{\sigma}_q^{(0)}}\right) + \sum_{k=1}^{N_{Faultmodes}} p_{fault,k} Q\left(\frac{H\breve{P}L_q - \breve{T}_{k,q} - \breve{b}_q^{(k)}}{\breve{\sigma}_q^{(k)}}\right) = \\ = \frac{1}{2} PHMI_{HOR}\left(1 - \frac{P_{sat,notmonitored} + P_{const,notmonitored}}{PHMI_{VERT} + PHMI_{HOR}}\right). \end{aligned} \tag{5.11}$$

with $H\breve{P}L = \sqrt{H\breve{P}L_1^2 + H\breve{P}L_2^2}$. These equations provide an updated value for the protection levels, taking into account HAS-corrected measurements and the updated continuity model that characterizes Galileo HAS performance through $\sigma_{URE,i}^{HAS}$.

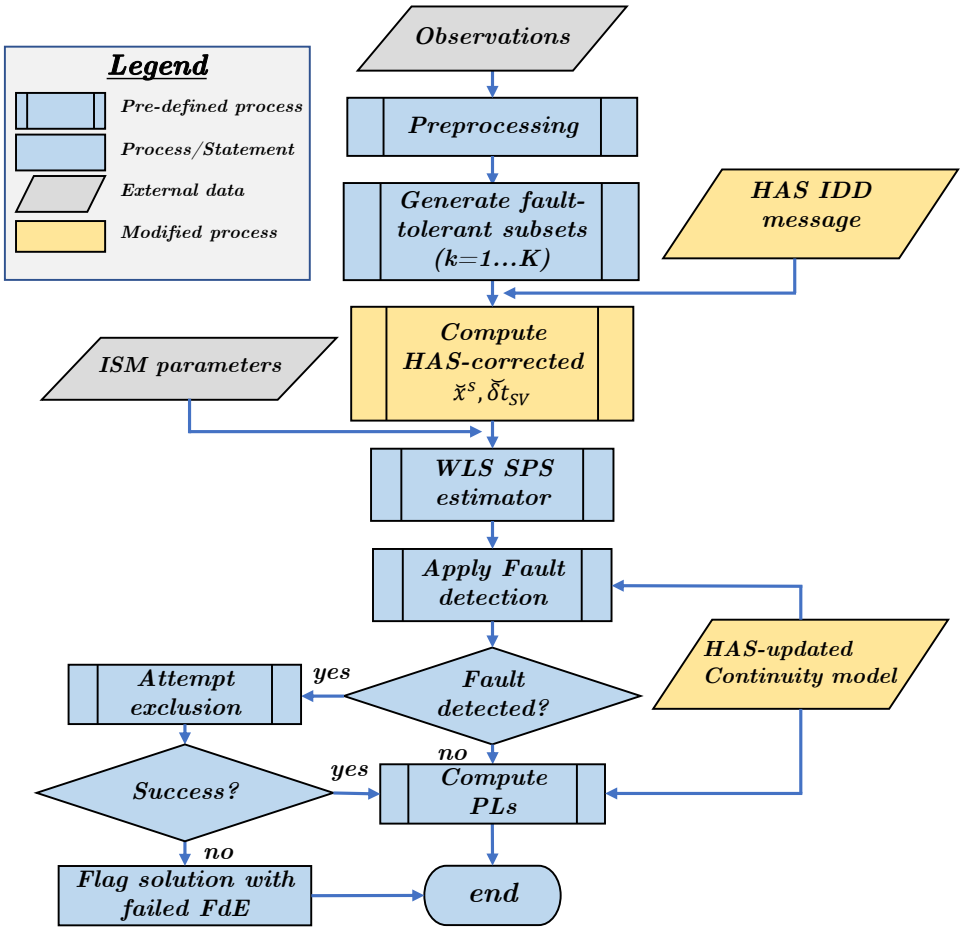

Figure 5.1: Flowchart of the modified ARAIM user algorithm integrating HAS IDD corrections. The variations introduced are marked in yellow.

5.2. Implementation

Figure 5.1 shows the flowchart of the proposed algorithm. In this flowchart, those blocks in yellow indicate variations introduced by the integration of Galileo HAS IDD into ARAIM.

Given a set of observations from a receiver, the collected measurements are preprocessed. This process includes several steps that prepare the input data before delivering it to the rest of the pipeline. The acquired measurements should correspond to L1/L2C and E1/E5b code pseudorange measurements for GPS and Galileo, respectively, as required by [4].

Firstly, those measurements coming from satellites flagged as unhealthy in the last $T_{recov} = 300$ seconds are removed. While [3] does not provide a specific value for T_{recov}, 5 minutes is assumed to be an appropriate value.

Then, the code ionospheric free linear combination is produced from the individual pseu-

dorange observations which is then used in the rest of the pipeline. This allows to remove the first-order ionospheric delay, as discussed on Section 2.2.

K fault-tolerant subsets are generated according to the a prior probability of constellation and satellite faults, as indicated by the ARAIM baseline algorithm [17]. Each of these subsets correspond to the failure of one or more SV and a certain probability is associated to each of them. The case $k = 0$ corresponds to the all-in-view solution (i.e. no SV is excluded).

In order to compute the positioning solution, it is necessary to compute the HAS-corrected satellite position and clock biases. These are obtained by combining the LNAV/INAV together with the corrections provided by the HAS IDD message. Then, a Weighted Least-squares estimator is used for computing the positioning solution. For the weight matrix, the ISM integrity model is used as $\mathbf{W} = \mathbf{C}_{int}^{-1}$. The specific algorithm used for the position estimation is described in Appendix B.

Then, fault detection is applied by performing the statistical tests

$$|\breve{\hat{x}}_q^{(k)} - \breve{\hat{x}}_q^{(0)}| \leq \breve{T}_{k,q} \tag{5.12}$$

for each of the K subsets. For this purpose, the HAS continuity model is used on the computation of each threshold $\breve{T}_{k,q}$. If no faults are detected, then the PLs equations (5.11) and (5.10) are solved. On the other hand, if a fault is detected, exclusion is attempted with those subsets k for which any of the q (q = East, North, Up) tests have failed. If at any point a consistent solution is found, PLs are computed. If exclusion is not successful, then the positioning solution is flagged with failed FDE attempt.

5.3. Proposed evaluation of ARAIM-HAS algorithm

The integration of HAS into ARAIM would potentially lead to an increased global coverage for ARAIM beyond what is achievable with broadcast ephemeris, as a reduction on the Protection Levels derived from the user geometry is expected.

In order to validate this approach, it is interesting to perform a world-wide coverage analysis. Simulations are performed using nominal orbits and specific error models that allow to compute the expected protection levels and coverage based on a set of parameters characterizing the ISM. In particular, a parametric analysis is performed using as reference the values of σ_{URE}^{HAS} and σ_{URA}. This tool would allow to characterize the dependencies with respect to any improvement on the continuity and integrity error models. This analysis

is developed in Chapter 6.

Galileo High Accuracy Service currently offers a commitment in terms of the 95th percent of the constellation-wise RMS error for the 3D orbits and clocks. However, in order to test this methodology it is necessary to obtain a set of σ_{URE}^{HAS} values that characterize the error of Galileo HAS in the ranging domain. For this purpose two alternatives are explored: on the one hand, a set of σ_{URE}^{HAS} values are estimated based on the MPLs commitments of HAS; on the other hand, an independent evaluation of Galileo HAS SISRE performance is done based on the analysis of corrections emitted during 2024. The procedure followed for the latter analysis is discussed on Chapter 7.

Finally, the algorithm is tested using real observation data from a test flight campaign on Chapter 8. This is necessary to assess the actual performance improvement and the viability of the proposed methodology.

6 | ARAIM global performance analysis

The main goal of this chapter is to characterize the dependency of ARAIM's global performance with variations on the continuity (URE) and integrity (URA) error models. The objective is to be able to asses the potential improvement of the use of Galileo HAS within ARAIM.

In particular, this analysis will focus on how the main ARAIM metrics (protection levels, σ_{acc} and effective monitor thresholds) and global coverage under certain navigation requirements evolve when the integrity and continuity models are changed.

This analysis allows to quantify, not only the expected performance of the proposed ARAIM-HAS algorithm based on current HAS performance, but also enables to project the performance for future scenarios where, potentially, σ_{URE}^{HAS} and σ_{URA} values may change.

For this purpose a world-wide coverage analysis is performed for GPS and Galileo constellations. This analysis simulates a grid of users world-wide and the orbital position of the satellites extracted from the corresponding almanacs. For each simulated user, at each epoch, a positioning solution is obtained together with a set of protection levels, σ_{acc} and EMT based on the observed geometry and error models. Then this information is processed to obtain a full picture of the performance of the constellation under a specific combination of $\{\sigma_{URE}^{HAS}, \sigma_{URA}\}$.

For this analysis, it is proposed to perform a parametric analysis where σ_{URE}^{HAS} and σ_{URA} are varied in a set interval and the dependency of different performance indicators is discussed, such as

1. Vertical and Horizontal protection levels.
2. World-wide availability for LPV-200 and LPV-250.
3. Positioning accuracy evolution.

ISM parameter	Implemented value
$\sigma_{URA,GPS/GAL}$	$[0.75, 6]$ m
σ_{URE}	$[0.1, 1.5]$ m
$b_{nom,GPS/GAL}$	0.75 m
$P_{sat,GAL/GPS}$	10^{-5}
$P_{const,GPS}$	10^{-8}
$P_{const,GAL}$	10^{-4}

Table 6.1: Adopted values of ISM parameters for Galileo and GPS constellations. Based on [3]

In [3] a set of ISM values are proposed for characterizing ARAIM performance. In particular, a value of σ_{URA} of around 1.5 meters is used for both Galileo and GPS. For the continuity model, σ_{URE} is modeled as 2/3 of the integrity value which is a very conservative approach.

In order to perform this, MAAST tool for ARAIM, developed by GPS Lab of Stanford University is used as reference [27]. This tool uses almanacs containing the orbits for each of the SV of GPS and Galileo, as well as appropriate error models in order to simulate accurately ARAIM algorithm given a specific set of ISM parameters.

In particular, it is interesting to see the expected performance improvement with respect to the $\sigma_{URE} = 2/3\sigma_{URA}$ scenario as it is used as a reference in [3]. For the simulations developed on this section, the values listed on Table 6.1 are used. The simulation parameters are set to be consistent with those used by [3, 17]. In particular, users are simulated on a 10 by 10 degrees grid and a total of 10 siderial days are used for the simulation, which coincides with the repetition rate of Galileo constellation. All results are analyzed with a time step of 600 seconds.

6.1. Key performance indicators' dependency

The protection levels, vertical accuracy $\sigma_{acc,v}$ and effective monitor threshold (EMT) are computed at each epoch for each user given the ISM parameters from Table 6.1.

We first analyze the dependence of each of these parameters on the modified continuity (σ_{URE}^{HAS}) and integrity (σ_{URA}) models. For this purpose, let us focus the study on a single geographical location, of a user located near Munich (with coordinates 48°N11.58°E). The 99.5th percentiles of VPL, HPL, σ_{acc} and EMT during the time window are computed for each pair of $\{\sigma_{URA}, \sigma_{URE}^{HAS}\}$. In particular, for each combination of integrity and continuity models, the increase with respect to the pair $\{\sigma_{URE}, 2/3\sigma_{URE}\}$ is shown. This approach

is chosen because it further highlights the improvements with respect to the current references that are used for ARAIM availability simulations [3], while preserving the dependencies with respect to σ_{URE}^{HAS}.

Figures 6.1 shows the dependency of the vertical and horizontal protection levels while, on the other hand, Figure 6.2 shows the dependencies of $\sigma_{acc,v}$ and the EMT. Those cases where $\sigma_{URE}^{HAS} > 2/3\sigma_{URE}$ are removed from the analysis. First, it is necessary to notice that for a fixed σ_{URA}, the result associated to each of the σ_{URE}^{HAS} is referred to the same reference case, that corresponds to the pair $\{\sigma_{URA}, 2/3\sigma_{URA}\}$. As a consequence, fixing σ_{URA} it is possible to see the real dependence of each parameter with the continuity error model given a fixed integrity performance. Qualitatively, the behavior is very similar for each of the parameters only changing the order of magnitude of the variations.

In Figure 6.1a, by assuming a $\sigma_{URA} \in [0.75, 2]$ m a maximum decrease of around 10 meters on VPL can be expected assuming a conservative $\sigma_{URE}^{HAS} \simeq 0.4$ m. HPL shows a potential reduction of around 8 meters for the very same case. However, it is necessary to highlight that the expected values for σ_{URA} are lower than 2 meters and, as a consequence, smaller improvements may be expected in real operation in the future.

Figure 6.2 shows a maximum decrease for the vertical accuracy of around 1 meters, and 6 meters reduction of EMT using the same reference values for the integrity model. A more conservative value of 2 meters for the URA results on 0.5 meters decrease for σ_{acc} and 5 meters for EMT.

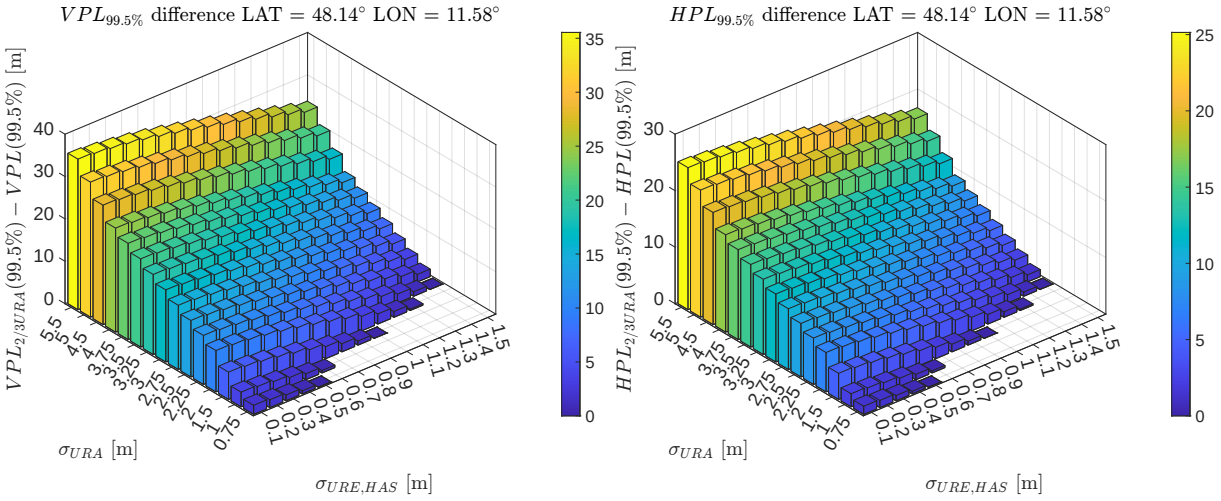

(a) (b)

Figure 6.1: Vertical and horizontal protection levels improvement with respect to $\sigma_{URE} = 2/3\sigma_{URA}$ dependency with $\sigma_{URE,HAS}$ and σ_{URA} for a specific location.

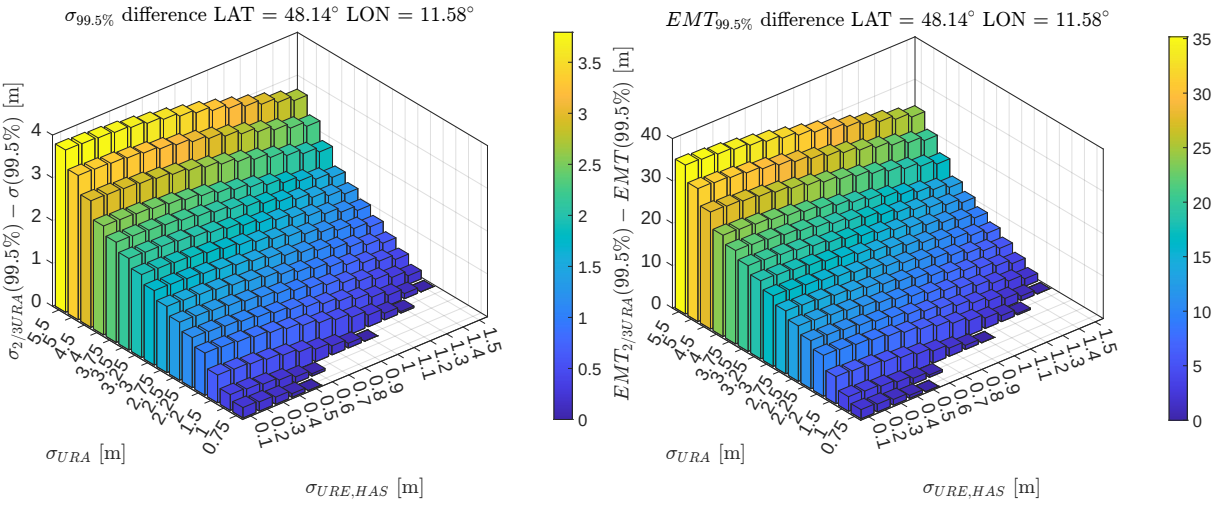

(a) (b)

Figure 6.2: σ_{acc} and EMT improvement with respect to $\sigma_{URE} = 2/3\sigma_{URA}$ dependency with $\sigma_{URE,HAS}$ and σ_{URA} for a specific location.

Overall, these results show non-negligible potential improvements for VPL, HPL, EMT and vertical accuracy. Moreover, these computations are made assuming a common URA and URE for each constellation. In reality, different URE/URA values are expected for each SV based on its specific performance. This would lead to a better ARAIM performance, as it is possible to model more accurately the actual behaviour of each constellation.

6.2. Global availability

It is now interesting to analyze the global coverage provided by ARAIM for a specific set of navigation requirements, described by a set of alert limits and accuracy and EMT thresholds. In particular, different requirements are selected corresponding to CAT-I autoland, LPV-200 and LPV-250 from Table 3.1. An additional requirement characterized by the same thresholds as LPV-200 but with a $VAL = 20$ m is also included for completing the overall analysis. For all cases, a value of $\sigma_{URA} = 1.5$ m is used.

Figures 6.3 to 6.12 show the global availability maps for different values of σ_{URE}^{HAS} and different operational requirements. Figures 6.3, 6.4 and 6.5 show that for LPV-250 global coverage is expected for more than 99% of the time even when considering the worse-case of $\sigma_{URE}^{HAS} = 0.7$ m.

On the other hand, Figures 6.6, 6.7 and 6.8 show that global coverage is expected more than 99% of the time, except when $\sigma_{URE}^{HAS} = 0.7$ m, for which there are areas with lower

expected coverage, mostly limited to polar regions where geometry is normally degraded. In any case, these regions are very limited and in general, coverage almost 100% of the time is expected.

Figures 6.9, 6.10 and 6.11 show the availability map when a tighter requirement is introduced for LPV-200 by changing the VAL to 20 meters. As expected, this condition leads to poorer availability worldwide. However, in the worse case scenario ($\sigma_{URE}^{HAS} = 0.7m$) coverage is expected to be $\geq 60\%$ in most locations. HAS is expected to provide better performance which indicates that the real behavior would be closer to that of Figure 6.9. Moreover, note that for this analysis a single value of URE and URA is used for both constellations. Using a SV-specific model will lead to a better performance overall thus providing acceptable availability even for operating requirements tighter than those of LPV-200.

Finally, Figure 6.12 shows the expected global availability for CAT-I Autoland operations. It can clearly be seen that the performance is very poor as CAT-I requirements are too strict. Only the case where $\sigma_{URE}^{HAS} = 0.2$ m is shown as there is no coverage for the others.

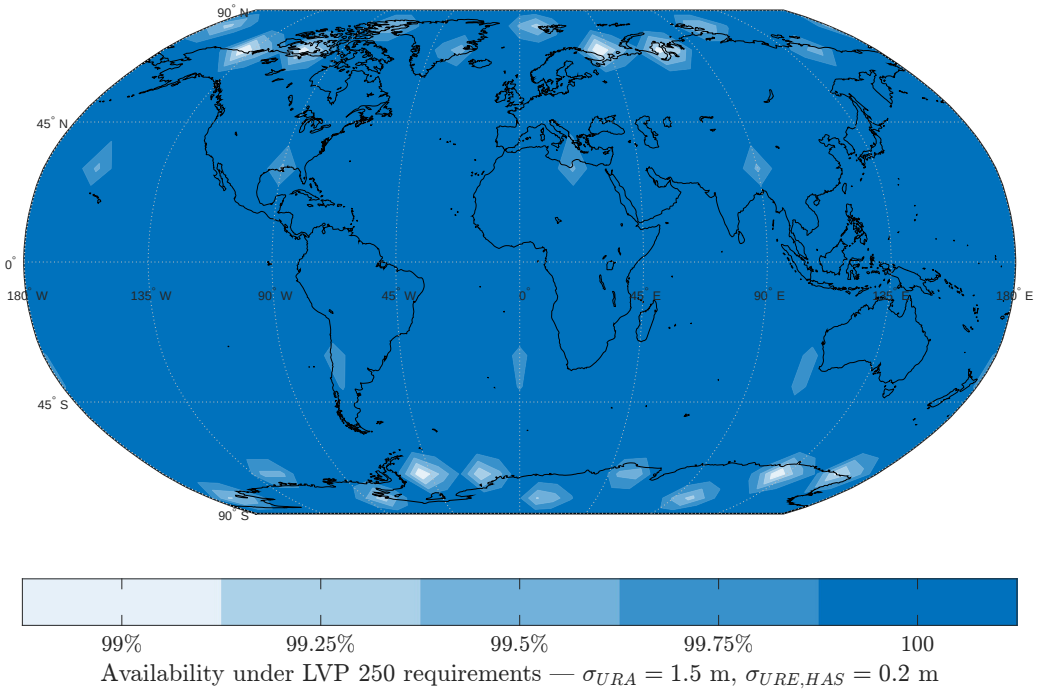

Figure 6.3: Global availability for $\sigma_{URA} = 1.5\,m$ and $\sigma_{URE}^{HAS} = 0.2$ m under LPV-250 operation.

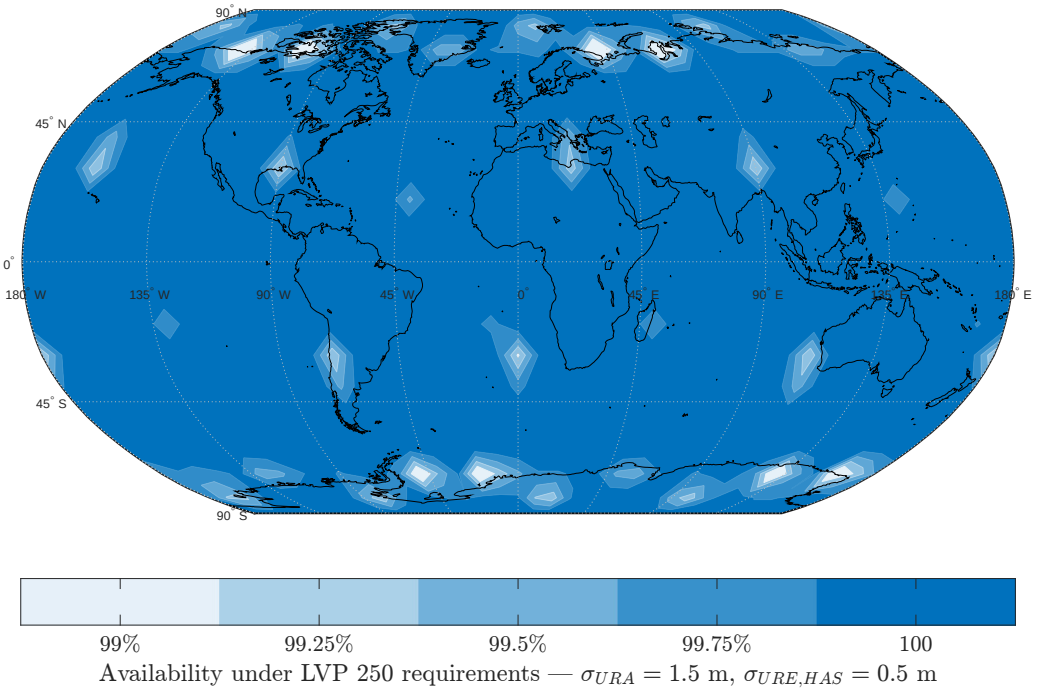

Figure 6.4: Global availability for $\sigma_{URA} = 1.5\,m$ and $\sigma_{URE}^{HAS} = 0.5$ m under LPV-250 operation.

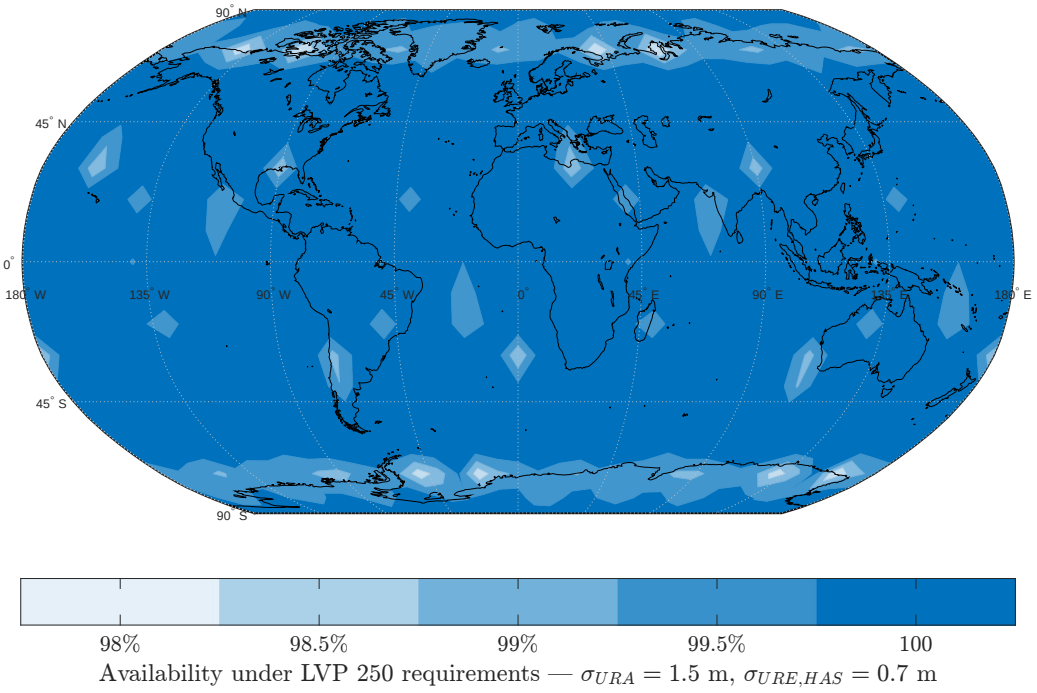

Figure 6.5: Global availability for $\sigma_{URA} = 1.5\,m$ and $\sigma_{URE}^{HAS} = 0.7$ m under LPV-250 operation.

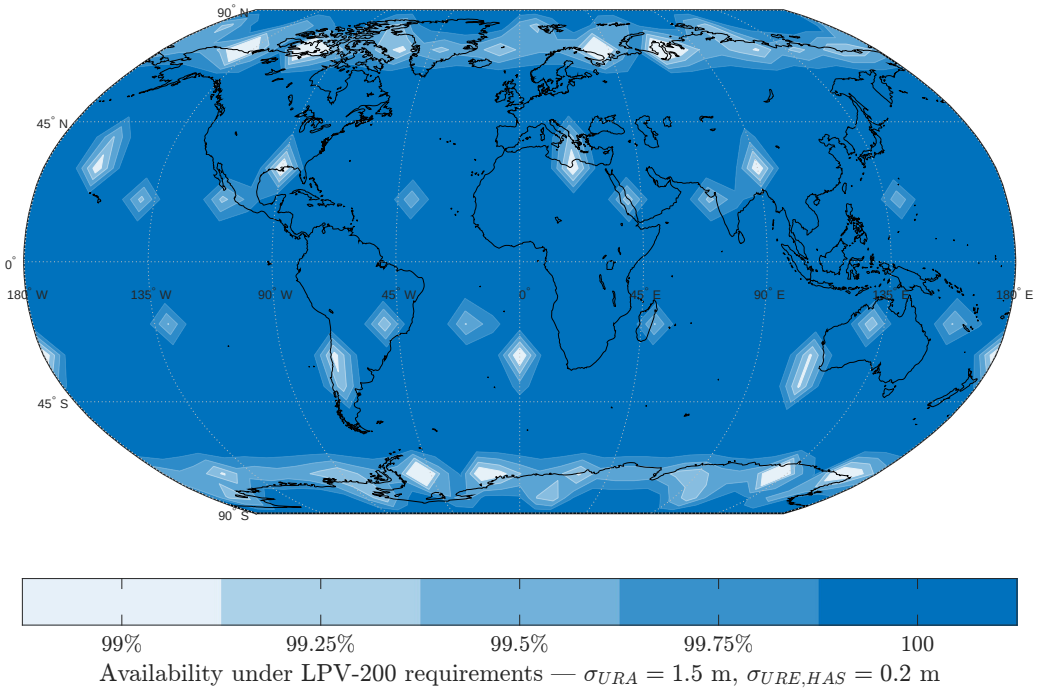

Figure 6.6: Global availability for $\sigma_{URA} = 1.5\,m$ and $\sigma_{URE}^{HAS} = 0.2$ m under LPV-200 operation.

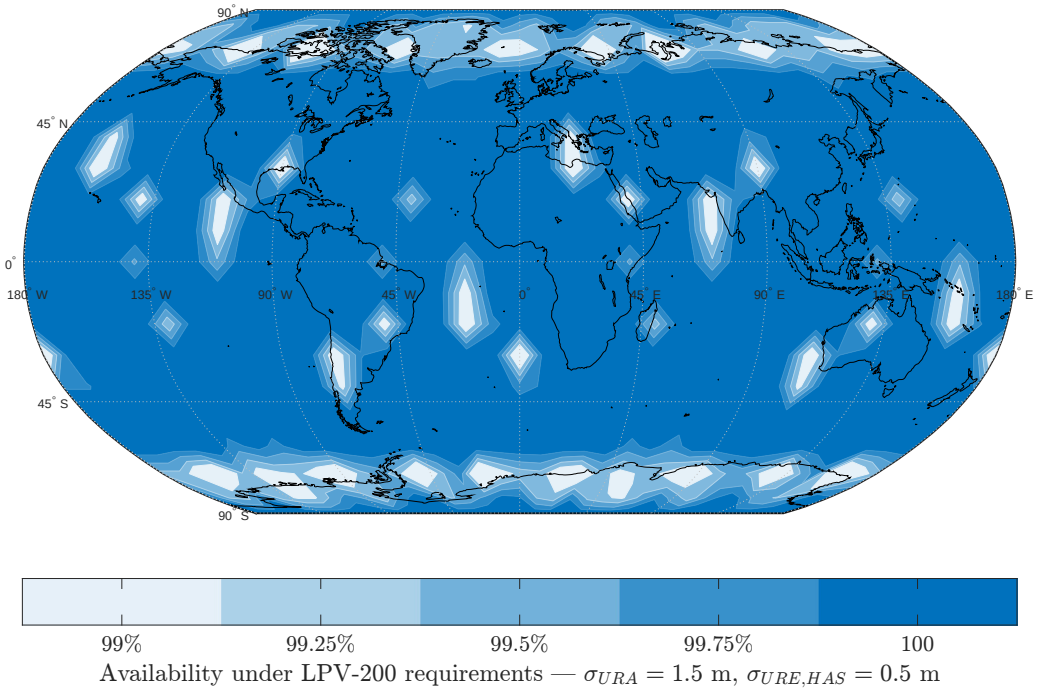

Figure 6.7: Global availability for $\sigma_{URA} = 1.5\,m$ and $\sigma_{URE}^{HAS} = 0.5$ m under LPV-200 operation.

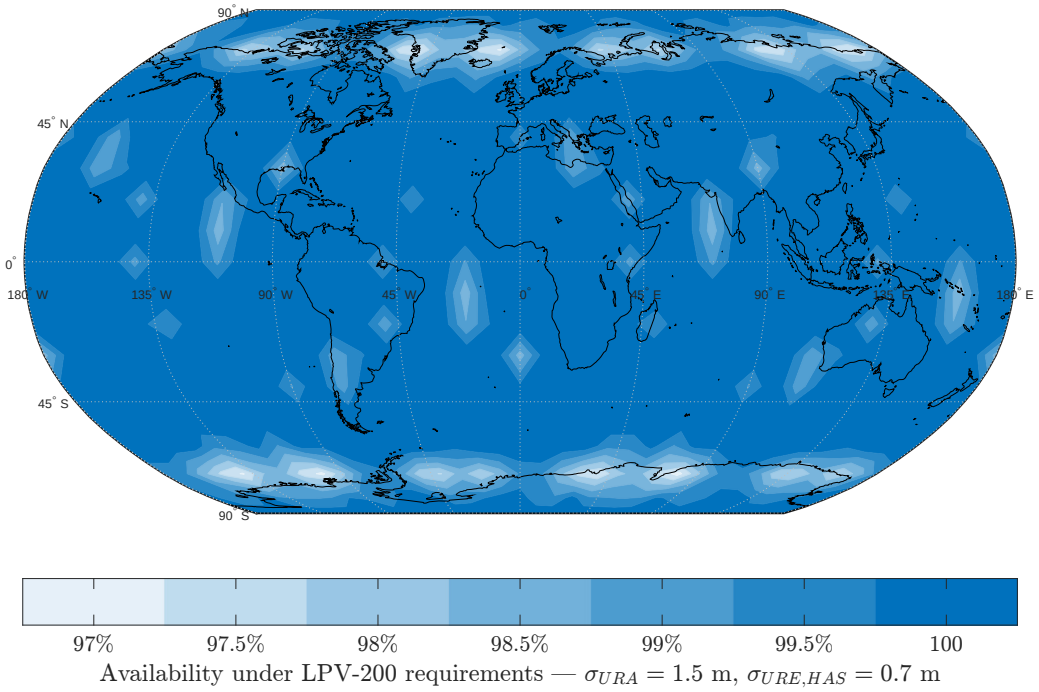

Figure 6.8: Global availability for $\sigma_{URA} = 1.5\,m$ and $\sigma_{URE}^{HAS} = 0.7$ m under LPV-200 operation.

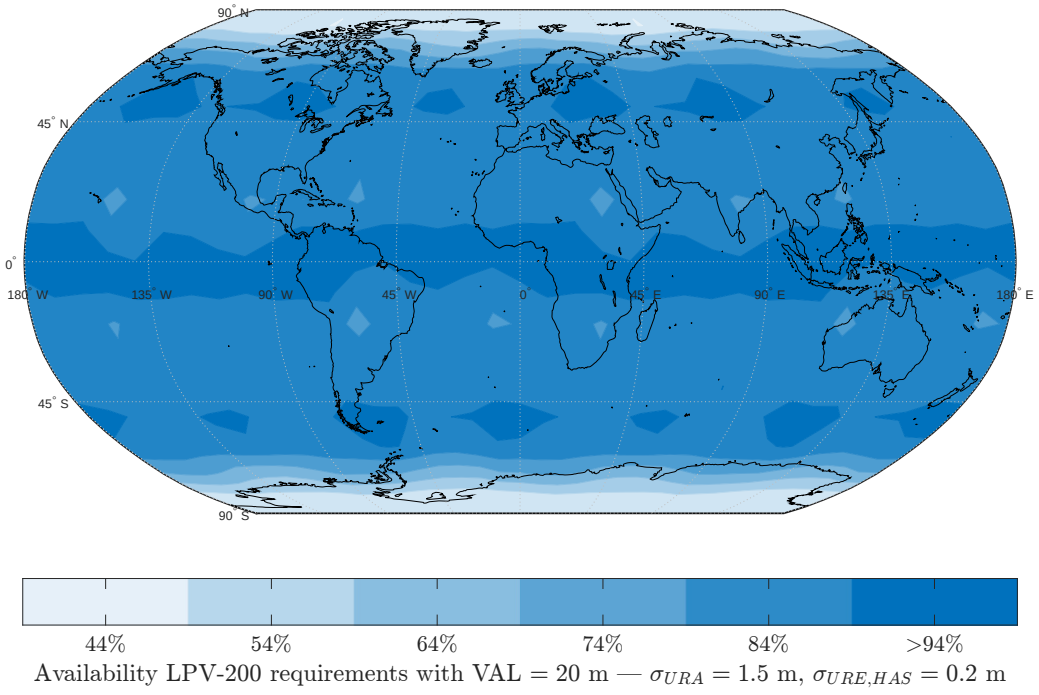

Figure 6.9: Global availability for $\sigma_{URA} = 1.5\,m$ and $\sigma_{URE}^{HAS} = 0.2$ m under LPV-200 operation with VAL lowered to 20 m.

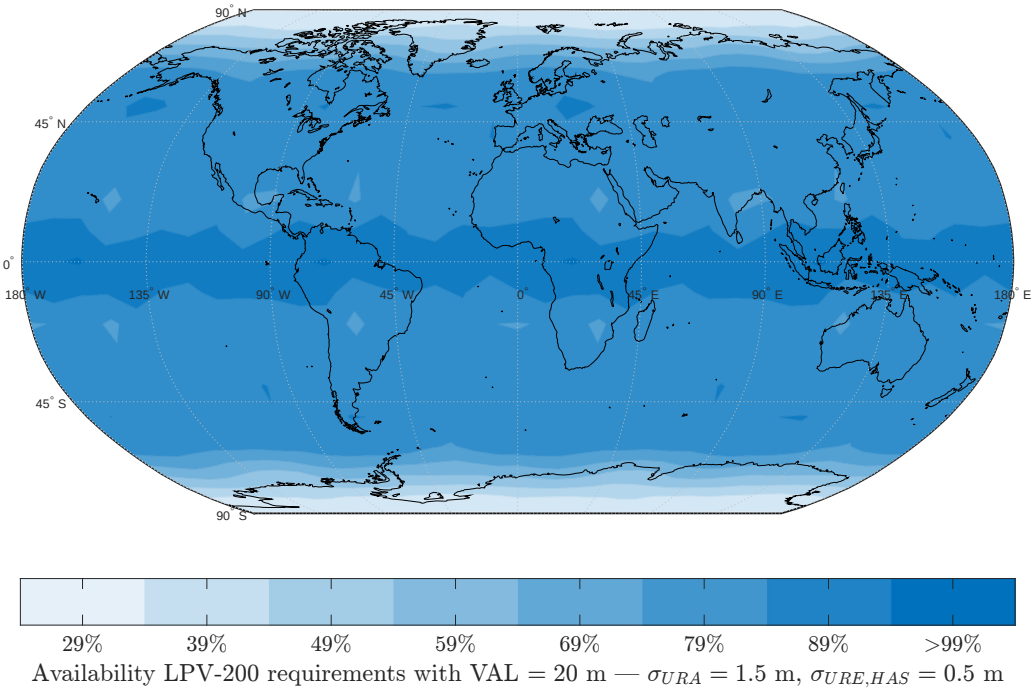

Figure 6.10: Global availability for $\sigma_{URA} = 1.5\,m$ and $\sigma_{URE}^{HAS} = 0.5$ m under LPV-200 operation with VAL lowered to 20 m.

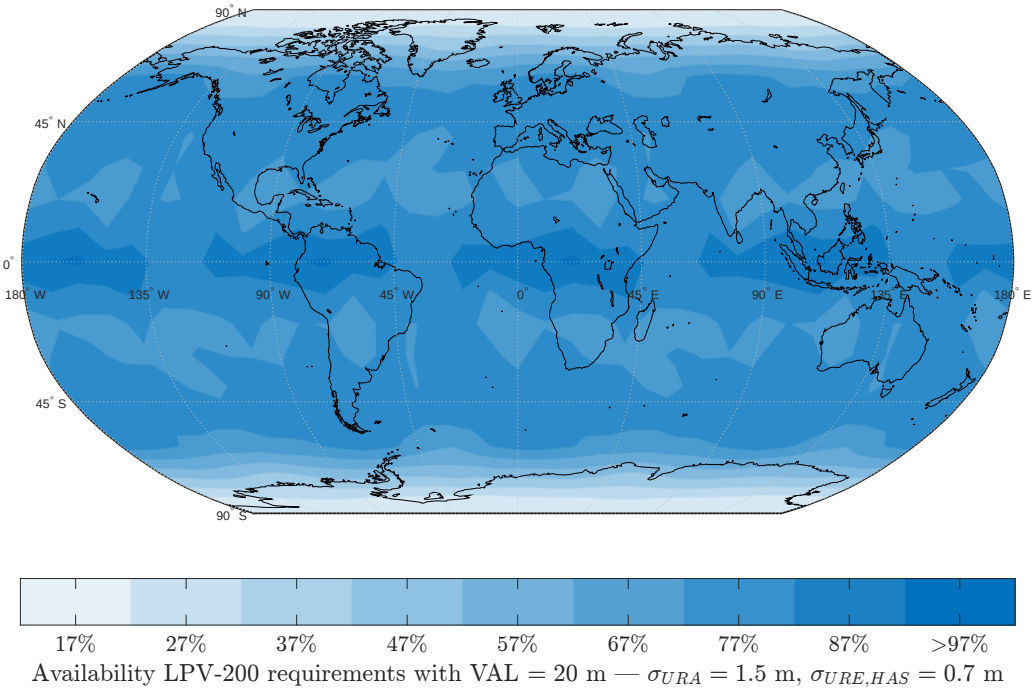

Figure 6.11: Global availability for $\sigma_{URA} = 1.5\,m$ and $\sigma_{URE}^{HAS} = 0.7$ m under LPV-200 operation with VAL lowered to 20 m.

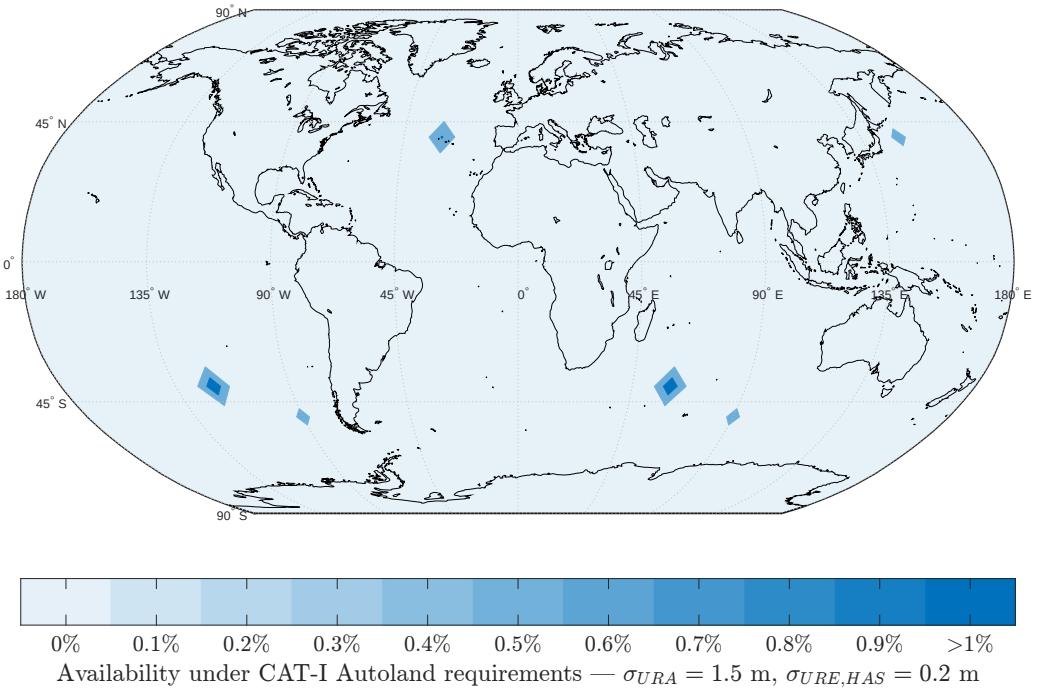

Figure 6.12: Global availability for $\sigma_{URA} = 1.5\ m$ and $\sigma_{URE}^{HAS} = 0.2$ m under CAT-I Autoland operation.

6.3. Availability parametric analysis

It is interesting now to study the dependency of global coverage with the continuity σ_{URA} and integrity σ_{URE}^{HAS} models, in a similar ways as the analysis performed on Section 6.1. In this particular case, the percentage of users that benefit from coverage at the 99.5th percentile when integrating HAS into ARAIM is used as objective function. For this analysis only three cases are considered: LPV-250, LPV-200 and a modification of LPV-200 with VAL = 20 m. Note that CAT-I Autoland is not analyzed due to the fact that the availability analysis does not provide any coverage for the range of σ_{URE}^{HAS} and σ_{URA} used. As was the case with the local parametric analysis, the increase is also shown with respect to the $\sigma_{URE}^{HAS} = 2/3\sigma_{URA}$ case.

Figure 6.13a shows the percentage of users that meet LPV-250 requirements. It can be seen that global coverage is 100% for the range $\sigma_{URA} = [0.75, 2]$ m and $\sigma_{URE}^{HAS} = [0.1, 0.4]$ m which is taken as a good approximation of the expected performance of the system. This means that, under these conditions, it is expected that ARAIM+HAS enables operations up to LPV-250 worldwide 99.5 % of the time. Additionally, Figure 6.13b shows the improvement with respect to the reference case. Firstly, the improvement is zero when URA exhibits great accuracy. This is because in that case the coverage is already 100%

for any URE value used. However, when URA increases to a more realistic value such as 1.5 m, it can be seen that the improvement is almost 20 % and reaches 80% when URA moves closer to 2 m.

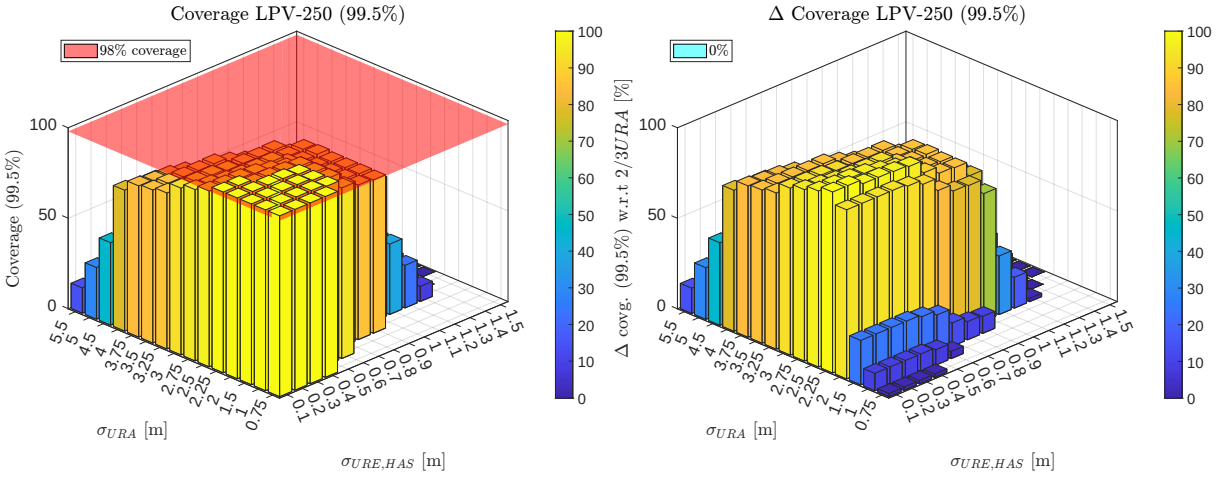

(a) (b)

Figure 6.13: Global coverage (99.5th percentile) for LPV-250 (a) and increase of global coverage with respect to the $2/3\sigma_{URA}$ base case (b).

Figure 6.14a shows the parametric analysis for LPV-200 requirements. As expected, this case exhibits less coverage overall. However, when URA is below 2 meters one can expect global coverages larger than 80 %. Moreover, it is interesting to notice that, when URE is low, the evolution of the global coverage appears to be almost constant with $\sigma_{URE,HAS}$. However, when focusing on Figure 6.14b, it is clear that there is an increase of up to 10 % coverage when $\sigma_{URE}^{HAS} = 1.5$ m as the URE varies from 0.3 to 0.7 meters. Overall, taking into account the expected values of σ_{URE}^{HAS}, the integration of ARAIM with Galileo HAS could lead to more than 80% global coverage for LPV-200 operational requirements. It is necessary to stress again that this analysis is performed using rather conservative hypothesis the use of a single URE and URA value. In reality, even better performance could be expected.

Finally, Figure 6.15a shows the worldwide coverage at the 99.5th percentile of the time when the LPV-200's VAL is lowered to 20 meters. As already anticipated by Figure 6.9, only when the system is characterized by very low values of σ_{URA} and σ_{URE}^{HAS}, there is a noticeable amount of users benefiting of coverage for 99.5% of the time. Since in the reference case there was very little coverage, the increase is very noticeable, showing a strong dependency on the continuity model.

Overall, these results prove that improving the accuracy model used in ARAIM leads

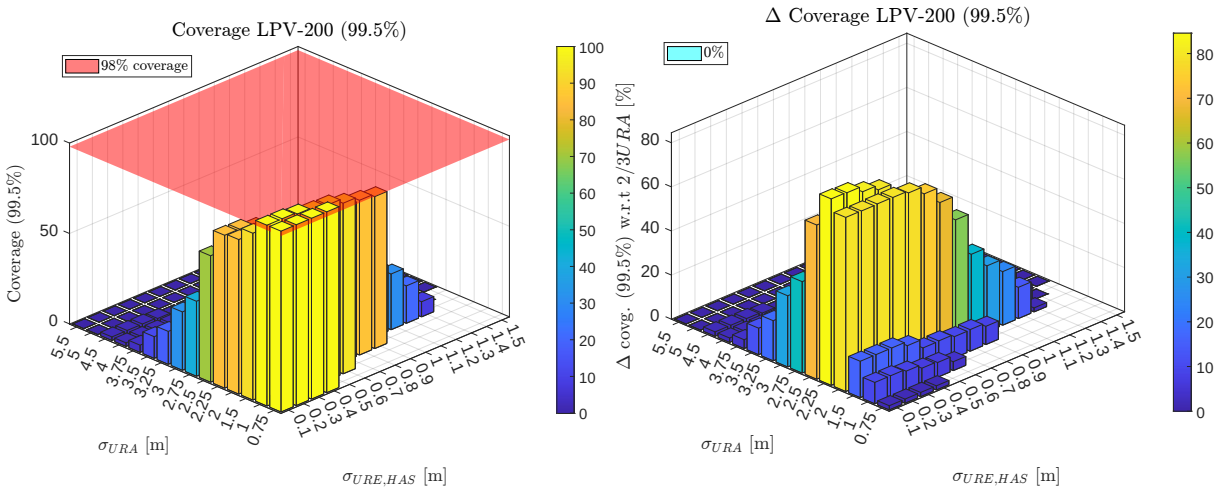

(a) (b)

Figure 6.14: Global coverage (99.5th percentile) for LPV-200 (a) and increase of global coverage with respect to the $2/3\sigma_{URA}$ base case (b).

to significant performance improvements even under very tight operational conditions such as LPV-200 greatly increasing the overall coverage, that can potentially reach 100% values in the most optimistic cases. As a consequence, it is interesting to properly assess the actual values of σ_{URE} and σ_{URE}^{HAS} that are expected based on historical data in order to provide an actual performance expectation from the integration of Galileo HAS into ARAIM.

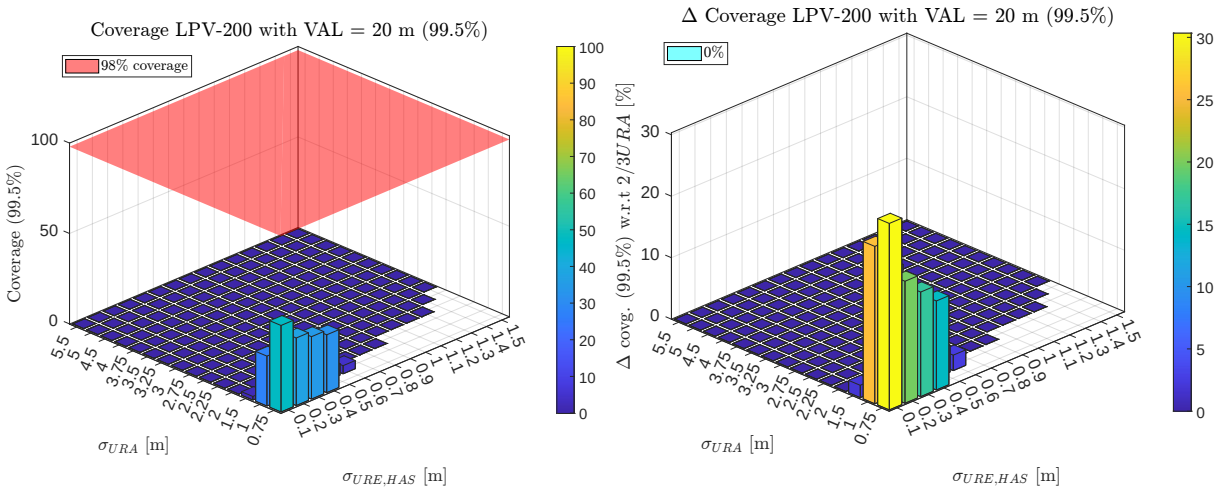

(a) (b)

Figure 6.15: Global coverage (99.5th percentile) for LPV-200 modified with VAL = 20 m (a) and increase of global coverage with respect to the $2/3\sigma_{URA}$ base case (b).

7 | Signal-In-Space error analysis

In order to properly asses the performance of the proposed methodology it is useful to have an estimation of the Signal-In-Space Range Error for Galileo HAS IDD. Currently, HAS IDD [24] offers a commitment on a set of Minimum Performance Levels. While these values offer a good reference for the expected Signal-In-Space error (SISE) performance of HAS, it has to be taken into account that only information about the 3D orbit error is provided.

As a consequence, this requires assuming a spherical orbit error distribution where the radial, cross-track and in-track components are characterized by the same accuracy. In general this is not true, as the radial component normally benefits from a better accuracy as the orbit determination is more precise along this direction. As a consequence, the use of the MPLs as a reference for computing the error in the range domain (i.e. the projection of the clock and orbit errors onto the line of sight vector of the user) leads to a rather conservative approach.

This chapter aims to analyze the results obtained when comparing estimations with the orbital positions and satellite clock biases provided by precise products. These products are taken as "ground truth" for the evaluation of the errors. In this way, it is possible to obtain an estimate of the actual SISRE that characterizes Galileo HAS IDD.

The objective is two-fold: firstly, it will provide an independent evaluation of the performance of HAS during a large time window of almost a year; and secondly, it will support the derivation of an error model that describes the potential achievable performance of ARAIM-HAS.

Firstly, a comprehensive description of the data used for this work is provided, with its source, format and characteristics. Then, Galileo HAS IDD corrections are characterized by analyzing its typical values, its availability and the expected performance according to quarterly reports provided by GSC.

Finally, the orbital and clock errors are characterized for each direction (radial, in-track and cross-track). Afterwards, a value of SISRE is estimated based on the projection of

the observed SISEs onto the ranging domain.

7.1. Data pocessing considerations

For the analysis of the Signal-In-Space error, it is necessary to analyze large amounts of data coming from different sources. In particular:

1. **Broadcast Navigation Messages**: RINEX files containing the broadcast navigation messages of each constellation, provided by the International GNSS service (IGS).
2. **Clock and Orbit precise products:** SP3 and CLK files that contain the products for the orbit and clock of each satellite, generated by the Center of Orbit Determination of Europe (CODE).
3. **Differential Clock Bias (DCB) products:** The DCBs are required to perform the clock translations between references in order to align clock biases referred to different code observables. These products are made available by the Chinese Academy of Sciences (CAS).
4. **Antenna Phase Center offsets (ANTEX files):** These files are necessary to perform the reference point translations consistent with Table 7.4. The IGS ANTEX files are used for this purpose.
5. **HAS IDD corrections:** HAS corrections obtained from the Internet Data Distribution of Galileo HAS.

An observation window of 337 days is analyzed, spanning from January 8th to December 14th of 2024. No data is available for HAS IDD between day of year (DoY) 16 and 24. However, no Notice Advisory for Galileo Users (NAGU) has been published regarding this data gap. After careful examination, this gap appears to be linked to a loss of connection of the computer recording the corrections. No more days have been affected by this issue for the considered time window.

In order to handle the large amount of data, NASA's Crustal Dynamics Data Information System (CDDIS) FTP service is used to automatically download the necessary Broadcast Navigation messages, clock and orbit precise products and DCBs. These are organized daily, and parsed for its processing. On the other hand, HAS IDD corrections are retrieved and recorded in plain text using BKG Ntrip Client. A parser has been developed and the resulting binary files are storaged and integrated in the analysis pipeline. Table 7.1 provides a summary of the source and format of each of the products used during the

Data file	Source	Format
Orbit and Clocks	CODE	SP3, CLK
DCB products	CAS	SINEX-BIAS
APC offsets	IGS	ANTEX
INAV/LNAV	IGS	RINEX
HAS IDD	BKG Ntrip Client	HAS IDD

Table 7.1: Data source summary for performing the necessary analyses.

development of this work.

7.2. HAS IDD corrections evaluation

7.2.1. Corrections magnitude

Galileo HAS IDD provides orbit and clock corrections with a nominal frequency of 10 seconds. HAS orbit corrections are provided as a set of 6 parameters per SV collected in two vectors $\{\delta\mathbf{r}_{HAS}, \dot{\mathbf{r}}_{HAS}\}$. In general, it was found that the $\delta\dot{\mathbf{r}}_{HAS}$ component is very close to zero and, as a consequence, the corrections are almost constant during its 40 seconds maximum validity interval.

Figure 7.1 shows the value of the orbit corrections during November 3rd, 2024 (DoY 304). Firstly, there is a noticeable difference in the magnitude of corrections between GPS and Galileo. This is explained by the fact that GPS broadcast orbit errors are larger than those of Galileo. As a consequence, larger corrections are needed. Moreover, there is a large difference between radial and cross-track GPS corrections and those corresponding to the in-track direction. Due to the characteristics of the SV's dynamics, the in-track component suffers from larger uncertainties thus requiring larger corrections to reach comparable accuracy levels.

Regarding Galileo satellites, corrections are smaller (≤ 0.5 m), and tend to be more similar between components. This is explained by the better accuracy of Galileo Broadcast ephemeris, that leads to a more homogeneous behavior in between components.

Figure 7.2 shows the clock corrections for each of the SVs during the very same day. GPS corrections tend to be larger as GPS broadcast clock corrections tend to be less accurate (mainly due to the use of different clocks on-board and larger gap in between consecutive navigation messages).

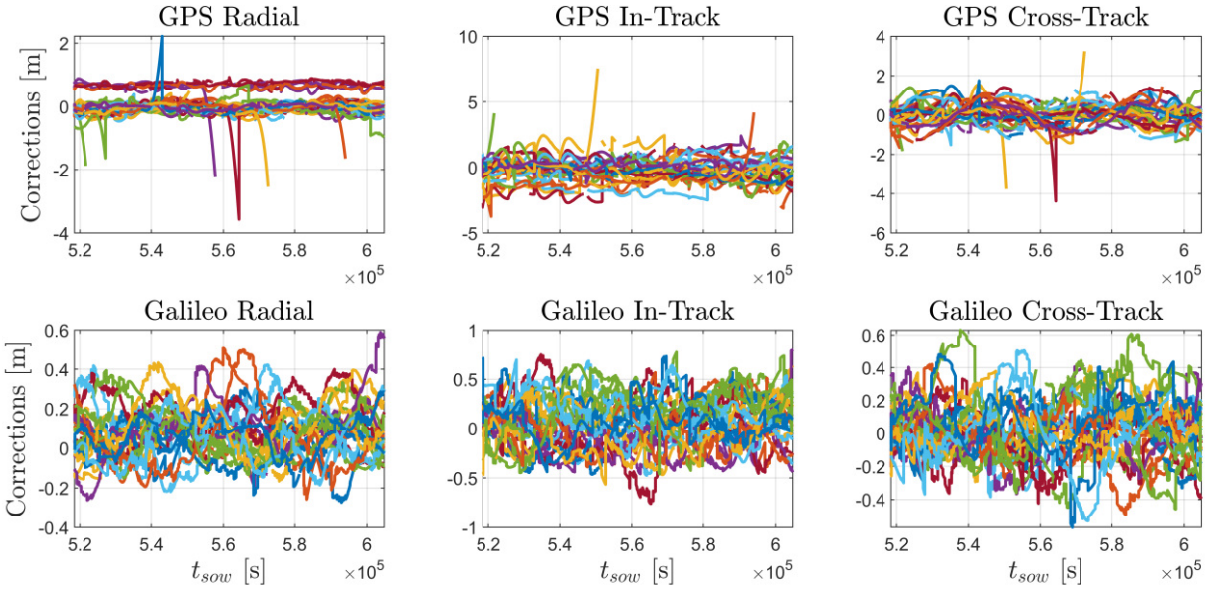

Figure 7.1: Galileo HAS IDD orbit corrections for GPS and Galileo constellations on DoY 304, 2024. Each color corresponds to one SV.

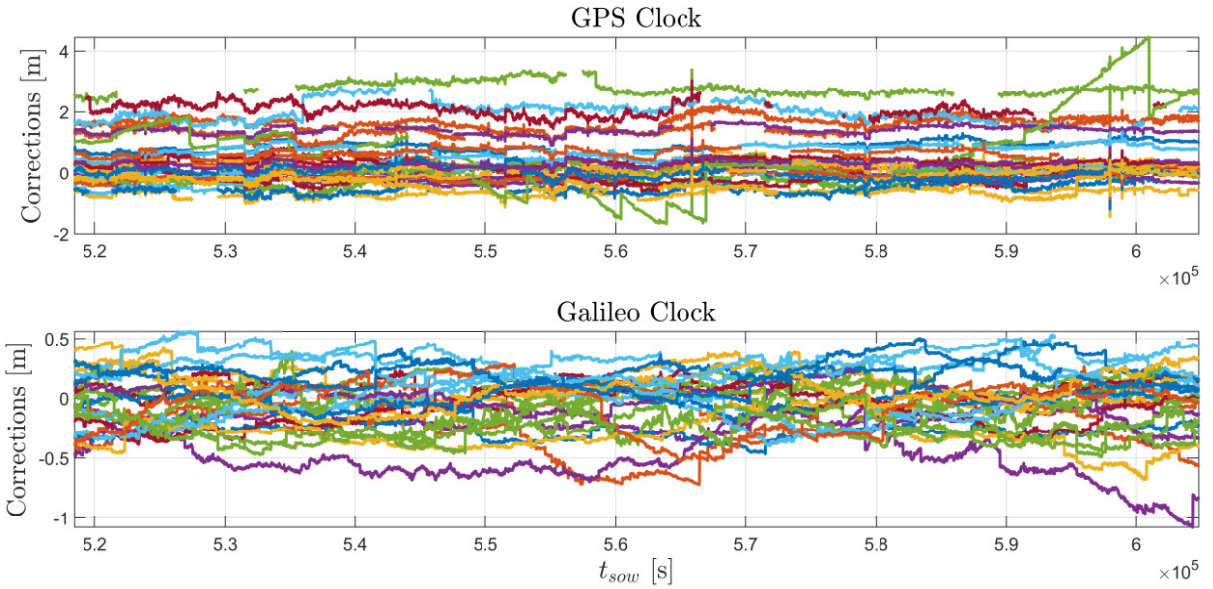

Figure 7.2: Galileo HAS IDD clock corrections for GPS and Galileo constellations on DoY 304, 2024. Each color corresponds to one SV.

7.2.2. HAS IDD availability analysis

In order to complete the characterization of HAS IDD corrections, it is interesting to asses the actual availability for each SV. As mentioned on Section 7.1, HAS corrections were recorded for 337 days between January 8th to December 14th of 2024.

Figure 7.3 shows the frequency at which orbital and clock corrections messages where received during DoY 305 of 2024. Note that receiving a message does not mean that there is a correction available for every healthy satellite from Galileo and GPS constellations. Each message normally has some satellites that do not receive corrections. For example, GPS PRN 22 did not receive any corrections for the analyzed period. The specific cause for this unavailability is unknown for the author of this work.

According to its Interface Control Document [24], HAS IDD corrections are broadcast nominally every 10 seconds. Additionally, when the user loses connection to the server the last batch of corrections remains valid for up to 40 seconds. However, in the case that no corrections are provided for a specific satellite at one epoch, every previous correction should be immediately discarded.

It can be seen that the nominal correction frequency is followed in general for the whole day. However, there are some instances where no message arrives and the user has to wait another 10 seconds for a new set of corrections. In any case, and according to the ICD, the previously-received corrections remain valid for this time, thus not affecting availability.

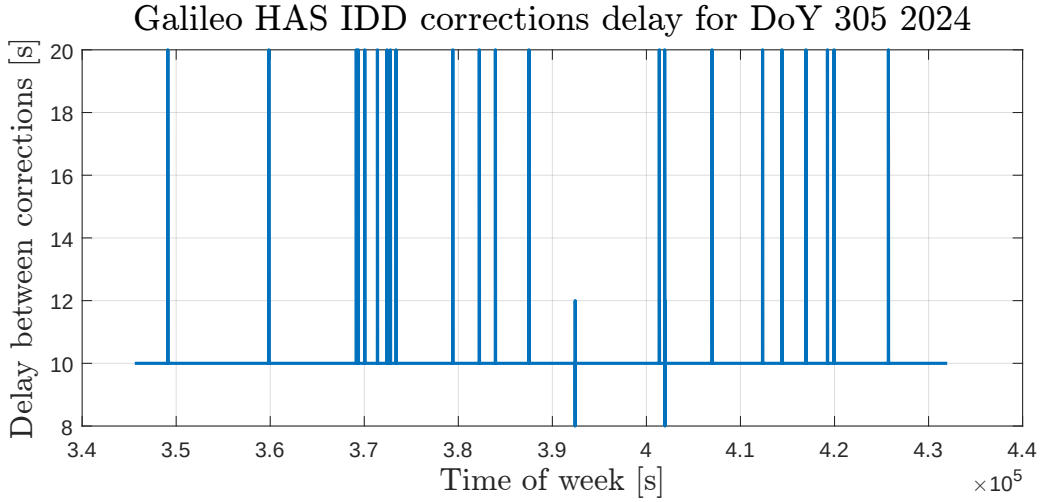

Figure 7.3: Galileo HAS IDD message frequency during DoY 305 of 2024.

Taking the aforementioned logic, the overall availability is computed for each SV i as

$$\text{HAS IDD corrections Availability for SV}_i = \frac{\#\text{ Epochs with valid corrections for i}}{8639} 100 \tag{7.1}$$

where 8639 is the number of 10-seconds time slots in a day. This computation is performed for orbit and clock corrections of each constellation. It is necessary to highlight that the definition of availability provided by Eq. (7.1) differs from that of the HAS SDD [4]. As a consequence, the availability estimated on this section should not be compared with that of the quaterly reports released by EUSPA, as they refer to different metrics.

Table 7.2 sums up the HAS IDD correction availability per SV during the analyzed period of 337 days. While the availability for orbit and clocks for a given SV are almost equal, there are some cases where there is a slight difference such as in the case of G26, where there is a very subtle difference. In any case, these differences are very small (in the order of 0.001%). As a consequence, almost every time there is an orbit correction available for a certain satellite, a clock correction is also provided.

In general, Galileo satellites benefit from a higher availability of HAS IDD corrections. For the availability computation of PRN E06 it had to be taken into account that it became operational on September 9th, 2024 (NAGU 2024034).

While the availability of HAS IDD corrections is as low as 75% for some SV, note that the user is generally seeing many satellites at each epoch. And those satellites for which there are no corrections available may still be used with the broadcast ephemeris information. In particular, assume that all SV from both constellations have the worst-case availability from Table 7.2, which is found for GPS satellite G27 of 75.097%. If 12 satellites are in view between GPS and Galileo, the probability of having half or more of the satellites using only OS is $2.4 \times 10^{-}4$. In reality, this probability is much smaller, as HAS IDD availability per SV is better in general.

7.2.3. Galileo HAS IDD expected performance

The European GNSS Service Center (GSC) regularly monitors Galileo HAS performance metrics since the EU declared the availability of HAS Initial Service on January 24th, 2023. GSC releases quarterly reports on the performance of the service. Particularly, these reports include information about the accuracy delivered by both SIS and IDD services, availability of HAS corrections and availability of HAS Coverage inside the SA. Currently, seven quarterly reports are available (Q1-Q4 2023, Q1-Q3 2024). This section

PRN	Orbit [%]	Clocks [%]
G02	85.741	85.741
G03	89.418	89.418
G04	75.690	75.689
G05	90.256	90.256
G06	86.377	86.377
G07	79.946	79.945
G08	81.364	81.363
G09	81.054	81.053
G10	77.744	77.743
G11	88.458	88.458
G12	89.738	89.738
G13	69.663	69.663
G14	75.360	75.359
G15	81.933	81.933
G16	82.095	82.095
G17	83.595	83.595
G18	86.220	86.219
G19	86.304	86.304
G20	89.992	89.992
G21	86.677	86.676
G23	85.785	85.785
G24	84.971	84.971
G25	82.315	82.315
G26	75.509	75.508
G27	75.097	75.097
G28	89.842	89.842
G29	85.142	85.141
G30	85.134	85.134
G31	88.790	88.790
G32	78.805	78.804

(a) GPS

PRN	Orbit [%]	Clocks [%]
E02	94.817	94.817
E03	94.105	94.105
E04	91.425	91.425
E05	94.512	94.512
E06	96.602	96.602
E07	94.104	94.104
E08	94.713	94.713
E09	93.772	93.772
E10	94.410	94.410
E11	94.577	94.577
E12	94.068	94.068
E13	92.988	92.988
E15	94.136	94.136
E19	94.349	94.349
E21	94.286	94.286
E24	94.810	94.810
E25	94.104	94.104
E26	93.535	93.535
E27	94.082	94.082
E29	27.255	27.255
E30	93.566	93.566
E31	94.337	94.337
E33	94.535	94.535
E34	94.637	94.637
E36	94.575	94.575

(b) Galileo

Table 7.2: Summary of HAS IDD corrections availability for GPS and Galileo between DoY 9 and DoY 342 of 2024. DoY 16 to DoY 24 are excluded from the analysis.

will focus on orbit and clock errors reported during this period. However, information about clock bias accuracy, availability and coverage can be found on [28–34]. Monthly orbits and clocks accuracy values reported for HAS IDD are summarized on Table 7.3.

Firstly, data for January is not available as the service was only declared operational by the end of the month. It can be seen that overall the performance of HAS IDD is within the MPLs defined on Table 4.3. The only time HAS IDD failed to meet the MPLs for the Galileo constellation was in June 2024. In this particular case, both HAS SIS and HAS IDD provided poor orbit accuracy for Galileo satellites.

GPS orbit error was below 0.31 m for all cases, with an average value of 0.2 m for the available months. On the other hand, GPS clock error was below 0.15 m with an average value of 0.1 m. Galileo exhibited slightly better performance, with maximum orbit error of 0.19 m and average error of 0.16 m (excluding June, 2024). Galileo clock errors were below 0.1 m, with an average value of 0.07 m.

Finally, although its values are not reported on Table 7.3, HAS SIS exhibited similar performance during the analyzed period.

Galileo HAS IDD proves to consistently deliver substantial improvements on orbit and clock errors with respect to broadcast ephemeris on nearly real time, consistent with the MPLs commitment described on [4].

Additionally, the SDD [4] requires that Notice Advisories for Galileo Users (NAGUs) should be published at least 48 hours before any planned event, and for unplanned events, with a delay of up to 30 hours. However, the latter limit has been violated at some instances such as on Advisory 2024025 of June 2024 where the information was published 63 hours after an unplanned HAS outage event.

7.3. Signal-In-Space error characterization

7.3.1. Orbit and clock errors computation

The orbit and clock errors are assessed by comparing the predicted orbit position and clock biases from HAS and OS, and comparing them to the one predicted by precise orbits and clock products.

Precise orbit and clock products (from now on Precise Products, PPs) are highly accurate post-processed estimates of the GNSS satellite clock biases and orbital positions based on a large set of observations. In general, different types of precise products are available, each of them characterized by a certain latency and accuracy. Specifically, for this work the

Galileo HAS IDD accuracy summary. [28–34]

DATE	GNSS	Orbit [m] (95%)	Clock [m] (95%)	DATE	GNSS	Orbit [m] (95%)	Clock [m] (95%)
Jan-23	GPS	- [1]	- [1]	Jan-24	GPS	0.19	0.10
	Galileo	- [1]	- [1]		Galileo	0.14	0.06
Feb-23	GPS	0.16	0.10	Feb-24	GPS	016	0.10
	Galileo	0.20	0.08		Galileo	0.16	0.07
Mar-23	GPS	0.23	0.11	Mar-24	GPS	0.19	0.12
	Galileo	0.16	0.07		Galileo	0.17	0.08
Apr-23	GPS	≤ 0.21	0.10	Apr-24	GPS	0.17	0.09
	Galileo	0.17	0.07		Galileo	0.16	0.07
May-23	GPS	0.31	0.07	May-24	GPS	0.30	0.11
	Galileo	0.19	0.10		Galileo	0.18	0.07
Jun-23	GPS	≤ 0.21	0.10	Jun-24	GPS	0.16	0.09
	Galileo	0.15	0.07		Galileo	0.34[2]	0.08
Jul-23	GPS	0.31	0.10	Jul-24	GPS	0.16	0.09
	Galileo	0.16	0.10		Galileo	0.16	0.07
Aug-23	GPS	0.15	0.09	Aug-24	GPS	0.28	0.15
	Galileo	0.17	0.06		Galileo	0.17	0.07
Sep-23	GPS	≤ 0.19	≤ 0.10	Sep-24	GPS	0.16	0.09
	Galileo	0.15	0.06		Galileo	0.17	0.07
Oct-23	GPS	0.16	0.10	Oct-24	GPS	- [3]	- [3]
	Galileo	0.15	0.06		Galileo	- [3]	- [3]
Nov-23	GPS	0.15	0.09	Nov-24	GPS	- [3]	- [3]
	Galileo	0.15	0.07		Galileo	- [3]	- [3]
Dec-23	GPS	0.23	0.10	Dec-24	GPS	- [3]	- [3]
	Galileo	0.15	0.07		Galileo	- [3]	- [3]

[1] HAS entered service oficially on January 24th, 2023.
[2] Above the Minimum Performance Level according to Table 4.3.
[3] Quarterly report not available.

Table 7.3: Summary of Galileo HAS IDD orbit and clock RMS error according to available quarterly reports.

final PPs provided by IGS through the MGEX project [35, 36] are used as "ground truth" for the computation of the Signal-In-Space error provided by the broadcast ephemeris and HAS. These products are released with a latency of 12 to 19 days and offer an accuracy of 2.5 cm in orbit position and 75 ps of RMS clock error (with standard deviation of $\sigma_{clk,final} = 20$ ps).

Satellite orbit errors are defined as the deviation between the SV's Antenna Phase Center (APC) position (based on broadcast ephemeris or HAS), and that provided by the PPs. It

Summary of references used for orbit positions and clock biases. [6, 37, 38]

Source:	**PP**		**BRDC** (LNAV/INAV)		**HAS IDD**	
Type:	Orbit	Clocks	Orbit	Clocks	Orbit	Clocks
GPS	CoM[1]	C1W/C2W[2]	L1/L2[2]	C1P/C2P[2]	L1	C1C/C2P
Galileo	CoM[1]	C1C/C5Q[2]	E1/E5ab/E6[3]	C1C/C7Q[2]	E1	C1C/C5Q[2]

[1] Center of mass. [2] Ionospheric free combination. [3] Arithmetic mean of APC offsets.

Table 7.4: Summary of reference points for orbit positions and satellite clock biases for precise products (PP), HAS IDD and broadcast ephemeris (BRDC). LNAV for GPS and INAV for Galileo. Clocks references are based on the IGS RINEX 4.02 standard [6].

is important to note that while broadcast ephemeris, HAS and PP offer the orbit position in the same reference frame (ECEF), they refer to different points of the spacecraft. In particular: precise products refer to the center of mass [6]; broadcast ephemerids refer to the L1/L2 ionospheric free APC for GPS and the arithmetic mean of the APC position of E1, E2 and E6 [37] for Galileo; and HAS IDD refers to the L1/E1 single frequency APCs [24]. Table 7.4 summarizes the points to which each product is referring to. In this work, the LNAV (GPS) and INAV (Galileo) navigation messages will be used, as these are the ones supported by Galileo HAS [4].

Given a certain SV, and the orbital position $\mathbf{x}_{ECEF}$ based on either HAS IDD or broadcast ephemeris, the orbital positioning error with respect to precise products is computed as

$$\boldsymbol{\epsilon}_{orb}^{ECEF} = \mathbf{x}_{ECEF} - (\mathbf{x}_{ECEF}^{PP} + \mathbf{R}_{BF}^{ECEF}\boldsymbol{\Delta}_{APC}), \tag{7.2}$$

where $\mathbf{R}_{APC}^{ECEF}$ represents the time-dependent rotation matrix from body axes to ECEF [1], and Δ_{APC} is the antenna phase center position with respect to the center of mass. This value is provided by IGS through the corresponding IGS ANTEX file [6]. This error can be rotated to any other frame of reference. For instance, for the NTW frame defined on Figure 4.2: $\boldsymbol{\epsilon}_{orb}^{NTW} = \mathbf{R}_{ECEF}^{NTW}\boldsymbol{\epsilon}_{orb}^{ECEF}$.

Regarding the clocks, it is necessary to translate them to a common code combination using the appropriate differential code bias (DCB) products

$$\epsilon'_{clk} = \delta_{clk} - (\delta_{clk}^{PP} + B). \tag{7.3}$$

where the actual value of B depends on the constellation and source used for the error computation (BRDC, HAS IDD), as it is associated to each code signal combination.

Group delays B for SISRE monitoring using CAS DCB products.

System	GPS	Galileo
PP	-	-
BRDC	-	$-\frac{f_{E5a}^2}{f_{E1}^2-f_{E5a}^2}DCB_{C1C-C5Q}+\frac{f_{E5b}^2}{f_{E1}^2-f_{E5b}^2}DCB_{C1C-C7Q}$
HAS IDD	$\frac{f_{L1}^2}{f_{L1}^2-f_{L2}^2}DCB_{C1C-C1W}$	-

Table 7.5: Group delays B for SISRE monitoring using CAS DCB products. f_i corresponds to the frequency of signal i for the associated GNSS.

Table 7.5 shows the applied clock offsets for each clock. A detailed discussion on how to obtain the specific values of B is provided on Appendix A.

It is important to note that due to different time synchronization between PP, HAS and BRDC for each constellation (i.e. GST for HAS and Galileo-BRDC, IGS Time Reference for PP and GPS System Time for GPS-BRDC), it is necessary to remove the epoch-wise mean for each constellation. In the positioning solution, this bias is absorbed by the receiver's clock bias.

7.3.2. SISRE computation

Once SIS errors are characterized, it is necessary to define a measure of how these errors are projected onto the ranging domain. This leads to the definition of the Signal-In-Space Range Error (SISRE). In the literature there are different variants of SISRE. For this work, it is proposed to apply the definition of Instantaneous User Projection SISRE, $SISRE_{IUP}$, provided by [1]. For this purpose, a grid of equally-spaced users are placed on the surface of the Earth. Then, for each instant and each satellite i of constellation j, the users that see the satellite with an elevation angle $\geq 10°$ are selected. For each of these users k, the line-of-sight (LOS) vector $\mathbf{e}_k^{ij}$ is computed in ECEF based on the user's and the SV's locations $\mathbf{x}_k^{ECEF}$ and $\mathbf{x}_{ij}^{ECEF}$, respectively.

$$\mathbf{e}_k^{ij} = \frac{\mathbf{x}_k^{ECEF} - \mathbf{x}_{ij}^{ECEF}}{|\mathbf{x}_k^{ECEF} - \mathbf{x}_{ij}^{ECEF}|}. \tag{7.4}$$

Then, the SISRE is obtained as the projection onto the LOS vector of the orbit and clock errors

$$SISRE_{IUP,k}^{ij} = \left(\mathbf{e}_k^{ij}\right)^T \boldsymbol{\epsilon}_{orb}^{ECEF} - \epsilon_{clk}^{ij}. \tag{7.5}$$

Note that, since clock errors affect equally all range measurements for a given satellite,

they are subtracted after the projection. Figure 7.4 shows an schematic representation of $SISRE_{IUP}$ setup. The grid size is limited to 520 users, mainly due to data handling limitations. With about 200 users in view for each time instant, this means roughly 36 million data points per day assuming a time step of 30 seconds. When extending the time window for a whole year, this already requires careful handling of the whole data set.

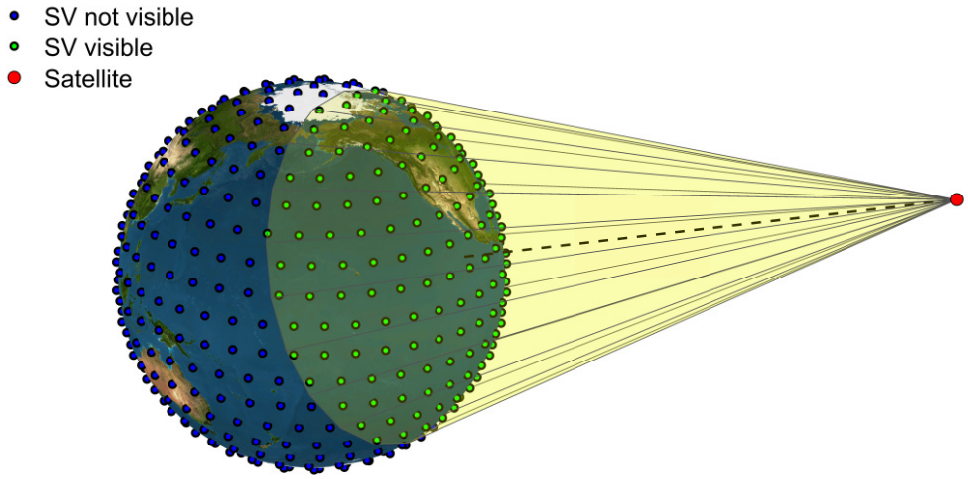

Figure 7.4: Schematic representation of Instantaneous User Projection SISRE.

While there are other definitions, such as the globally-averaged SISRE [37], $SISRE_{IUP}$ follows a unimodal, symmetric distribution, which is interesting for computing gaussiand bounds for the error as discussed on Section 3.2.3. However, it is important to note that while this approach greatly increases the number of samples, these are not truly independent. [1].

7.3.3. Orbit and clock errors characterization

In this section, the obtained orbit and clock errors are analyzed for HAS and OS of GPS and Galileo constellation. In particular, these errors are estimated by comparing the orbit positions and clock biases obtained using the broadcast navigation message and HAS IDD with the orbit and clock biases provided by CODE precise products.

Each orbit position estimation (PP, HAS and OS) is referred to a difference reference point of the SV. As a consequence, it is necessary to use the appropriate phase center offset (PCO) values (rotated to ECEF) in order to refer everything to the same point. For this analysis, everything was moved to the reference point used by the broadcast ephemeris, that is listed on Table 7.4. IGS ANTEX files [6] are used as source of the APO of each SV.

The APC info contained in the file `igs20.atx` was used for all cases. However, during the

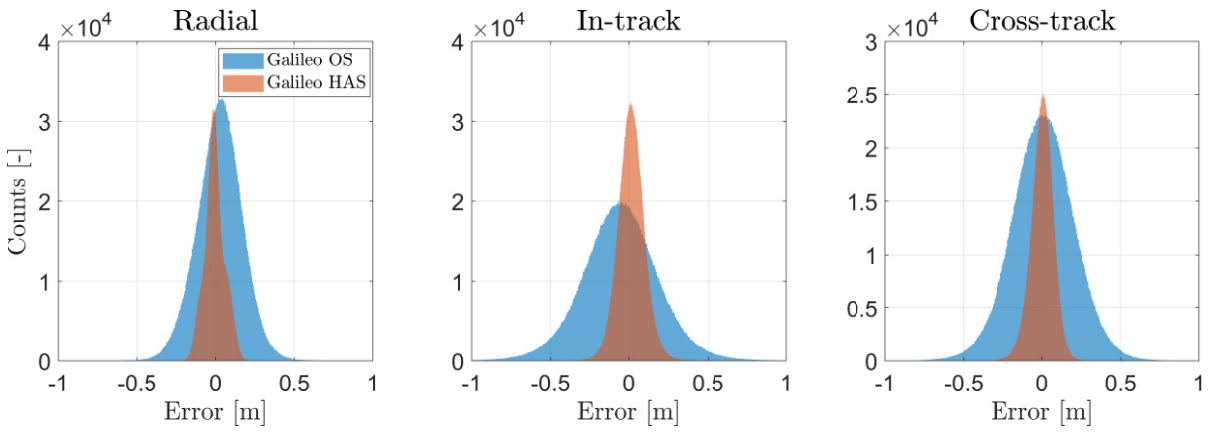

Figure 7.5: Galileo orbit errors for broadcast ephemeris (OS) and HAS IDD for 337 days between January 8th and December 14th of 2024.

processing it was noticed that GPS satellites exhibited a slight bias on the radial direction for the HAS-corrected orbital position. This bias dissapears when using the APC reported in `igs14.atx`. It seems that for GPS satellites, the HADG is using the APC described on `igs14.atx` as the reference for computing the corrections.

A total of 337 days were analysed, spanning from January 8th to December 14th of 2024. The period between DoY 16 and DoY 24 is excluded due to the lack of HAS IDD corrections. Figures 7.6 and 7.5 show the orbit error distribution for each constellation for HAS IDD and OS. It is clear that HAS brings a substantial improvement to the orbital errors of both constellations, leading to errors in the order of a few decimeters for all three components. In particular, the radial component achieves accuracy below 2 decimeters for both constellations. As expected, the largest improvement is provided in the cross-track and in-track components, specially for GPS. However, these components have the least impact on the ranging accuracy when projected on the line of sight vector.

Figure 7.7 shows the clock error distributions for GPS and Galileo. There is a noticeable improvement in performance with respect to OS. The achieved accuracy in orbit and clock determination of Galileo SVs was below 3 dm, while for GPS a smaller improvements are achieved.

Figures 7.8 and 7.9 show the average value and 2σ range for each satellite vehicle. In the orbit error domain, it is clear how HAS manages to lower the orbit error and remove any observed bias from the broadcast ephemeris. This leads to decimeter-level accuracy in terms of satellite positioning both for GPS and Galileo. Additionally, GPS satellites from Block III-A appear to suffer from larger errors in the radial component. Orbit errors for OS are consistent with those of [1, 39], while those for HAS are consistent with the ones

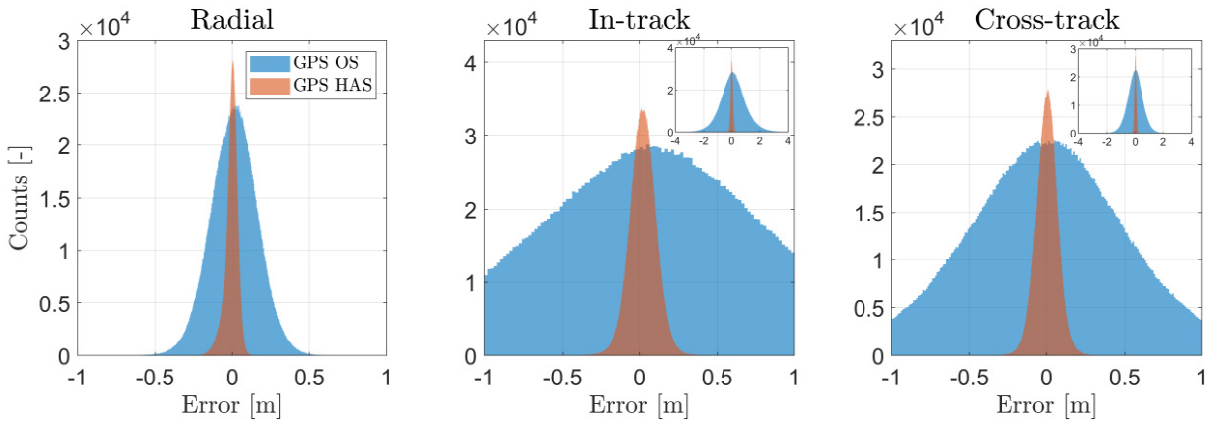

Figure 7.6: GPS orbit errors for broadcast ephemeris (OS) and HAS IDD for 337 days between January 8th and December 14th of 2024.

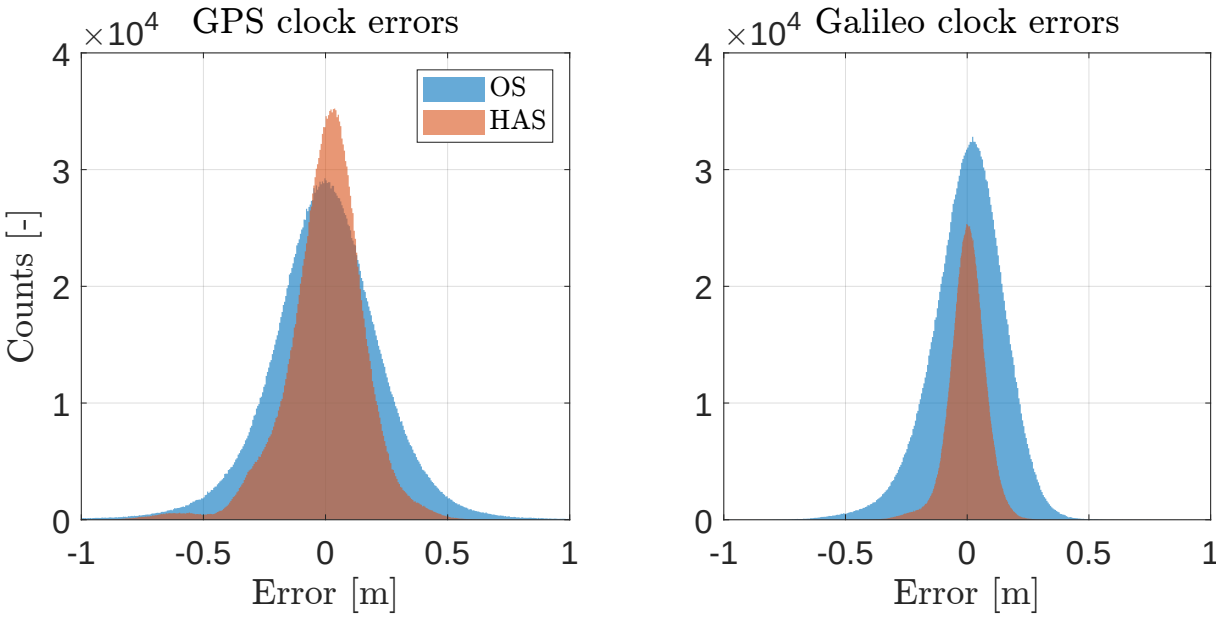

Figure 7.7: GPS and Galileo clock errors for broadcast ephemeris (OS) and HAS IDD for 337 days between January 8th and December 14th of 2024.

provided by [40–42].

A small bias is present in the radial direction of Galileo satellites for both HAS and OS cases . The reference for the broadcast is taken as the arithmetic mean of E1, E5 and E6 signals as stated on Table 7.4. The source of this information comes from [37] back on 2017 and this might have changed during these years, leading to slight bias for each SV. However, these biases are below 0.1 meters for all cases (see Table 7.6), so its effect may be neglected when compared to other error sources when processing real measurements.

Focusing now on the Galileo clocks of Figure 7.8, overall HAS IDD manages to provide a noticeable improvement with respect to broadcast. However, slight biases are found for satellites from the IOV block but in those cases HAS manages to reduce the bias that was provided by OS. Table 7.6 presents a summary of the SISE errors found for the Galileo constellation using HAS IDD.

GPS clocks on Figure 7.9 show noticeable biases of GPS clock errors for HAS on different satellites. G28 (SVN 44) is showing a specially large bias in the order of 0.5 m, but it is worth noting that this satellite was decommissioned on December 14th, 2024. In an attempt to fully characterize the source of these biases, Figure 7.10a shows the histogram of the clock errors for GPS satellites. PRN 6, 8, 12, 19, 21, 28, 29 and 32 exhibit a bimodal distribution of errors with two clearly differentiated peaks. By analyzing the time evolution of the error for these SVs, it was found that at some point on August 2024 there was a shift in the bias. Figure 7.10b shows the clock error histogram from September to December, where only one peak is found that corresponds to the new offset.

Currently, there is no official source that states the references that the HADG uses for Galileo HAS IDD while producing the clock and orbit corrections of GPS satellites. In this work, those listed on Table 7.4 are assumed, but to the knowledge of the author of this work, no previous published research has addressed the clock errors for GPS satellites using HAS neither in a SV per SV fashion nor for a long period of time. Additionally, HAS is a system in a rather early stage of development and these changes may be expected as the system evolves towards phase 2. As a consequence, it is assumed that during August 2024 there has been a shift in the reference for those SV in the HADG, which is then translated into a bias on the errors. However, this only explains the bimodality of the distribution but not the noticeable bias that is observed after removing the first half of 2024.

Note that for successfully comparing the precise products with the HAS-corrected GPS measurements, it is necessary to use the differential clock bias $DCB_{C2W-C2P}$ (according to RINEX4 format), which is not provided by the CAS products. For this work this bias

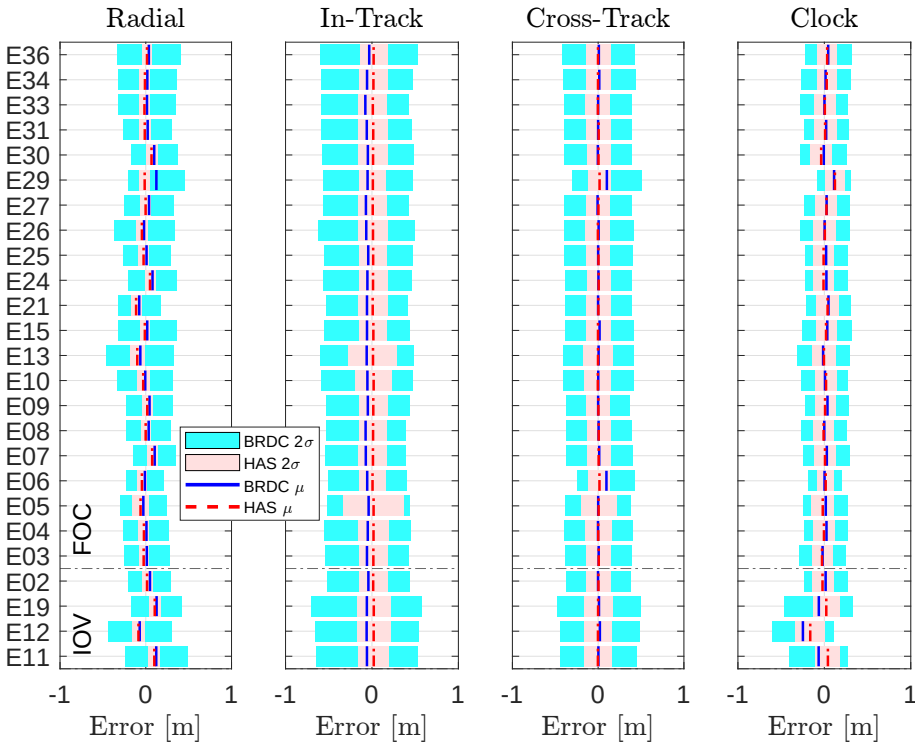

Figure 7.8: SISE error per satellite vehicle for Galileo constellation, organized per blocks. Both the 2σ interval and the mean values are shown for OS and HAS IDD.

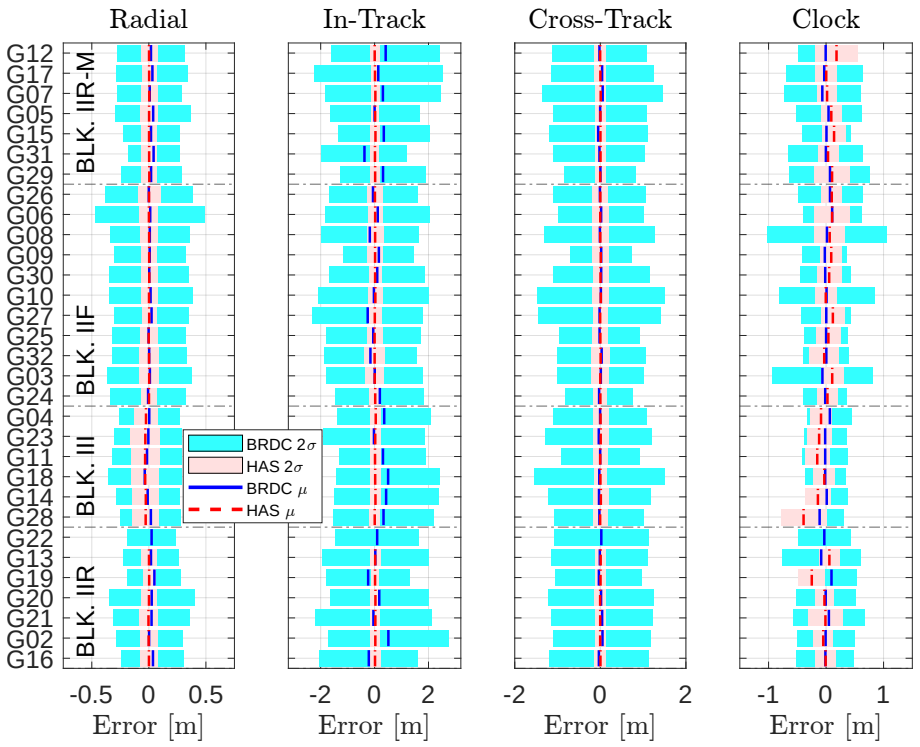

Figure 7.9: SISE error per satellite vehicle for GPS constellation, organized per blocks. Both the 2σ interval and the mean values are shown for OS and HAS IDD.

has been neglected, following the same approach as [43]. This step might be introducing a small additional offset for some satellites that is only seen when comparing HAS orbits and clocks with precise products.

Additionally, for the GPS orbits it was found that probably the reference of the APC was not aligned with that of the latest ANTEX file published by IGS, but a previous one. A similar effect might be taking place here. Note that the broadcast clock error distributions are practically unbiased for all SV which was also observed by other works [1, 39]. This further supports the idea that HAS-corrected clocks should show nominally a bias at most equal to that of the broadcast.

As a consequence, it is proposed to assume that the observed bias in the HAS-corrected GPS clocks is due to a misalignment in the references used between the precise products and Galileo HAS. In this case, the final user would not be able to "see" this bias, as long as the appropriate pseudorange observations are used (L1+L2C, [4]). As a consequence, when overbounding the SISRE distributions for estimating the values of σ_{URE}^{HAS} this bias will be removed from clock errors.

Tables 7.7 and 7.8 show the summary of the SISE error characteristics for GPS when using HAS IDD. This analysis is split in two due to the observed change of reference on August 2024. It is clear that there is a non-negligible bias on the SV that showed the bimodal behavior of Figure 7.10. Additionally, by comparing the mean clock errors between both periods the shift on August 2024 becomes clear.

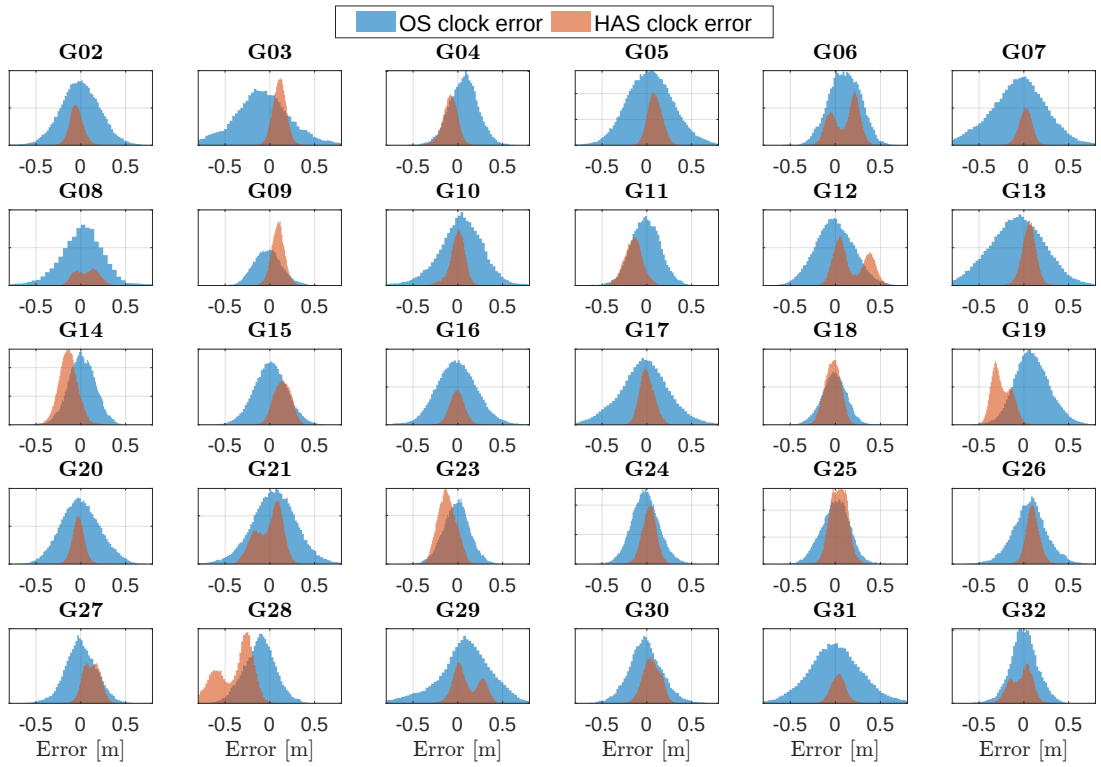

(a)

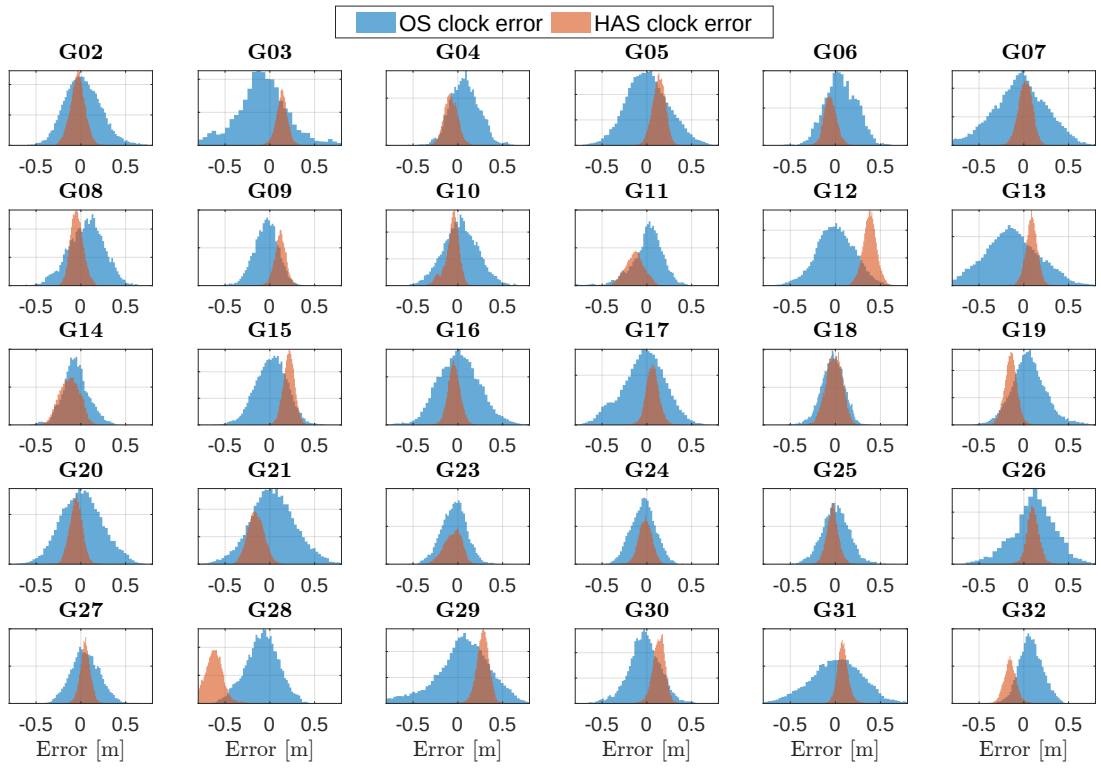

(b)

Figure 7.10: Clock error histogram for GPS constellation from January to December, 2024 (a) and from September to December, 2024 (b).

Galileo SISE summary

Block	PRN	Radial		In-Track		Cross-Track		Clock	
		μ	σ	μ	σ	μ	σ	μ	σ
IOV	E11	9.95	3.33	2.07	8.89	-0.31	7.88	4.13	7.09
	E12	-8.55	3.53	1.97	9.55	-0.24	8.11	-16.32	8.44
	E19	10.45	3.49	2.09	9.74	-0.08	8.43	2.25	7.63
FOC	E02	1.47	3.07	1.41	8.30	0.32	7.05	-2.11	6.11
	E03	-2.46	2.80	1.62	8.29	0.67	7.02	-2.68	5.85
	E04	-2.14	3.19	1.79	8.78	0.13	7.63	-0.44	6.22
	E05	-6.11	4.68	1.88	17.42	0.51	10.39	-1.83	6.63
	E06	-4.49	2.64	0.65	7.58	1.53	6.18	1.55	4.85
	E07	7.44	2.96	1.14	8.17	0.59	6.81	0.76	6.24
	E08	-0.11	2.76	1.28	7.86	0.62	6.85	-0.85	5.95
	E09	1.73	3.01	1.53	8.11	0.29	6.97	0.85	6.05
	E10	-3.00	3.65	1.94	10.67	-0.38	7.86	1.97	6.21
	E13	-9.92	4.19	1.19	14.09	-0.17	8.56	-0.47	6.92
	E15	-1.09	2.91	1.62	8.06	-0.18	7.01	1.96	5.80
	E21	-11.27	3.09	0.87	8.54	0.27	7.05	3.76	6.48
	E24	4.94	3.00	1.22	8.24	0.58	6.90	-0.95	5.85
	E25	-2.56	2.96	1.36	7.99	0.36	6.88	-0.85	5.79
	E26	-4.51	3.31	1.17	8.50	-0.32	7.11	0.55	6.41
	E27	-0.19	3.06	0.89	8.23	0.33	6.93	2.48	6.33
	E29	-1.28	3.12	1.03	7.56	1.65	6.43	12.25	5.60
	E30	6.69	3.28	1.24	8.58	0.40	6.92	-3.67	6.34
	E31	-1.16	3.22	1.46	8.44	0.60	7.21	0.88	6.38
	E33	-1.54	3.01	0.99	8.26	-0.30	7.11	0.55	6.16
	E34	-0.97	2.94	1.69	8.28	-0.17	7.11	2.75	5.59
	E36	1.42	2.82	1.92	7.91	-0.17	7.11	3.28	5.70

Table 7.6: Galileo HAS IDD SISE mean (μ) and standard deviation (σ) summary from January to December of 2024. All measurements are in cm.

GPS SISE summary 01/2024 - 08/2024

Block	PRN	Radial		In-Track		Cross-Track		Clock	
		μ	σ	μ	σ	μ	σ	μ	σ
IIR	G02	-0.17	3.58	3.21	9.20	-0.07	6.54	-5.51	7.64
	G13	0.11	3.96	1.99	10.83	-0.51	5.99	4.20	9.03
	G16	0.19	3.72	1.83	9.48	0.13	6.55	0.67	8.97
	G19	0.25	2.79	1.94	7.02	0.65	6.65	-29.01	9.64
	G20	0.15	3.28	2.84	8.71	-0.78	7.22	-1.76	7.20
	G21	-0.20	3.86	3.03	9.32	0.04	6.59	4.54	12.29
III	G04	-2.75	5.41	6.03	9.80	-2.99	8.06	-9.23	9.43
	G11	-3.27	6.13	0.61	9.67	1.11	8.35	-16.05	10.43
	G14	-2.55	5.27	2.66	9.62	2.34	9.38	-14.74	10.75
	G18	-3.22	6.01	0.77	9.57	1.37	7.61	-3.64	8.89
	G23	-3.02	6.05	2.69	9.16	-0.86	8.55	-14.67	9.39
	G28	-2.63	5.70	2.00	9.71	-1.74	8.39	-29.73	13.45
IIF	G03	0.36	4.64	0.27	19.88	1.16	10.38	9.57	10.21
	G06	0.08	4.38	2.17	14.86	2.00	9.65	17.27	12.46
	G08	0.37	4.41	1.80	17.61	-0.48	10.56	11.32	12.36
	G09	0.29	3.81	1.91	15.82	0.42	10.28	7.95	9.03
	G10	0.11	3.97	2.70	15.13	2.66	9.38	2.20	8.23
	G24	0.06	3.62	2.74	11.30	-1.20	7.90	4.19	8.38
	G25	-0.22	4.05	0.49	15.97	-1.17	9.38	7.36	10.21
	G26	0.05	3.12	1.90	9.39	-1.38	7.92	9.75	8.18
	G27	0.27	2.91	1.14	9.23	-0.68	8.84	15.14	9.03
	G30	0.47	3.57	2.05	12.89	-1.23	9.09	2.12	9.40
IIR-M	G32	0.15	4.79	0.04	21.39	0.38	11.73	1.40	11.23
	G05	0.28	3.77	1.92	7.71	-0.44	6.28	7.23	8.53
	G07	0.47	3.42	3.10	8.40	0.35	6.41	1.78	7.71
	G12	0.19	3.34	0.67	8.77	-0.29	6.70	9.78	14.32
	G15	0.12	3.59	2.91	9.45	-0.21	6.31	10.85	9.27
	G17	0.15	3.18	1.71	7.30	0.59	6.71	-2.09	8.12
	G29	0.35	3.60	1.94	8.68	-0.51	5.84	2.73	10.79
	G31	0.26	3.34	2.33	7.84	0.52	6.60	1.33	8.92

Table 7.7: GPS HAS IDD SISE mean (μ) and standard deviation (σ) summary from January to August of 2024. All measurements are in cm.

GPS SISE summary 09/2024 - 12/2024

Block	PRN	Radial		In-Track		Cross-Track		Clock	
		μ	σ	μ	σ	μ	σ	μ	σ
IIR	G02	-0.16	4.19	1.48	8.51	-1.06	5.68	-3.56	10.08
	G13	0.18	2.38	2.77	6.61	3.08	4.90	8.63	8.28
	G16	-0.15	3.81	1.22	9.75	0.66	6.28	-4.30	7.67
	G19	0.34	2.74	1.32	8.27	-0.02	5.68	-14.61	8.15
	G20	0.03	3.75	3.68	7.65	0.42	5.89	-5.48	8.77
	G21	-0.60	4.54	2.31	9.08	-1.17	5.68	-15.58	10.86
III	G4	-1.90	4.05	0.01	7.88	8.50	6.55	-7.73	8.30
	G11	-3.23	6.38	4.11	9.80	-3.26	6.85	-13.61	11.08
	G14	-2.92	7.20	4.40	10.64	-1.86	7.72	-12.80	11.47
	G18	-3.26	6.11	5.79	9.75	-2.71	6.28	-1.49	10.15
	G23	-3.18	7.08	1.60	9.78	4.98	8.04	-5.65	10.25
	G28	-3.19	6.08	-3.14	9.94	2.86	7.21	-62.73	11.28
IIF	G03	0.17	3.12	1.06	8.68	-2.85	8.57	13.28	7.70
	G06	0.03	3.58	2.10	8.40	-5.23	8.45	-5.63	8.01
	G08	0.01	2.64	2.34	7.99	0.57	6.49	-4.38	7.96
	G09	0.33	2.34	1.71	8.79	2.47	6.45	11.48	9.30
	G10	0.23	2.83	3.04	7.89	-2.46	8.55	-6.56	8.44
	G24	0.26	3.00	1.27	9.14	3.23	7.38	-1.92	9.07
	G25	0.01	3.07	-0.80	8.98	2.75	7.74	-3.15	7.60
	G26	0.48	7.79	-0.53	23.24	3.65	11.54	10.21	11.32
	G27	0.37	3.56	0.05	16.95	0.32	7.62	4.78	8.46
	G30	0.10	3.76	1.77	8.93	4.38	6.93	13.27	9.40
IIR-M	G32	0.24	2.22	0.50	7.18	1.47	6.64	-15.37	8.27
	G05	0.11	3.85	2.38	6.62	1.63	5.67	13.36	8.70
	G07	0.08	3.77	2.37	7.54	1.91	5.30	1.61	9.89
	G12	0.13	4.05	-0.21	9.13	-0.64	6.13	38.18	8.47
	G15	0.37	2.40	3.91	7.01	1.32	5.34	21.18	8.22
	G17	0.55	3.23	1.10	6.92	-0.99	5.50	6.31	10.07
	G29	0.51	3.14	2.28	7.78	0.28	6.13	27.77	8.38
	G31	0.29	3.30	-0.72	8.57	0.23	5.73	8.39	7.30

Table 7.8: GPS HAS IDD SISE mean (μ) and standard deviation (σ) summary from September to December of 2024. All measurements are in cm.

7.3.4. SISRE characterization

Once the SISE error is characterized, it is interesting to study the effect of these errors in the ranging domain (i.e. the projection of these errors that is translated into errors for the pseudorange measurements), which is known as the Signal-In-Space Range Error (SISRE). This is computed following the approach described on Section 7.3.2. A total of 520 equally-spaced users is used for the computation with an elevation mask of 10°.

Moreover, the HAS Service Area, described on [4] is taken into account for the computation of the SISRE for HAS. However, no noticeable differences have been found with respect to using the whole set of users. Figure 7.11 shows the user grid used for this computation. A time step of 5 minutes is used, as lower time steps would yield unmanageable amounts of data points and also yield higher time correlation between measurements.

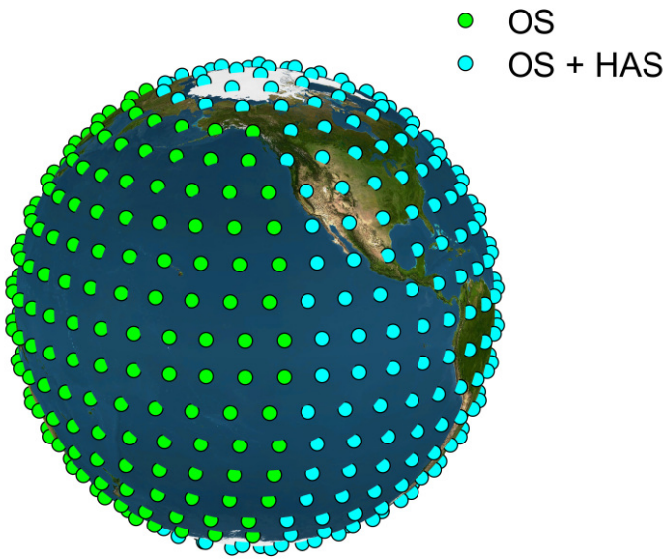

Figure 7.11: User grid used for SISRE computation for HAS only (green) and OS (green + blue).

The HAS IDD clock error biases observed in the previous section for GPS and Galileo SVs is removed by removing the temporal average of the clock errors in a SV per SV basis. Since we are only interested on characterizing the 99.5% bound URE for the HAS error distributions, the removal of the clock biases observed in the previous section would only have impact on the predicted biases for the continuity model, that are anyways not included in the baseline ARAIM algorithm. Additionally, as previously discussed, these biases are most likely linked to misalignment on the evaluation of the clock errors. As a consequence, would not affect the final users when computing the positioning solution.

Figure 7.12 shows the folded CDF of Galileo SISRE errors for OS and HAS IDD. Firstly,

the slight bias observed in the orbit radial direction for both Broadcast and HAS is reflected on both cases. Moreover, it is clear how HAS manages to improve the tails of the distribution, leading to errors below 1.5 meters with a probability of 99.99%.

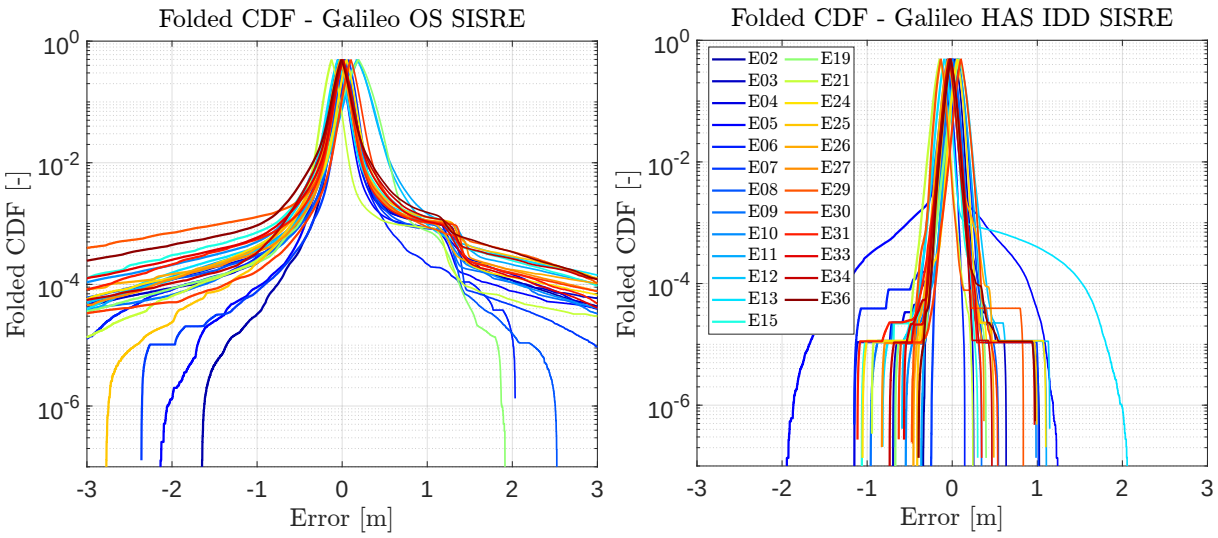

Figure 7.12: Folded CDF for Galileo SISRE using broadcast ephemeris (a) and Galileo HAS IDD (b).

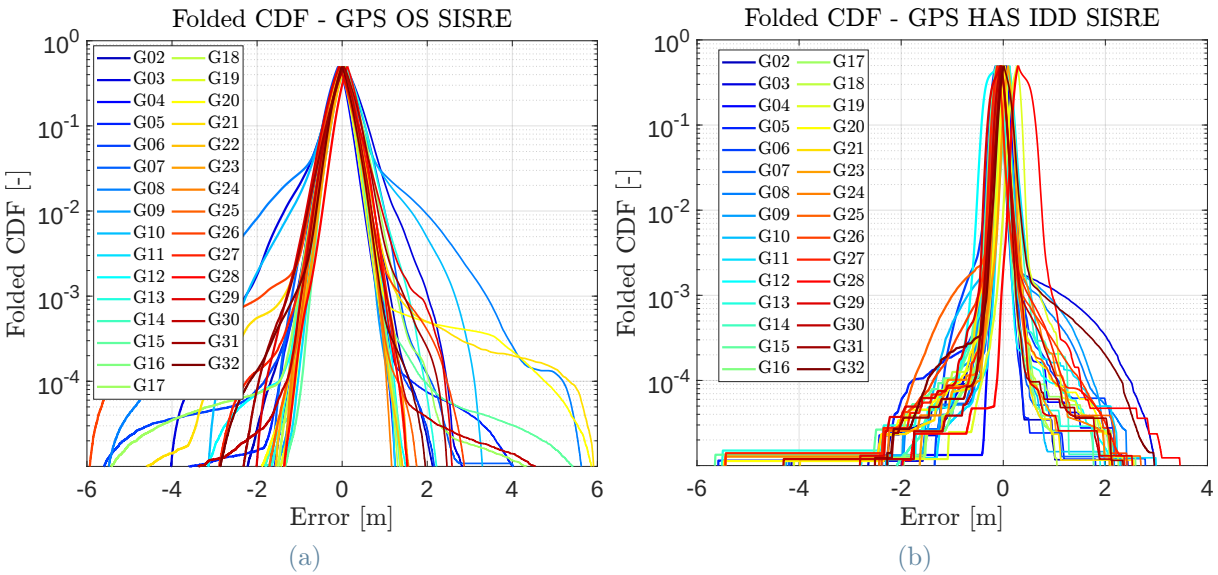

Figure 7.13: Folded CDF for GPS SISRE using broadcast ephemeris (a) and Galileo HAS IDD (b).

On the other hand, Figure 7.13 analyzes the folded GPS for the corrected and uncorrected cases. In this case, although the corrected errors are larger than those from Galileo, the

improvement in relative terms is larger, since maximum errors of almost 6 meters (99.99%) are reduced to less than 3 meters. A noticeable bias can be seen for some satellites. This is due to the observed bias on the clock errors from the previous section. According to Eq. (7.5), clock errors are directly translated into SISRE thus producing this offset.

8 | ARAIM-HAS performance

The objective of this chapter is to test the proposed methodology in a real flight scenario by processing data taken during a experimental flight campaign. This analysis aims to asses the performance of the integration of HAS within ARAIM and its viability on the current state of Galileo HAS.

In particular, two main cases are considered using different values for the accuracy and continuity models. On the one hand, the navigation solution is obtained using a continuity model for HAS based on the MPLs provided by [4], which is consistent with the current commitments of Galileo HAS. On the other hand, the continuity model derived from the SISRE analysis performed on Section 7.3.2.

Finally, it is also interesting to asess which is the dependency of the performance with the a priori constellation-wide fault probability of Galileo. This value is currently set to 10^{-4} mainly because of the recent commissioning of Galileo with respect to GPS. However, it is expected to lower as Galileo gain maturity and, as a consequence, the potential future performance of the proposed approach is assessed with a reduction of $P_{const,GAL}$.

8.1. Experimental setup

The real observation data used for this work was obtained from a measurement campaign performed by the German Aerospace Center (DLR) on the vicinity of Braunschweig-Wolfsburg airport, in Germany. A Dornier 228 aircraft, equipped with a JAVAD Delta receiver and a Trimble AV39 receiver antenna is used during the campaign. Figure 8.1 shows a picture of the aircraft and receiver used.

Measurements of L1/L2 and E1/E5a ionospheric free combination are used, taken with a frequency of 5 Hz during a total time span of 96 minutes, starting at 12:30 pm (GPS time) on the 12th of November, 2024. According to Table 7.4, Galileo INAV navigation message refers to the E1/E5b combination. However, since E5b measurements were not recorded, the corresponding DCB from CAS is used to translate the clock biases to the appropriate code combination.

(a) (b)

Figure 8.1: DLR's Dornier 228 aircraft and JAVAD Delta receiver used during the flight measurement campaign.

Measurements of each signal (L1, L2, E1, E5a) are carrier smoothed using a Hatch filter with a window of $T_{smooth} = 100$ s and the ionospheric free linear combinations are produced for each visible SV at each epoch. An elevation mask of 5° is implemented, together with a $T_{recovery}$ of 300 seconds.

A post processed ground truth solution is used that allows for the estimation of the positioning error. This solution is computed using GrafNav 9.00.2207, by combining measurements from two master antennas with IDs LEIJ00DEU and PTBB using differential GNSS techniques and precise products.

Three positioning soltuions are computed based on the OS broadcast navigation message, HAS and CODE precise porducts. For computing the positioning solution in each of the cases (PP, OS and HAS), the algorithms described in Appendix B are implemented.

This process provides a set of ECEF coordinates for each measurement epoch, that can then be used to compute the real positioning error provided by each approach.

Figure 8.2 shows recorded aircraft trajectory. The dataset covers from push-back at the gate until the aircraft arrives back to the same airport. Additionally, both reference stations used for the differential GNSS solution are shown in the map.

8.2. Integrity and continuity error models

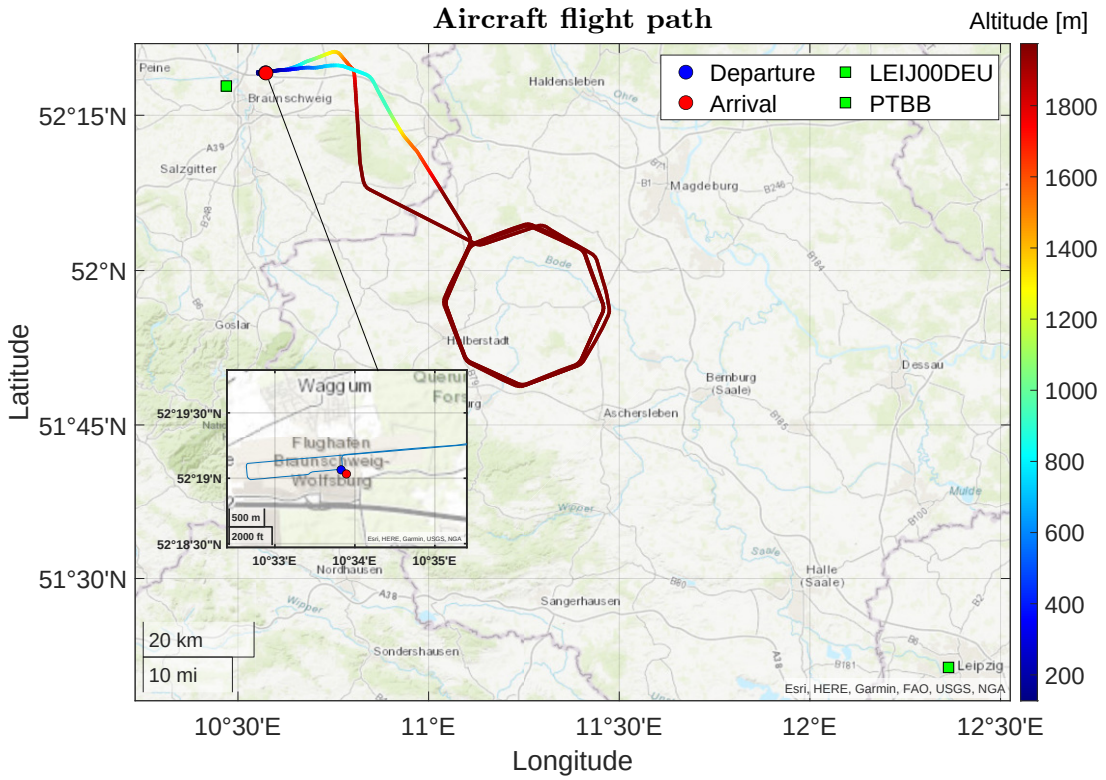

Figure 8.2: Flight path and reference stations corresponding to the flight measurement campaign.

8.2.1. SISRE-based OS integrity and HAS continuity models

Since ISM messages are at the moment of writing of this thesis not transmitted by neither GPS nor Galileo, in order to perform a more realistic evaluation of the proposed ARAIM-HAS algorithm, a set of possible ISM parameters has been derived by analyzing the SISRE from Chapter 7.

In order to obtain the appropriate values of URE and URA, a bounding Gaussian distribution is generated for 99.99999% (URA) and 95% (URE) of the probability masses.

Figures 8.3 and 8.4 show the computed overbounding distribution for the observed SISRE for integrity purposes. This overbound covers the CDF of the ranging error at least down to probabilities of 1E-7. It can be seen that for all cases, the obtained solution satisfies the imposed integrity requirement.

Figures 8.5 and 8.6 show the computed bounding distributions for SISRE of HAS (down to 95%) for GPS and Galileo constellation. The SISRE observed on Section 7.3.4 exhibited a bias for HAS, which can be directly linked with the clock biases observed during the Signal-In-Space error analysis. This bias is assumed to come from misalignment between

precise products and HAS and will be ignored when computing the integrity and continuity models (as the final user is assumed to not "see" them).

The URE and URA values for each case of each SVs are collected on Table 8.1. It can be seen that, compared to the reference value of $\sigma_{URE} = 2/3\sigma_{URA}$, there is a noticeable improvement of almost one meter in the continuity model when using Galileo HAS. The values of σ_{URA} obtained are found to be consistent with those provided by [1] for the single Gaussian overbound.

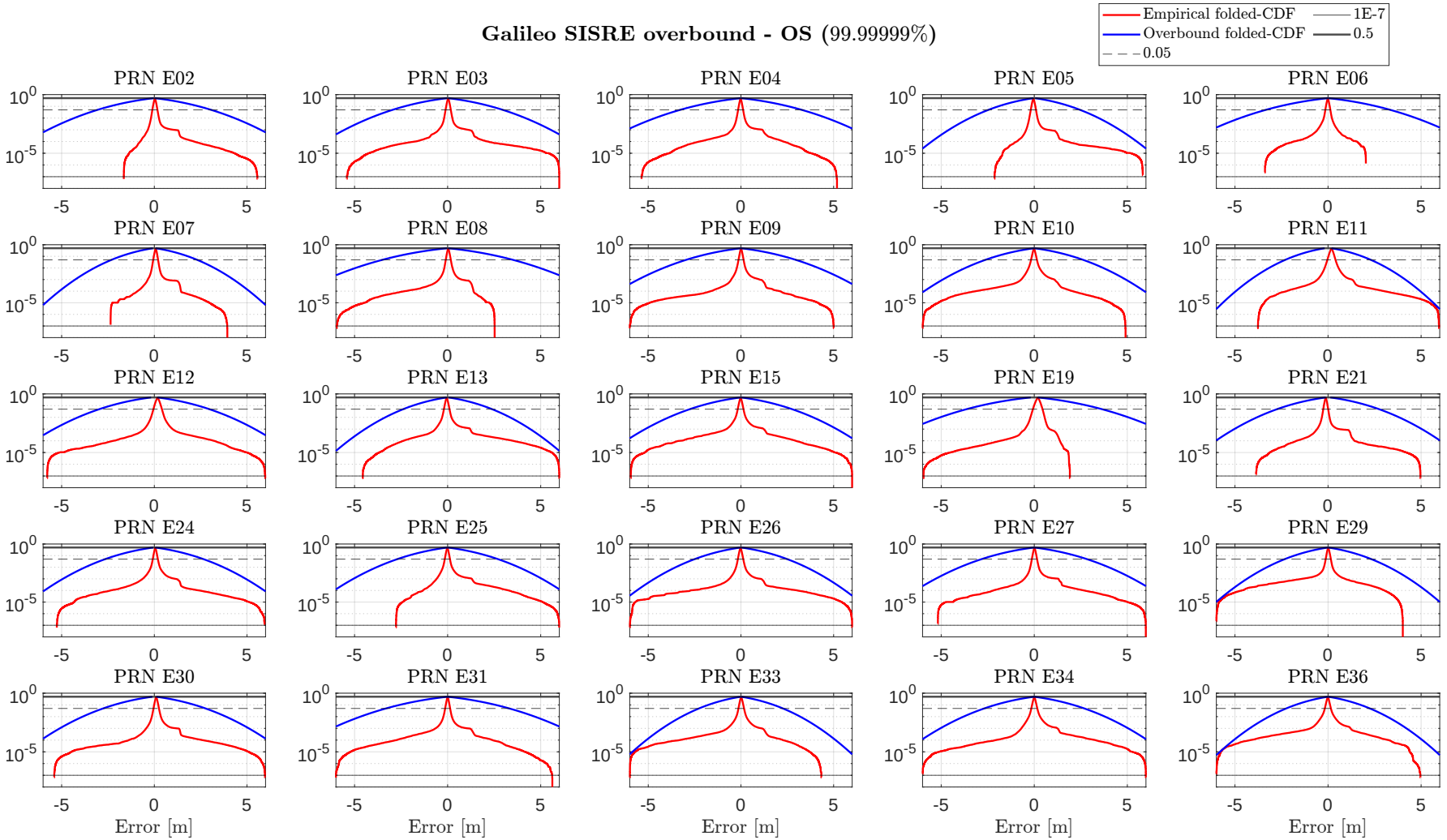

Figure 8.3: Overbound of Galileo OS SISRE distributions for 99.9999% of the probability mass.

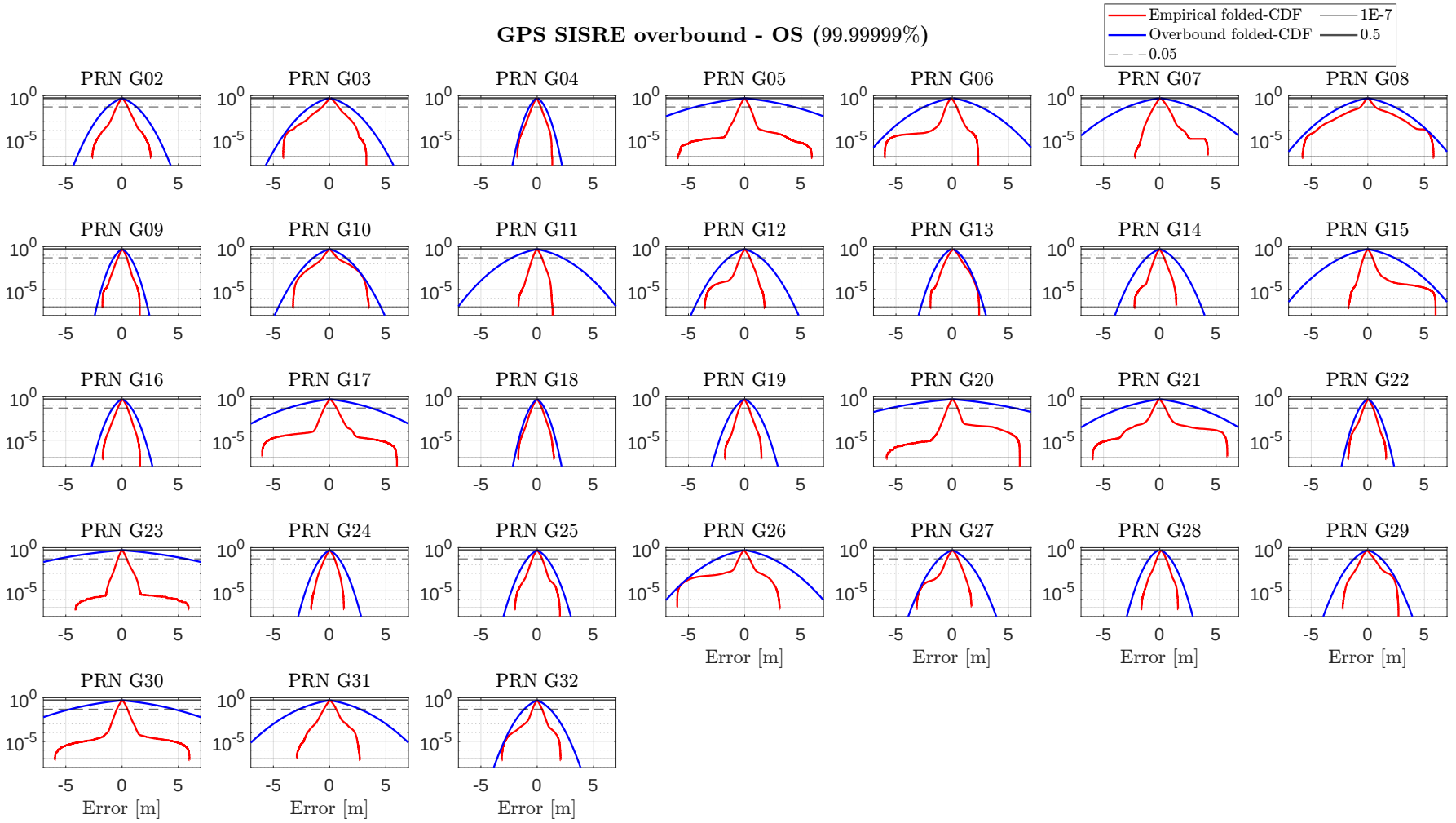

Figure 8.4: Overbound of GPS OS SISRE distributions for 99.9999% of the probability mass.

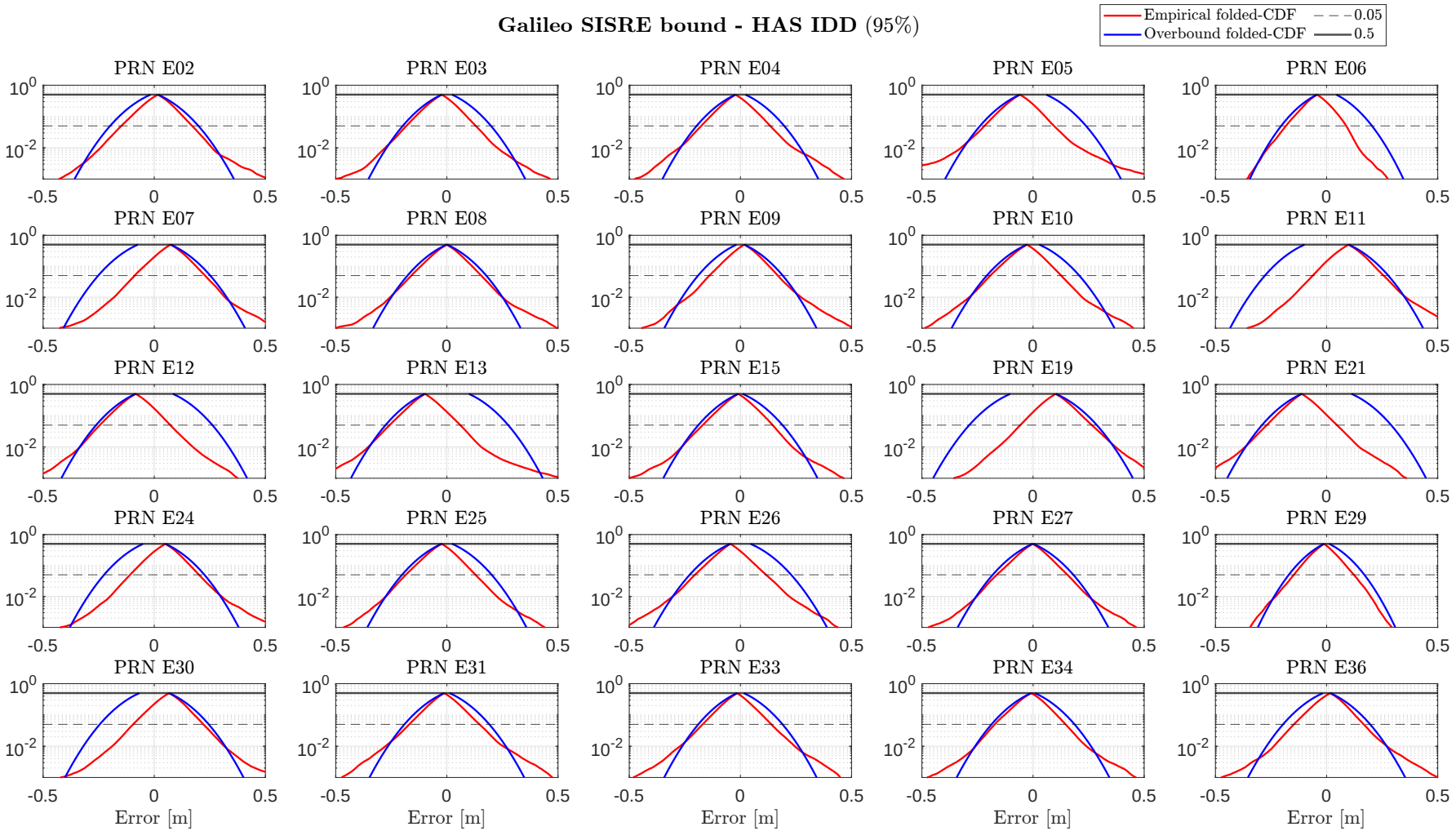

Figure 8.5: Bound of Galileo HAS IDD SISRE distributions for 95% of the probability mass.

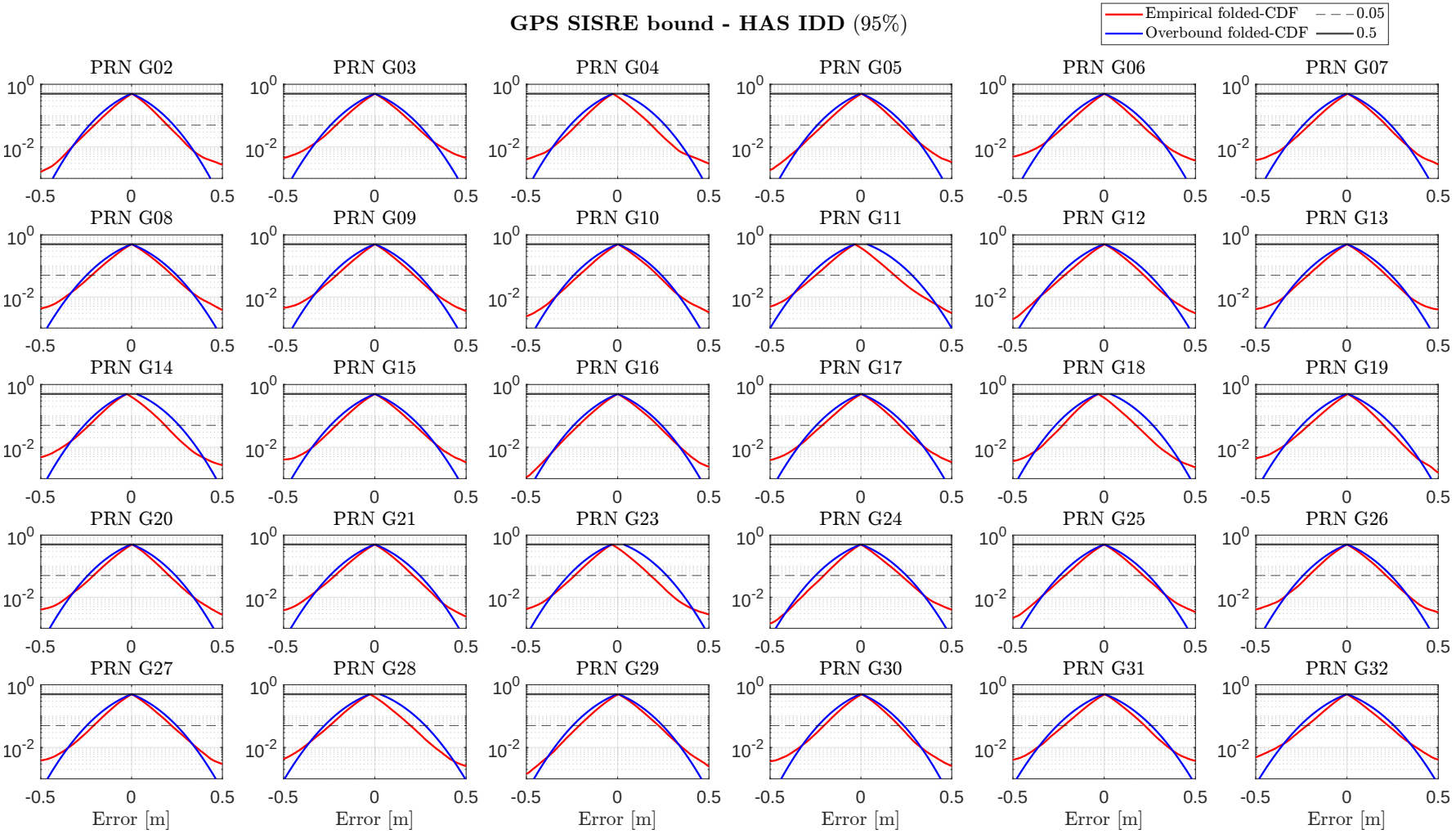

Figure 8.6: Bound of Galileo HAS IDD SISRE distributions for 95% of the probability mass.

URE and URA values obtained after SISRE assesment.

(a) GPS

PRN	σ^{ob}_{URA} [m]	$\sigma^{ob}_{URE,HAS}$ [m]
G02	0.768	0.140
G03	0.997	0.147
G04	0.383	0.142
G05	2.654	0.144
G06	1.460	0.145
G07	1.715	0.143
G08	1.412	0.151
G09	0.427	0.146
G10	0.870	0.145
G11	1.353	0.151
G12	0.851	0.150
G13	0.517	0.147
G14	0.707	0.142
G15	1.413	0.148
G16	0.473	0.146
G17	2.198	0.148
G18	0.384	0.142
G19	0.516	0.148
G20	3.305	0.145
G21	2.031	0.149
G22	0.405	- [1]
G23	3.452	0.144
G24	0.496	0.151
G25	0.533	0.148
G26	1.444	0.146
G27	0.694	0.150
G28	0.500	0.151
G29	0.690	0.147
G30	2.765	0.141
G31	1.602	0.154
G32	0.686	0.155

(b) Galileo

PRN	σ^{ob}_{URA} [m]	$\sigma^{ob}_{URE,HAS}$ [m]
E02	1.845	0.111
E03	1.782	0.107
E04	1.984	0.106
E05	1.468	0.109
E06	2.026	0.098
E07	1.358	0.108
E08	2.111	0.107
E09	1.792	0.105
E10	1.586	0.110
E11	1.282	0.109
E12	1.696	0.108
E13	1.419	0.108
E15	1.665	0.109
E19	2.092	0.112
E21	1.589	0.109
E24	1.579	0.107
E25	1.635	0.108
E26	1.504	0.111
E27	1.714	0.109
E29	1.407	0.096
E30	1.617	0.108
E31	2.013	0.109
E33	1.370	0.106
E34	1.633	0.109
E36	1.360	0.109

[1] No HAS IDD corrections available for G22.

Table 8.1: Obtained URA (from OS) and URE (from HAS IDD) estimations based the observed SISRE distributions for GPS and Galileo constellations.

8.2.2. MPLs-based HAS continuity model

The MPLs defined by HAS SDD and summarized on Table 4.3 represent the current commitments on HAS performance for the (constellation average) 3D orbit and clock error. For this purpose, it is proposed to derive a URE value for GPS and Galileo that is consistent with the commitments provided by HAS SDD.

Let us assume that the orbital errors in the radial, in-track and cross-track directions are identically independently distributed (i.i.d), following a zero-mean Gaussian distribution with variance $\sigma_{orb}^{HAS,MPL}$. Let $\boldsymbol{\epsilon}_{orb,i}^{j}$ be the orbit error of satellite i of constellation j. The RMS of the norms of the orbital errors for constellation j can be written as the sum of the squares of each component as

$$RMS_{orb,j} = \sqrt{\frac{1}{N_j}\sum_{i=1}^{i=N_j}\left(|\boldsymbol{\epsilon}_{orb,i}^{j}|^2\right)} = \sqrt{\frac{1}{N_j}\sum_{i=1}^{i=N_j}\left(\left(\epsilon_{N,i}^{j}\right)^2+\left(\epsilon_{T,i}^{j}\right)^2+\left(\epsilon_{W,i}^{j}\right)^2\right)} \tag{8.1}$$

where $\{N,T,W\}$ refers to the radial, in-track and cross-track components, respectively. It can be proven that, since $\epsilon_{N,i}^{j},\epsilon_{T,i}^{j},\epsilon_{W,i}^{j} \sim \mathcal{N}\left(0,\sigma_{orb,j}^{HAS,MPL}\right)$, each of the i terms inside the summation follow a chi-squared distribution of 3 degrees of freedom

$$\left(\epsilon_{N,i}^{j}\right)^2+\left(\epsilon_{T,i}^{j}\right)^2+\left(\epsilon_{W,i}^{j}\right)^2 \sim \chi_3^2\left(\sigma_{orb,j}^{HAS,MPL}\right)^2. \tag{8.2}$$

This distribution is equivalent to a gamma distribution with shape parameter 3/2 and scale parameter $2\left(\sigma_{orb,j}^{HAS,MPL}\right)^2$. Then, provided the additive and scaling properties of gamma distributions, the sum of the 3D errors from each of the SV of constellation j, multiplied by the $1/\left(N_j\right)$ factor is distributed as

$$X^j = \frac{1}{N_j}\sum_{i=1}^{i=N_j}\left(\left(\epsilon_{N,i}^{j}\right)^2+\left(\epsilon_{T,i}^{j}\right)^2+\left(\epsilon_{W,i}^{j}\right)^2\right) \sim \Gamma\left(\frac{3N_j}{2},\frac{2}{N_j}\left(\sigma_{orb,j}^{HAS,MPL}\right)^2\right). \tag{8.3}$$

Finally, the square root of X^j, $Y^j=\sqrt{X^j}$ follows a Nakagami distribution with shape parameter equal to that of the original distribution, $3N_j/2$, and scale parameter equal to the product of the shape and scale parameters of the gamma distribution, $3\left(\sigma_{orb,j}^{HAS,MPL}\right)^2$

$$Y^j = RMS_{orb,j} = \sqrt{X^j} \sim \text{Nakagami}\left(\frac{3N_j}{2},3\left(\sigma_{orb,j}^{HAS,MPL}\right)^2\right). \tag{8.4}$$

Let $F^j(y)$ be the CDF of the Nakagami distribution of Y^j. Then, it is possible to solve numerically for $\sigma_{orb,j}^{HAS,MPL}$ when imposing the 95th percentile condition

$$F^j(MPL_{orb}^j) = 0.95 \rightarrow \sigma_{orb,j}^{HAS,MPL}. \tag{8.5}$$

Following an analogous procedure, it is possible to prove that the RMS of the satellite clock errors, $RMS_{clk,j}$, also follows a Nakagami distribution

$$RMS_{clk,j} \sim \text{Nakagami}\left(\frac{N_j}{2}, \left(\sigma_{clk,j}^{HAS,MPL}\right)^2\right), \tag{8.6}$$

from which the value of $\sigma_{clk}^{HAS,MPL}$ can be obtained. As a consequence, the following orbit and clock errors are obtained

$$\begin{aligned} \sigma_{orb,GPS}^{HAS,MPL} &= 16.99 \text{ cm}, \quad \sigma_{orb,Galileo}^{HAS,MPL} = 10.20 \text{ cm}, \\ \sigma_{clk,GPS}^{HAS,MPL} &= 12.42 \text{ cm}, \quad \sigma_{clk,Galileo}^{HAS,MPL} = 9.77 \text{ cm}. \end{aligned}$$

Assuming that clock and orbit errors are uncorrelated, a URE model can be derived for GPS and Galileo based on the commitments of Galileo HAS as

$$\begin{aligned} \sigma_{URE,GPS}^{HAS,MPLs} &= \sqrt{\left(\sigma_{orb,GPS}^{HAS,MPL}\right)^2 + \left(\sigma_{clk,GPS}^{HAS,MPL}\right)^2} = 21.01 \text{ cm}, \\ \sigma_{URE,Galileo}^{HAS,MPLs} &= \sqrt{\left(\sigma_{orb,Galileo}^{HAS,MPL}\right)^2 + \left(\sigma_{clk,Galileo}^{HAS,MPL}\right)^2} = 14.13 \text{ cm}. \end{aligned} \tag{8.7}$$

These values have been computed under the assumption that all three orbit error components are characterized by the same variance $\sigma_{orb,j}^{HAS,MPL}$. However, this is not true in general. As it was observed on Chapter 7, radial direction benefits from a larger accuracy with respect to the in-track and cross-track components (as could be seen in Figures 7.6 and 7.5), due to the dynamics of the spacecraft as well as the orbit determination procedure. Moreover, it is the radial component the one having the largest impact on the ranging error seen by the user, as it is dependent on the orbit error vector's projection onto the line of sight vector, which always is "closer" to the radial direction due to the geometry of the problem, seen in Figure 7.4.

As a consequence, this methodology is conservative in the sense that it is overestimating the radial orbit error at the expense of underestimating the in-track and cross-track components, which leads to an overall larger $\sigma_{URE,j}^{HAS,MPLs}$. In fact, by comparing the obtained

values with those of Table 8.1, GPS URE is 6 to 7 cm larger for all SVs when estimated based on the MPLs and Galileo URE is 3 cm larger.

However, on the other hand, this value is based on the actual commitments of Galileo HAS. This provides a good baseline of the expected minimum performance of the proposed algorithm, as in general HAS provides better accuracy (see Tables 7.3 and 8.1).

Moreover, if at any point in the future Galileo HAS provides a specific commitment for each of the error components, it would be possible to obtain less conservative continuity models for HAS and also remove the need to perform any independent analyses.

8.3. SVs in view and observation geometry

In this Section, the number of SVs in view during the observation window, as well as the availability of Galileo HAS IDD corrections for the tracked satellites.

Figure 8.7 shows the number of SVs in view for each constellation and epoch. It can be seen that there are frequent loss of some SVs at the beginning of the measurement window, specially for Galileo satellites. This period corresponds to the taxing of the airplane from the gate to the runway (as seen on Figure 8.2). This could be attributed to nearby buildings and obstacles obstructing the reception of the signal or introducing multipath. In order to discriminate this effect during the analysis, both the take-off and landing epochs have been identified based on position and altitude of the aircraft, as the first and last time instant at which the aircraft is 10 meters above the mean sea level altitude of the airport. These epochs are marked with a black dashed line.

On the other hand, Figure 8.8 shows the SV visibility during the whole period. Only those SV that were in view for at least one epoch are shown. Red corresponds to those epochs where no signal was acquired by the receiver from that SV; yellow means that OS was available for that SV, but no HAS corrections were found and green means that both OS and HAS were available.

HAS IDD messages were found to be available for Galileo and GPS satellites above 99.18% and 91.33% of the time, respectively. This availability was computed with respect to those epochs where OS was available. This is consistent with the expected availability described on Table 7.2.

Note that these results are obtained without taking into account the FDE mechanism. During taxi operations, FDE acted frequently, probably due to larger errors related with multipath and poor geometry. This, together with the fact that $p_{const,gal} = 10^{-4} \gg$

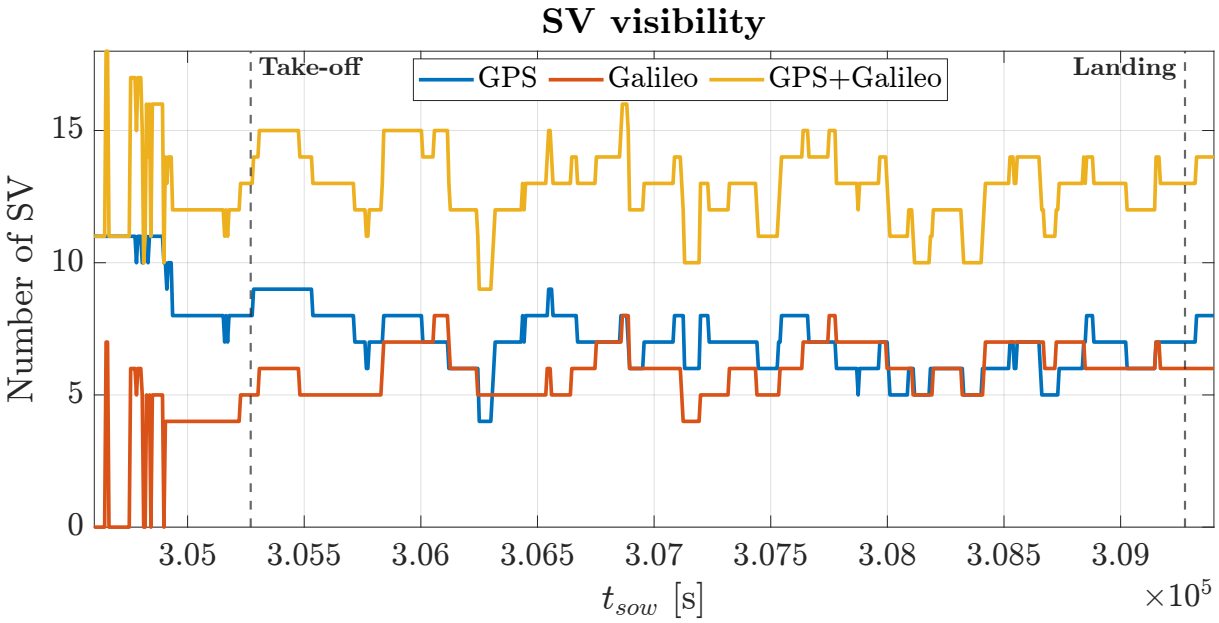

Figure 8.7: Number of visible GPS and Galileo satellites over time. Dashed lines indicate take off and landing epochs, respectively.

$p_{const,gps} = 10^{-8}$, leads to the exclusion of many Galileo satellites during the displacement from and to the gate. However, no faults were detected during the flight and thus no SV were excluded between take-off and landing.

Figure 8.9 shows the time evolution of the Geometric Dilution of Precision (GDOP), Position Dilution of Precision (PDOP) and Horizontal Dilution of Precision (HDOP). These metrics are a measure of the expected quality of the solution based on the geometry of the constellation at each epoch. First, a large GDOP is found during the taxi phase. This is expected, as geometry is greatly diminished during this phase, as shown in Figure 8.7. Then, there are some specific instants where the DOP is suddenly degraded. This is mainly linked to a reduction on the number of SVs in view during maneuvers, as they can be traced back to the information provided by Figures 8.7 and 8.8.

8.4. Algorithm performance

In this section, the performance of HAS+ARAIM algorithm is assessed using the experimental flight data. Three cases are considered: one using broadcast ephemeris and clock errors (OS); other using Galileo HAS IDD corrections - wherever available; and one using the post-processed precise products (PP). The latter is only used as a reference for the positioning error solution, and is not considered when assessing the obtained protection levels.

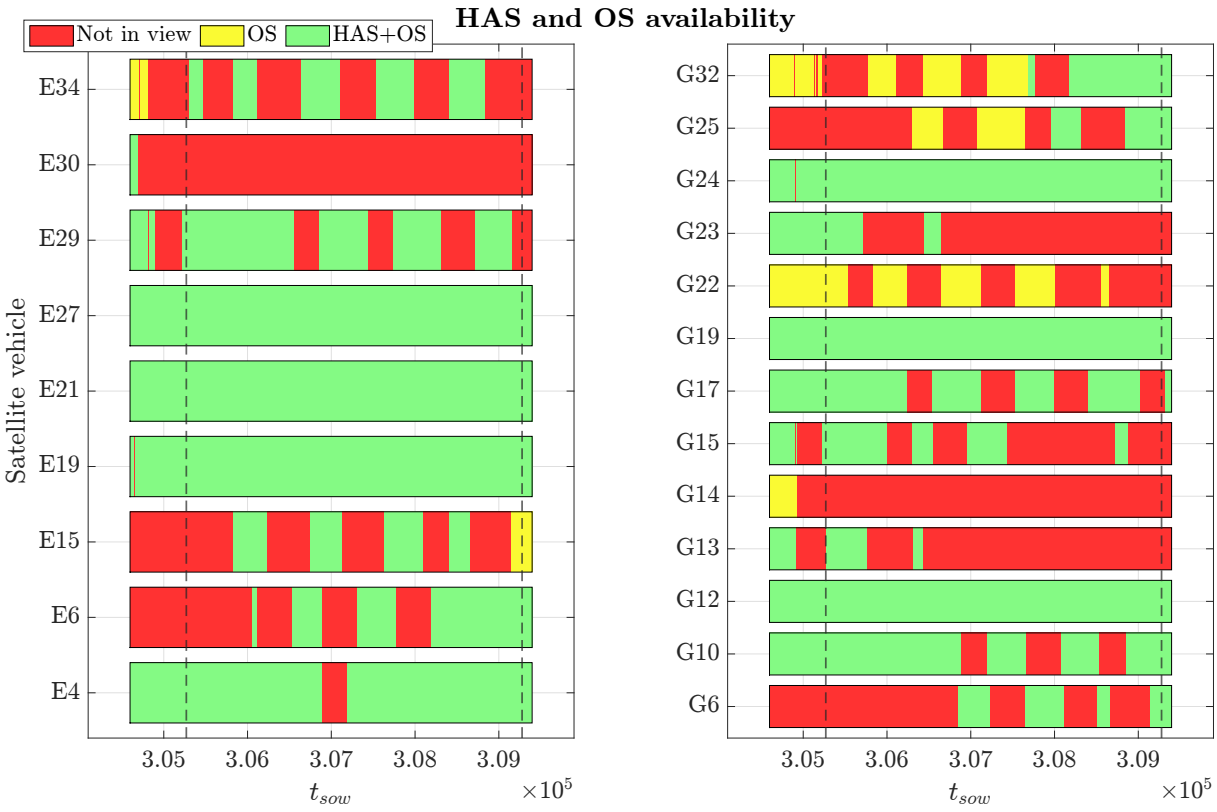

Figure 8.8: HAS IDD and OS corrections availability during the experimental campaign. Dashed lines indicate take off and landing epochs, respectively.

When computing the protection levels using HAS, two cases are considered depending on the continuity model used: using the one derived from SISRE on Section 8.2.1 and using the URE values derived from the Galileo HAS MPLs on Section 8.2.2.

If a SV i does not have any corrections available at some epoch (i.e. yellow in Figure 8.8), the broadcast ephemeris and clock errors are used instead. For this purpose, the corresponding σ^i_{URE} value for that SV is used, replacing $\sigma^i_{URE,HAS}$. Another alternative would be to discard completely the measurements corresponding to that SV. However, this would lead to a degraded geometry with respect to the OS case. As a consequence, it has been decided to follow the aforementioned approach.

8.4.1. Error performance

Figure 8.10 shows the time evolution of the error components in the ENU (East, North, Up) reference frame (with respect to the ground truth solution. It is possible to see that HAS solution follows much closer the time evolution of PP errors than OS. In particular, OS provides a RMS of the 3D error equal to 1.75 meters, while HAS IDD and PP provide

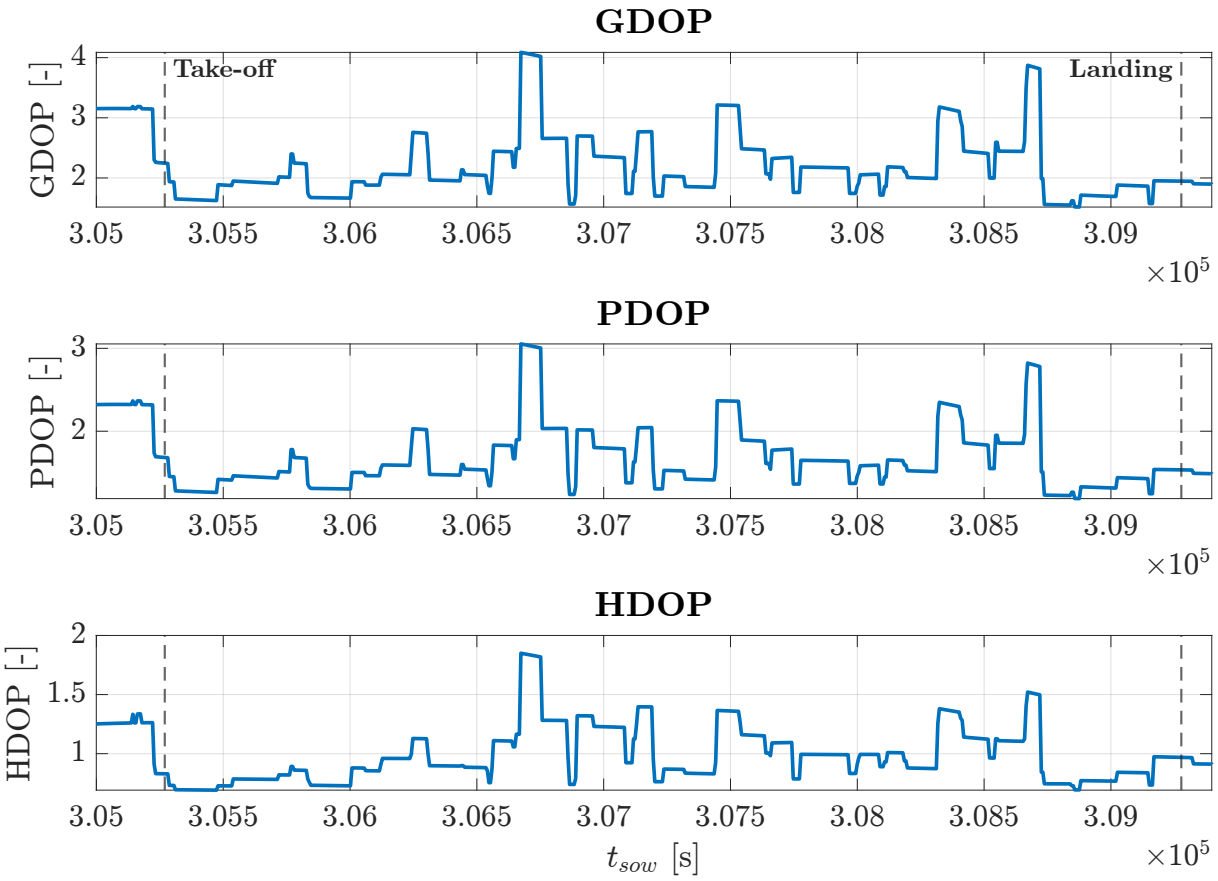

Figure 8.9: Dilution of precision during the observation window.

1.49 and 1.40 meters, respectively.

Additionally, there is a noticeable error increase during the taxi phase before and after the flight. By computing the RMS 3D error only during the flight, OS error is reduced to 1.59 meters, while HAS IDD and PP are 1.36 and 1.30 meters, respectively.

A noticeable improvement introduced by HAS IDD can be seen, as it is able - with live corrections - to exhibit a performance very close to that provided by precise products. Better positioning performance could be achieved by implementing a more complex position estimation such as a Kalman filter that uses additional information (such as the kinematic state or the inertial forces measured by an Inertial Measurement Unit, IMU) for obtaining a more refined solution. However, this is out of the scope of this work.

8.4.2. Protection levels

Once the positioning errors have been characterized, it is interesting to asses the protection levels provided by ARAIM. At each epoch, vertical and horizontal protection levels are computed after a successful application of the FDE mechanism. In particular, PLs are

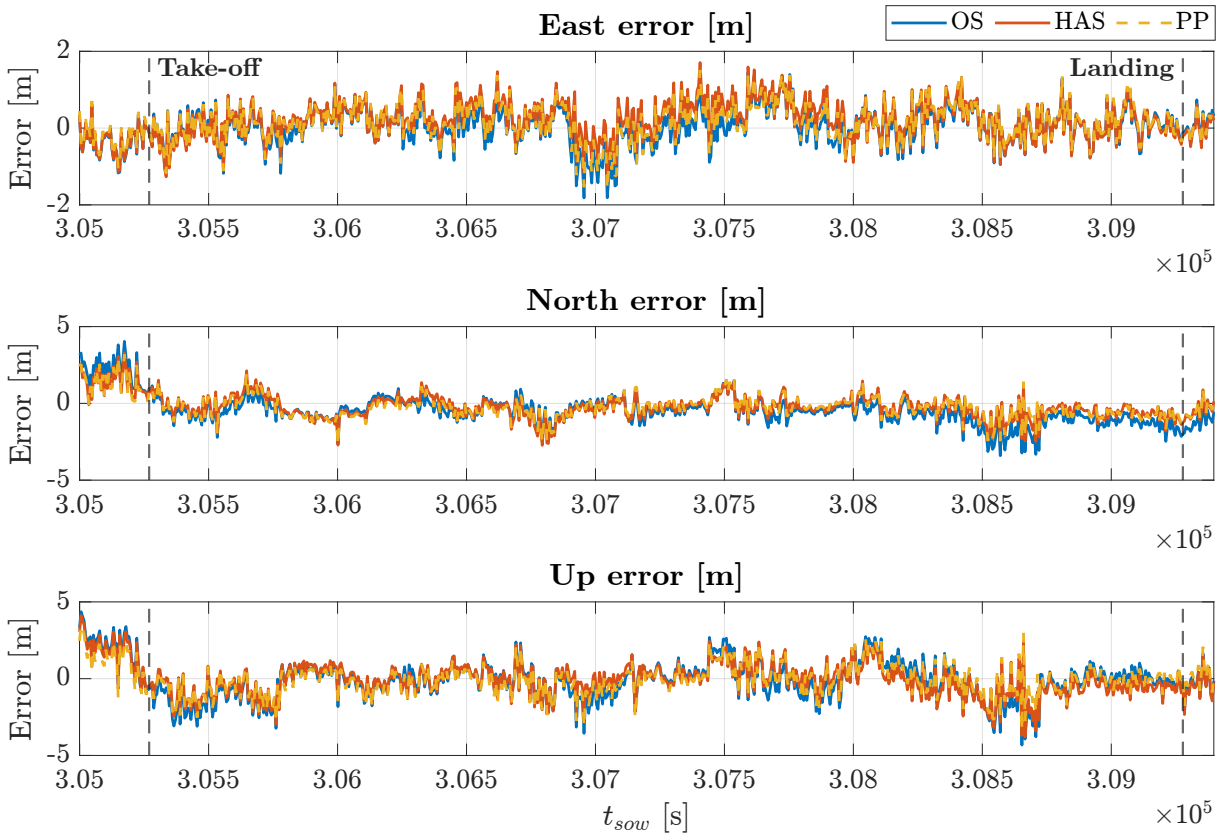

Figure 8.10: East, North Up (ENU) error evolution over time for Open Service (OS), HAS IDD and precise products (PP), using as reference the differential GNSS solution.

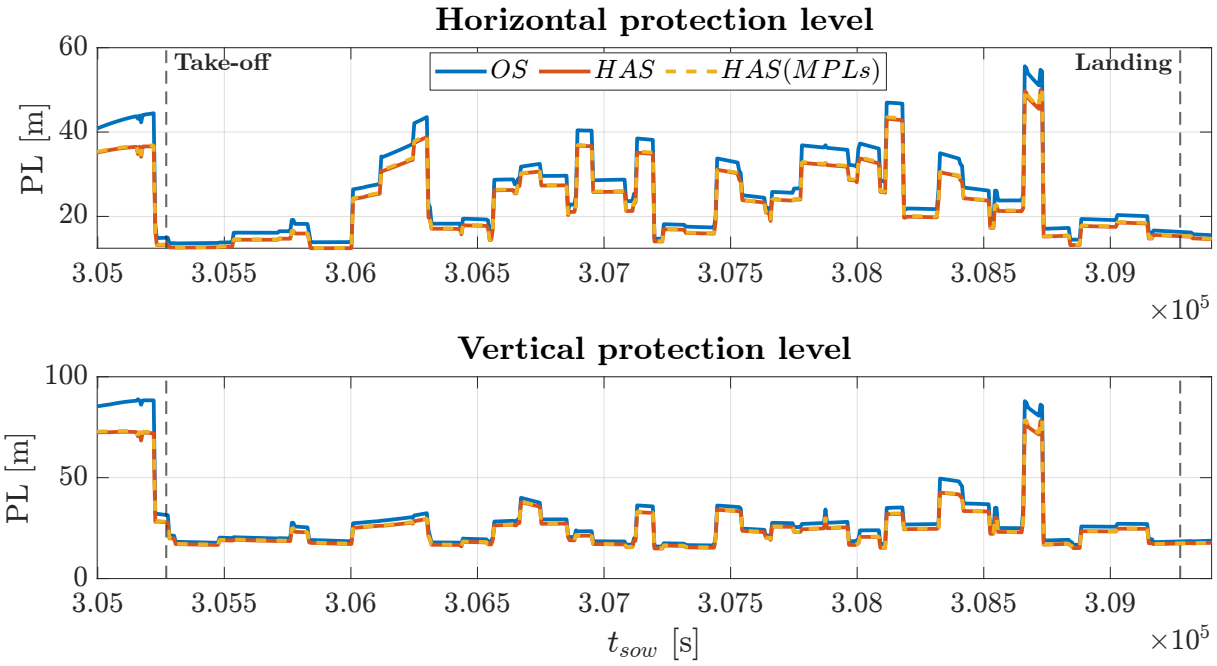

Figure 8.11: Vertical and horizontal protection levels obtained for the OS and HAS IDD cases.

shown for OS, and for both HAS using the continuity model derived from SISRE and that derived from the MPLs.

Figure 8.11 shows the vertical and horizontal protection levels for OS and HAS IDD with both continuity models. It is noticeable how PLs take very large values at the beginning of the observation window (which is probably linked with the poor geometry and interaction with nearby obstacles). Additionally, there is a great increase in VPL for both cases at around $t_{sow} \simeq 3.087 \times 10^5$ s, which can be traced back to a reduction on available GPS SV seen in Figures 8.7 and 8.8.

While all solutions follow a similar trend (that is mainly dominated by geometry), HAS IDD manages to provide a reduction of the horizontal and vertical protection levels, with very similar performance between SISRE-derived and MPL-derived URE values. In particular, 8.12 shows the percentual decrease in PLs delivered by HAS IDD when compared to OS. On average, a reduction between 5 to 15 % is expected for the horizontal and vertical protection levels between take-off and landing. This translates in a decrease between 1 to 10 meters for VPLs and between 1 to 5 meters for HPLs. Moreover, the difference on the reduction of PLs between both continuity models is below 1% of the OS value.

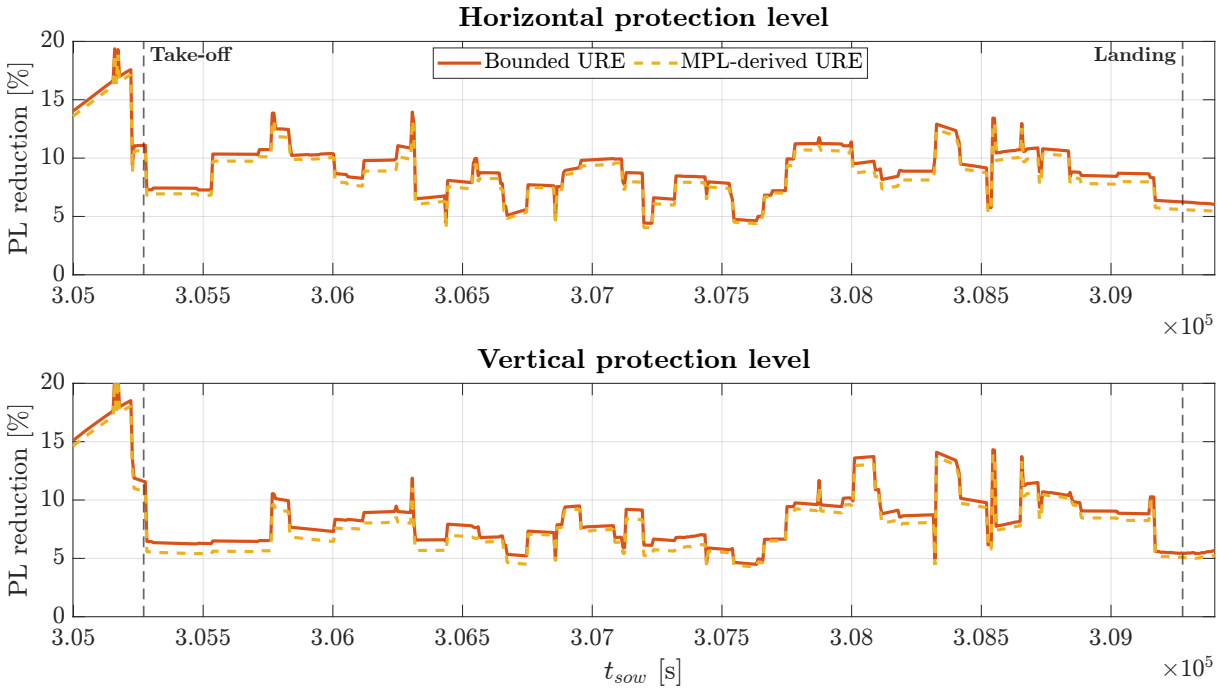

Figure 8.12: Percentual reduction on protection levels when using HAS IDD with respect to OS.

8.4.3. Navigation requirements compliance

The ESA - Stanford Integrity Diagram [44] is a tool that allows to integrate the error and protection levels computed for a certain set of observations in order to characterize the compliance with a set of navigation system requirements. In particular, given a certain Alert Limit it determines the epochs at which the system was in one of the following states:

- Nominal operation: In this case, the positioning errors are below the correspondent PLs, which are also below the Alert Limits.
- System Unavailable (SU): In this case, protection levels are larger than corresponding alert limit.
- Providing Misleading Information (MI): Errors are larger than the corresponding protection level.
- Hazardous Operation (HO): Errors are larger than the corresponding protection level and the PLs are below the AL.

In order to complete the proposed analysis, the Stanford-ESA integrity diagrams are shown for the vertical component using OS and HAS IDD. Figure 8.13 shows the OS

diagram, while Figure 8.14 and 8.15 correspond to HAS IDD using the SISRE and MPL derived continuity models, respectively.

All diagrams are computed using as reference the LPV-200 (35 m) alert limit, which corresponds to regions Nominal #1 and #2. Moreover, region #1 corresponds to a reduced VAL of 20 meters which allows for the assessment of the performance under tighter requirements.

Using HAS IDD manages to reduce system unavailability for more than half (from 14.83% down to 6.182%) for LPV-200 alert limit. Additionally, the availability with a VAL equal to 20 meters is increased by 7 points from 35.55% to 42.66%. Moreover, no sensible differences have been encountered between both continuity models for HAS.

These results suggest that the use of MPLs as a reference for computing the URE of HAS IDD is a good choice, in spite of the conservative assumption taken for the orbit error model. This approach is simpler and does not require the analysis of large quantities of data, and the differences between URE values do not translate on large performance gaps between both URE models.

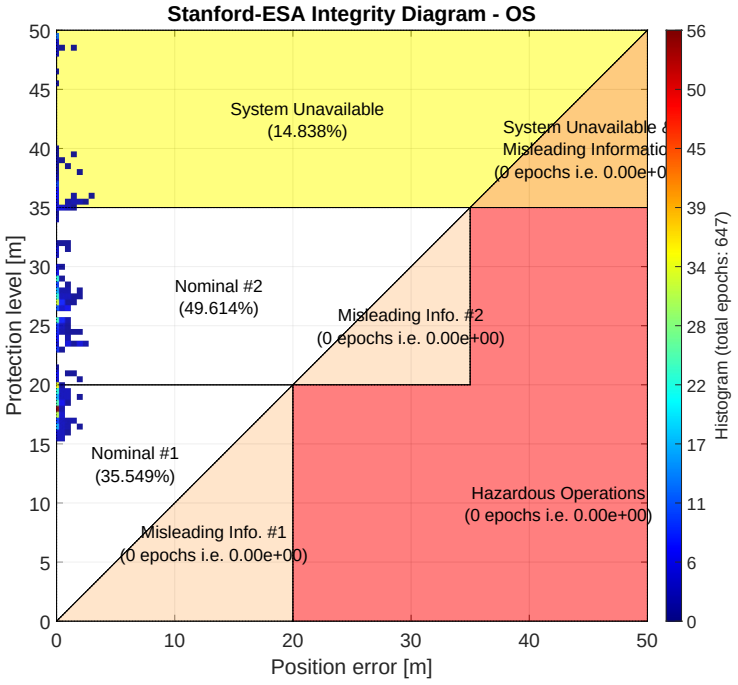

Figure 8.13: Stanford-ESA integrity diagram for OS case using LPV-200 navigation requirements as reference.

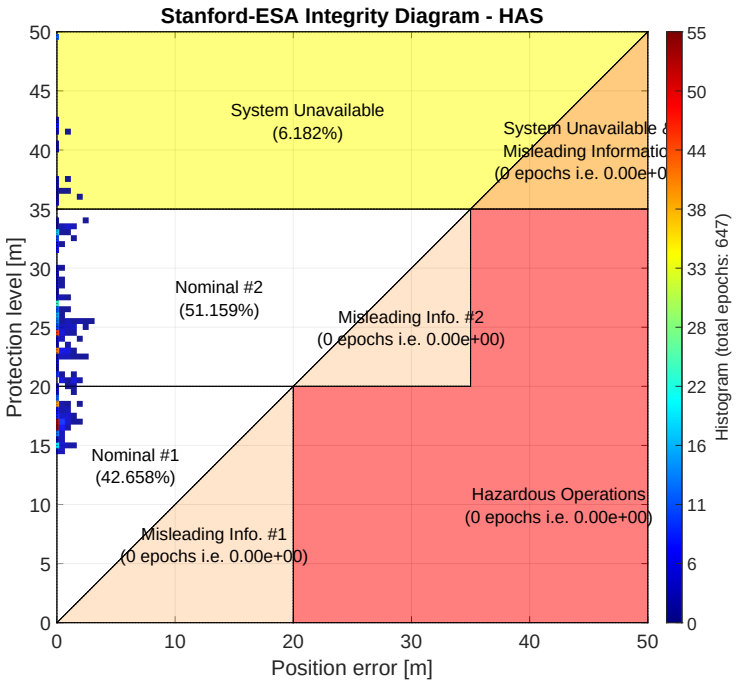

Figure 8.14: Stanford-ESA integrity diagram for HAS IDD with SISRE-derived continuity model. LPV-200 navigation requirements are used as reference.

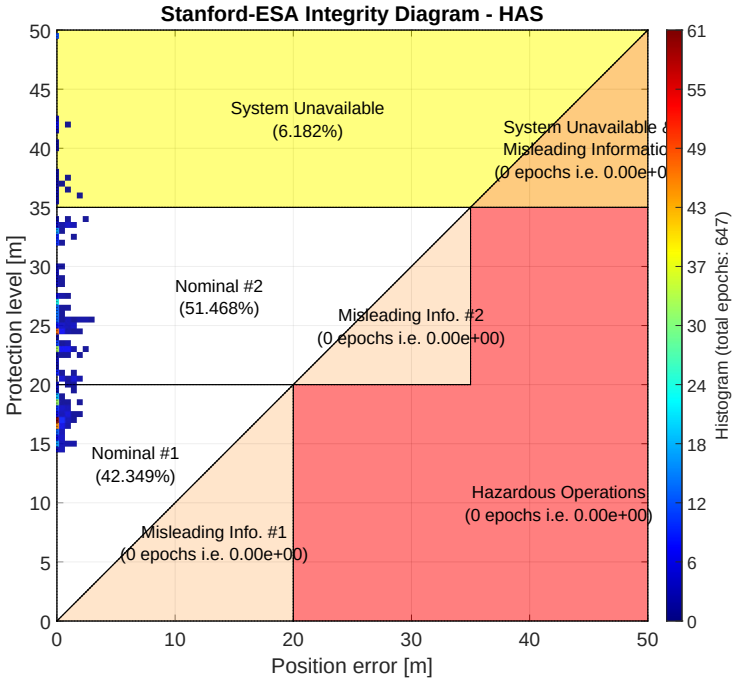

Figure 8.15: Stanford-ESA integrity diagram for HAS IDD with MPLs-derived continuity model. LPV-200 navigation requirements are used as reference.

8.5. Dependency on $P_{const,Galileo}$

Currently, the a priori probability for constellation-wide fault of Galileo is proposed to be 10^{-4} [3]. This is mainly explained due to the rather recent deployment of the constellation

Case	VPL	$P_{const,Galileo}$				
		1E-4	**1E-5**	**1E-6**	**1E-7**	**1E-8**
OS	>35 m	14.84%	12.83%	12.83%	12.83%	12.83%
	>20 m	49.61%	50.08%	49.92%	49.92%	48.99%
	<20 m	35.55%	37.09%	37.25%	37.25%	38.18%
HAS	>35 m	6.18%	6.18%	6.18%	6.18%	5.87%
	>20 m	51.16%	51.16%	49.46%	45.13%	28.59%
	<20 m	42.66%	42.66%	44.36%	48.69%	65.53%

Table 8.2: Vertical protection level dependence on $P_{const,Galileo}$.

with respect to GPS, which leads to smaller historic performance metrics. However, it is expected that this value is decreased progressively as the constellation matures. As a consequence, in this section a sensibility analysis with $P_{const,Galileo}$ is performed where the dependency of the performance improvements introduced by HAS are analyzed.

In particular, $P_{const,Galileo}$ is varied between 10^{-4} and 10^{-8}, while the rest of the parameters are fixed. Table 8.2 shows the result for each of the considered cases, as the percentage of epochs at which the VPL is below or above a certain threshold. Note that, since the errors are below 5 meters for all cases and does not depend on $P_{const,Galileo}$, only the obtained vertical protection levels are listed, as they directly translate onto a certain region of the Standford-ESA integrity diagram.

For OS, the reduction of $P_{const,Galileo}$ provides a limited impact on the VPL. In particular, the percentage of epochs for which $VPL > 35m$ (unavailability for LPV-200) is reduced a 13.48%, while VPL is found to be below 20 m 38.18% when $P_{const,Galileo} = 10^{-8}$ with respect to 35.55% that characterized the base case.

In the case of HAS, however, the behavior is slightly different. While the unavailability for LPV-200 ($VPL > 35$ m) is almost unchanged, there is a noticeable increase in the percentage of epochs for which $VPL < 20$ m of 53.6% (from 42.66% to 65.53%). It must be noted that the most noticeable change is between $P_{const,Galileo} = 10^{-7}$ and $P_{const,Galileo} = 10^{-8}$, which is the point at which both constellation fault probabilities are equal.

Figures 8.16 and 8.17 show the Standford-ESA integrity diagrams for OS and HAS IDD when using $P_{const,Galileo} = 10^{-8}$.

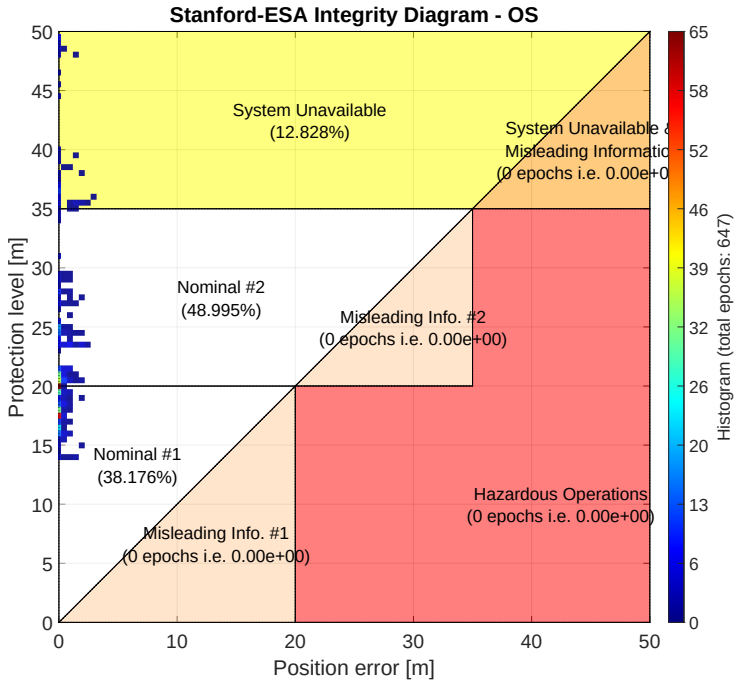

Figure 8.16: Stanford-ESA integrity diagram for OS with SISRE-derived continuity model and $P_{const,Galileo} = 10^{-8}$. LPV-200 navigation requirements are used as reference.

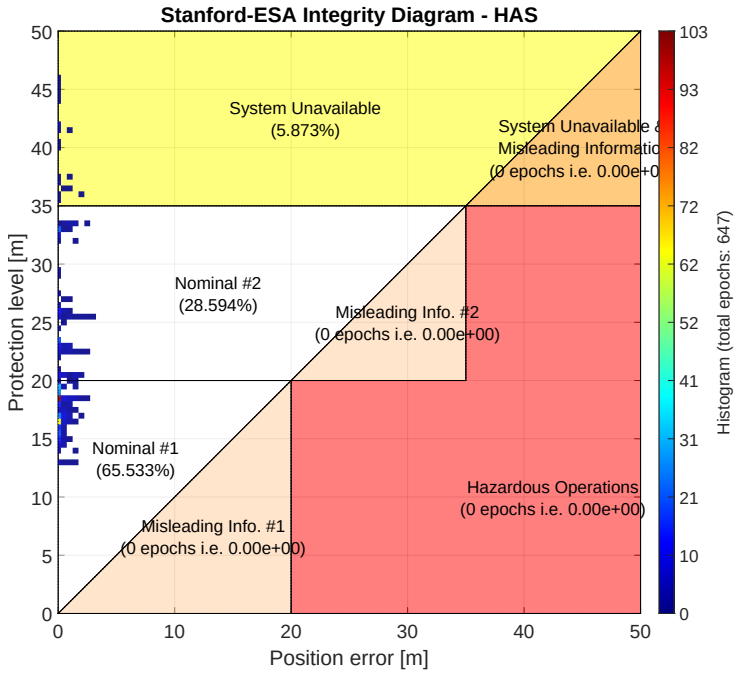

Figure 8.17: Stanford-ESA integrity diagram for HAS IDD with SISRE-derived continuity model and $P_{const,Galileo} = 10^{-8}$. LPV-200 navigation requirements are used as reference.

9 | Conclusions and future developments

9.1. Achievements

This work has presented a modified dual-frequency dual-constellation ARAIM algorithm that integrates Galileo High Accuracy Service. The new algorithm has been defined, implemented and evaluated using real measurements from a experimental flight campaign. In particular, the following activities have been carried out:

Firstly, a method to integrate Galileo HAS into a ARAIM has been proposed, detailing the modifications done to the original baseline algorithm as well as guidelines for its implementation in the user side.

Secondly, an availability simulation has been performed to characterize the dependence of the key performance indicators of ARAIM on the continuity and integrity models through the values of σ_{URA} and σ_{URE}. This analysis allows to predict current and potential future performances that can be achieved by implementing the proposed methodology.

Thirdly, an independent statistical assessment of the Signal-In-Space error characterizing HAS IDD during 2024 has been performed. This analysis has provided SV-specific information on the orbital and clock errors, as well as its projection onto the ranging domain by computing the instantaneous user projection on a grid of simulated users on Earth. A continuity error model for Galileo HAS has been proposed as a result of this analysis.

Lastly, the proposed algorithm is implemented and tested with real measurement data from a experimental flight campaign performed by DLR. A comprehensive analysis of the results has proven that reductions between 5 to 10 % on the vertical protection levels can be achieved, increasing system availability by more than 50% for LPV-200 navigation requirements.

Moreover, potential future performances of the proposed algorithm are assessed by studying the performance with decreased a priori constellation fault probability for Galileo.

Figure 9.1 summarizes the activities performed and the contributions associated to each of them.

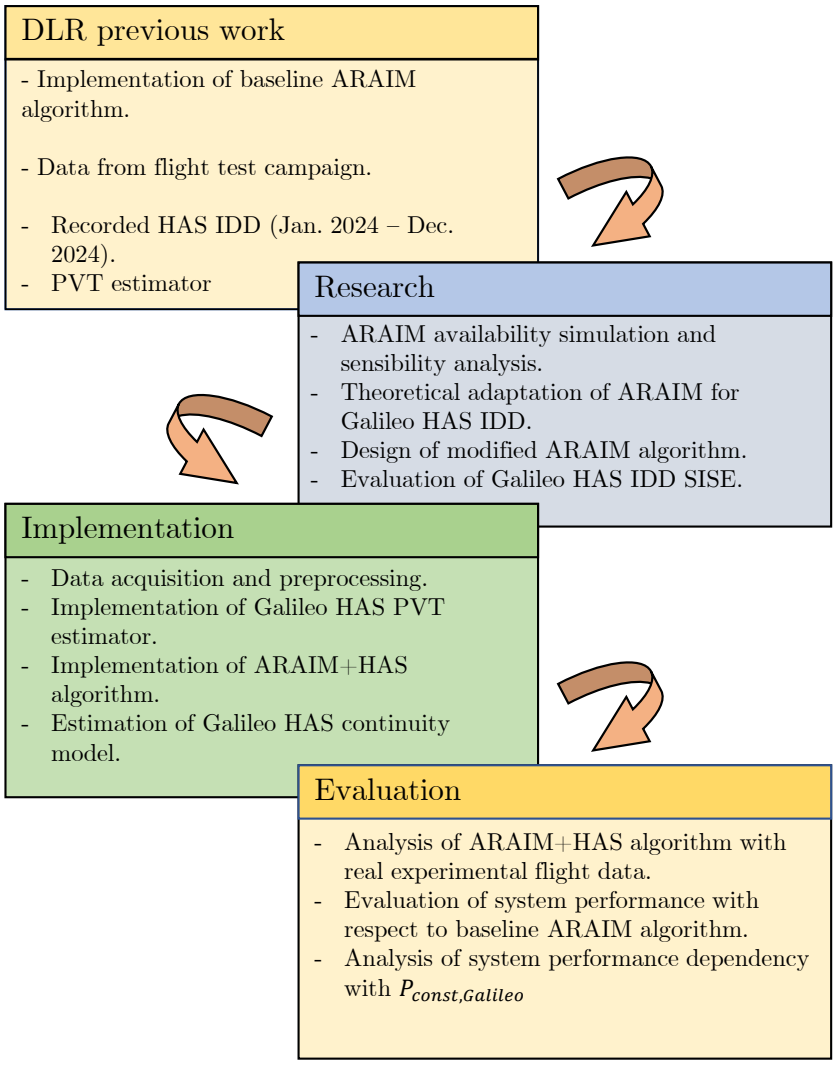

Figure 9.1: List of contributions and existing work.

9.2. Conclusions

In this work, a modified ARAIM algorithm that integrates Galileo High Accuracy Service has been proposed. The presented algorithm has proven to be able to improve the current performance of ARAIM for vertical guidance on commercial aviation assuming that HAS does not introduce any additional fault modes. The improvements in the continuity model delivered by HAS are translated in a reduction of the vertical and horizontal protection levels, as well as in an increase of system availability.

For this purpose, the availability simulation delivered valuable information on the ex-

pected performance enhancement that could be expected from an improvement of the continuity model. On the other hand, the signal-in-space error analysis provided valuable information on the current and future performance of Galileo HAS algorithm, providing SV-specific values for the user range error of Galileo and GPS constellations. The conclusions drawn from these studies were validated using real flight experimental observations, that proofed its applicability on a real scenario. Additionally, the dependency study with $P_{const,Galileo}$ showed that better performance may be expected in the future, as $P_{const,Galileo}$ is lowered, showing an increase on availability of up to 53.6% for a vertical alert limit of 20 meters.

The proposed algorithm does not limit its applicability to civil aviation. Due to its versatile nature, the proposed algorithm could potentially be implemented in the future for other safety-critical applications such as urban air mobility or train navigation, where the application of ARAIM integrated with Galileo HAS would augment the current performance, enhancing the integrity of the overall system.

9.3. Future developments

During the development of this work, some specific points have emerged that are worth exploring in the future. In particular:

- *Integrity model update:* Currently, Galileo HAS does not provide any integrity commitment based on its Service Definition Document [4]. For this project, it has been assumed that Galileo HAS does not introduce any additional fault modes. As a consequence, the integrity error and threat model used corresponds to the one provided by the ISM. If integrity commitments are provided by Galileo HAS in the future, it is interesting to asses the performance of the system when not only the continuity error model is updated, but also the integrity one.

- *Validation with Galileo SIS:* This work has been developed using Galileo HAS Internet Data Distribution service (IDD). However, in a real case scenario, the user would use the Signal-In-Space dissemination of HAS messages through the E6-b band from Galileo satellites. While, according to the SDD [4], the very same minimum performance levels apply to HAS IDD and HAS SIS, it is interesting to develop the framework to retrieve, process and apply HAS SIS corrections and evaluate its performance.

- *Evaluation of the proposed algorithm with larger datasets:* For this work, 96 minutes of experimental flight data were used on the final evaluation of the algorithm. It is

proposed that more datasets are used in order to offer a more complete picture of the actual performance of the algorithm in a real scenario.

Bibliography

[1] Santiago Perea Diaz. *Design of an integrity support message for offline advanced RAIM*. PhD thesis, Rheinisch-Westfälische Technische Hochschule Aachen, 2019.

[2] Omar Garcia Crespillo. *GNSS/INS Kalman Filter Integrity Monitoring with Uncertain Time Correlated Error Processes*. PhD thesis, 2022.

[3] Working Group C - ARAIM Technical Subgroup. Gps-galileo milestone 3 report. Technical report, 2016.

[4] Galileo High Accuracy Service Service Definition Document Issue 1.0. Technical report, European Union, 2023.

[5] EUSPA. Euspa eo and gnss market report. Technical report, EUSPA, 2024.

[6] Peter JG Teunissen and Oliver Montenbruck. *Springer handbook of global navigation satellite systems*, volume 10. Springer, 2017.

[7] J. Sanz Subirana, J.M. Juan Zornoza, M. Hernández-Pajares. GNSS Basic Observables. Online, 2011.

[8] Ron Hatch. The synergism of gps code and carrier measurements. In *International geodetic symposium on satellite doppler positioning*, volume 2, pages 1213–1231, 1983.

[9] Florian Röβl, Omar García Crespillo, Oliver Heirich, and Ana Kliman. A map based multipath error model for safety critical navigation in railway environments. In *2023 IEEE/ION Position, Location and Navigation Symposium (PLANS)*, pages 446–457. IEEE, 2023.

[10] Evgenii Munin, Antoine Blais, and Nicolas Couellan. Convolutional neural network for multipath detection in GNSS receivers. In *2020 International Conference on Artificial Intelligence and Data Analytics for Air Transportation (AIDA-AT)*, pages 1–10. IEEE, 2020.

[11] J.M. Juan Zornoza J. Sanz Subirana and M. Hernández-Pajares. GNSS Data Pro-

cessing Volume I: Fundamentals and algorithms. Technical report, European Space Agency, 2013.

[12] Bob Schutz, Byron Tapley, and George H Born. *Statistical orbit determination*. Elsevier, 2004.

[13] Annex 10 (Aeronautical Telecommunications) to The Convention On International Civil Aviation, Volume I - Radio Navigation Aids, International Standards And Recommended Practices (SARPs). Technical report, ICAO Doc. AN10-1, 2006.

[14] US Federal Radionavigation Plan. Technical report, Department of Defense, Department of Homeland Security and Department of Transportation., 2008.

[15] Doc 9613 performance based navigation manual. Technical Report Consoldated 4th edition, ICAO, 2013.

[16] Report on Aviation User Needs and Requirements GSA-MKD-AV-UREQ-250287. Technical report, GSA - European Global Navigation Satellite System Agency, 2019.

[17] Juan Blanch, Todd Walker, Per Enge, Young Lee, Boris Pervan, Markus Rippl, Alex Spletter, and Victoria Kropp. Baseline advanced raim user algorithm and possible improvements. *IEEE Transactions on Aerospace and Electronic Systems*, 51(1):713–732, 2015.

[18] NASVSTAR GPS Space Segment / User Segment L1C Interface. Technical report, US Space Force, 2020.

[19] European Union. (OS SIS ICD) Galileo Open Service Signal-In-Space Document (OS SIS ICD). Technical report, 2023.

[20] Boris S Pervan, Samuel P Pullen, and Jock R Christie. A multiple hypothesis approach to satellite navigation integrity. *Navigation*, 45(1):61–71, 1998.

[21] Gary A McGraw, Tim Murphy, Mats Brenner, Sam Pullen, and AJ Van Dierendonck. Development of the LAAS accuracy models. In *Proceedings of the 13th International Technical Meeting of the Satellite Division of The Institute of Navigation (ION GPS 2000)*, pages 1212–1223, 2000.

[22] Juan Blanch, Todd Walter, and Per Enge. Gaussian bounds of sample distributions for integrity analysis. *IEEE Transactions on Aerospace and Electronic Systems*, 55(4):1806–1815, 2018.

[23] Galileo High Accuracy Service Signal In Space Interface Control Document Issue 1.0. Technical report, European Union, 2022.

[24] Galileo High Accuracy Service Internet Data Distribution Interface Control Document Issue 1.1. Technical report, European Union, 2023.

[25] Ignacio Fernandez-Hernandez, Adrián Chamorro-Moreno, Simón Cancela-Diaz, J David Calle-Calle, Paolo Zoccarato, Daniel Blonski, Tommaso Senni, F Javier de Blas, Carmelo Hernández, Javier Simón, et al. Galileo high accuracy service: initial definition and performance. *GPS solutions*, 26(3):65, 2022.

[26] NAVSTAR GPS Space Segment/Navigation User Segment Interfaces - IS-GPS-200. Technical report, 2022.

[27] Jan, Shau-Shiun and Chan, Wyant and Walter, Todd and Enge, Per. Matlab simulation toolset for SBAS availability analysis. In *Proceedings of the 14th International Technical Meeting of the Satellite Division of The Institute of Navigation (ION GPS 2001)*, pages 2366–2375, 2001.

[28] Galileo High Accuracy Service Service quaterly performance report January - March 2023 Issue 1.0. Technical report, European Union, 2023.

[29] Galileo High Accuracy Service Service quaterly performance report April - June 2023 Issue 1.0. Technical report, European Union, 2023.

[30] Galileo High Accuracy Service Service quaterly performance report July - September 2023 Issue 1.0. Technical report, European Union, 2023.

[31] Galileo High Accuracy Service Service quaterly performance report October - December 2023 Issue 1.0. Technical report, European Union, 2023.

[32] Galileo High Accuracy Service Service quaterly performance report January - March 2024 Issue 1.0. Technical report, European Union, 2024.

[33] Galileo High Accuracy Service Service quaterly performance report April - June 2024 Issue 1.0. Technical report, European Union, 2024.

[34] Galileo High Accuracy Service Service quaterly performance report July - September 2024 Issue 1.0. Technical report, European Union, 2024.

[35] Oliver Montenbruck, Peter Steigenberger, Lars Prange, Zhiguo Deng, Qile Zhao, Felix Perosanz, Ignacio Romero, Carey Noll, Andrea Stürze, Georg Weber, et al. The Multi-GNSS Experiment (MGEX) of the International GNSS Service (IGS)–achievements, prospects and challenges. *Advances in space research*, 59(7):1671–1697, 2017.

[36] Oliver Montenbruck, Peter Steigenberger, Robert Khachikyan, Georg Weber, Richard

Langley, Leos Mervart, and Urs Hugentobler. IGS-MGEX: preparing the ground for multi-constellation GNSS science. *Inside Gnss*, 9(1):42–49, 2014.

[37] Oliver Montenbruck, Peter Steigenberger, and André Hauschild. Multi-GNSS signal-in-space range error assessment–Methodology and results. *Advances in Space Research*, 61(12):3020–3038, 2018.

[38] Lambert Wanninger, Susanne Beer, Anja Heßelbarth, et al. Der Galileo High Accuracy Service (HAS): Ein neues Kapitel der GNSS-Positionsbestimmung. *ZfV-Zeitschrift für Geodäsie, Geoinformation und Landmanagement*, (zfv 4/2023), 2023.

[39] Todd Walter and Juan Blanch. Characterization of GNSS clock and ephemeris errors to support ARAIM. In *Proceedings of the ION 2015 Pacific PNT Meeting*, pages 920–931, 2015.

[40] Paolo Zoccarato, Francesco Menzione, Ciro Gioia, Joaquim Fortuny-Guasch, Javier Ostolaza, Stefano Lagrasta, Dimitrios Vasileios Psychas, Matteo Paonni, Javier De Blas, Daniel Blonsk, et al. Galileo High Accuracy Service Reference User Algorithm Formulation and Verification. In *Proceedings of the 37th International Technical Meeting of the Satellite Division of The Institute of Navigation (ION GNSS+ 2024)*, pages 2111–2122, 2024.

[41] Ilaria Martini, Melania Susi, Luca Cucchi, and Ignacio Fernandez-Hernandez. Galileo high accuracy service performance and anomaly mitigation capabilities. *GPS solutions*, 28(1):25, 2024.

[42] Ilaria Martini, Melania Susi, and Ignacio Fernández-Hernández. PPP and Galileo high accuracy service with satellite selection strategies for kinematic applications. In *Proceedings of the 35th International Technical Meeting of the Satellite Division of The Institute of Navigation (ION GNSS+ 2022)*, pages 667–682, 2022.

[43] Peiyuan Zhou, Guorui Xiao, and Lan Du. Initial performance assessment of galileo high accuracy service with software-defined receiver. *GPS solutions*, 28(1):2, 2024.

[44] Sanz M. Hernández-Pajares, J.M. Juan, A.Tadjine and I. Delgado. The Stanford – ESA Integrity Diagram: Focusing on SBAS Integrity. Online, 2011.

[45] Oliver Montenbruck and André Hauschild. Code biases in multi-GNSS point positioning. In *Proceedings of the 2013 International Technical Meeting of The Institute of Navigation*, pages 616–628, 2013.

[46] M. Rothacher, R. Schmid. Antenna Exchange Format, version 1.4. Online, 2010.

[47] European GNSS Service Center (GSC). Galileo Satellite Metadata. Online, 2024.

[48] Oliver Montenbruck, Ralf Schmid, Flavien Mercier, Peter Steigenberger, Carey Noll, Roman Fatkulin, Satoshi Kogure, and Aiylam S Ganeshan. GNSS satellite geometry and attitude models. *Advances in Space Research*, 56(6):1015–1029, 2015.

A | Group delays computation for SISRE assesment

In order to perform a Signal-In-Space error assessment by comparing OS or HAS estimated orbital positions and satellite clock biases, with the ones provided by precise products, it is necessary to align each of the estimations to a same reference.

In particular, for the clock errors the group delays must be taken into account in order to remove spurious bias that otherwise would appear in the resulting error distributions. On the other hand, orbital positions are generally referred to different points of the spacecraft. A proper translation must be performed to remove any potential biases that may appear on any of the components (radial, in-track and cross-track).

A.1. Group delays

When computing the ionospheric free combination (IF) of two pseudorange observations P_1 and P_2, with frequencies f_1 and f_2, the result can be modeled as [45]

$$IF(P_1,P_2) = \frac{f_1^2}{f_1^2-f_2^2}P_1 - \frac{f_2^2}{f_1^2-f_2^2}P_2 = \rho + c\delta t^{rcv} - c\delta t^{sat} + T + \frac{f_1^2}{f_1^2-f_2^2}B_1 - \frac{f_2^2}{f_1^2-f_2^2}B_2 \tag{A.1}$$

where ρ is the geometric range, δt^{rcv} and δt^{sat} are the receiver and satellite clock biases, T is the tropospheric error and B_i is the bias term associated with each observation. These bias terms can be decomposed in a satellite component B^{sat} and receiver component, B^{rcv}. According to [45], these biases are lumped within the receiver and clock biases,

$$c\overline{\delta t}^{rcv}_{IF(P_1,P_2)} = c\delta t^{rcv} + \frac{f_1^2}{f_1^2-f_2^2}B_1^{rcv} - \frac{f_2^2}{f_1^2-f_2^2}B_2^{rcv}, \tag{A.2}$$

$$c\overline{\delta t}^{sat}_{IF(P_1,P_2)} = c\delta t^{sat} - \frac{f_1^2}{f_1^2 - f_2^2} B_1^{sat} + \frac{f_2^2}{f_1^2 - f_2^2} B_2^{sat}, \tag{A.3}$$

thus simplifying the expression of the ionospheric free combination to

$$IF(P_1, P_2) = \rho + c\overline{\delta t}^{rcv}_{IF(P_1,P_2)} - c\overline{\delta t}^{sat}_{IF(P_1,P_2)} + T. \tag{A.4}$$

As a consequence, whenever a satellite clock bias $c\overline{\delta t}^{sat}_{IF(P_1,P_2)}$ is obtained from a certain source (e.g. OS, HAS, PP), it must also be taken into account the code combination that it is referred to. From the user side, the appropriate signal combinations should be used in order to avoid the appearance of a SV-dependent bias in the measurements. On the other hand, whenever a comparison is performed between satellite clock biases, it is necessary to perform the appropriate translations to align both references.

Let $\overline{\delta t}^{sat,(1)}_{IF(P_1,P_2)}$ be the satellite clock bias from source (1) referred to the P_1, P_2 ionospheric free combination, with frequencies f_1 and f_2. On the other hand, let $\overline{\delta t}^{sat,(2)}_{IF(P_1,P_3)}$ be the satellite clock bias for the P_1, P_3 combination from source (2). We are interested on computing $\epsilon_{clk} = \delta t^{sat,(1)} - \delta t^{sat,(2)}$, that is the real error in the satellite clock bias determination from both sources. As a consequence, it is necessary to remove appropriately the group delay terms of Eq. (A.3). In particular, we have

$$\begin{aligned} \overline{\delta t}^{sat,(1)}_{IF(P_1,P_2)} &= \delta t^{sat,(1)} - \frac{f_1^2}{f_1^2 - f_2^2} B_1^{sat} + \frac{f_2^2}{f_1^2 - f_2^2} B_2^{sat}, \\ \overline{\delta t}^{sat,(2)}_{IF(P_1,P_3)} &= \delta t^{sat,(2)} - \frac{f_1^2}{f_1^2 - f_3^2} B_1^{sat} + \frac{f_3^2}{f_1^2 - f_3^2} B_3^{sat}. \end{aligned} \tag{A.5}$$

Applying the identity [45]

$$\frac{f_1^2}{f_1^2 - f_2^2} B_1 - \frac{f_2^2}{f_1^2 - f_2^2} B_2 = B_1 + \frac{f_2^2}{f_1^2 - f_2^2} DCB_{1-2} \tag{A.6}$$

where $DCB_{1-2} = B_1 - B_2$, is the differential clock bias between signals 1 and 2

$$\begin{aligned} \overline{\delta t}^{sat,(1)}_{IF(P_1,P_2)} &= \delta t^{sat,(1)} - B_1^{sat} - \frac{f_2^2}{f_1^2 - f_2^2} DCB^{sat}_{1-2}, \\ \overline{\delta t}^{sat,(2)}_{IF(P_1,P_3)} &= \delta t^{sat,(2)} - B_1^{sat} - \frac{f_3^2}{f_1^2 - f_3^2} DCB^{sat}_{1-3}. \end{aligned} \tag{A.7}$$

The difference between both equations leads to

$$\overline{\delta t}^{sat,(1)}_{IF(P_1,P_2)} - \overline{\delta t}^{sat,(2)}_{IF(P_1,P_3)} = \epsilon_{clk} - \frac{f_2^2}{f_1^2 - f_2^2} DCB^{sat}_{1-2} + \frac{f_3^2}{f_1^2 - f_3^2} DCB^{sat}_{1-3} \tag{A.8}$$

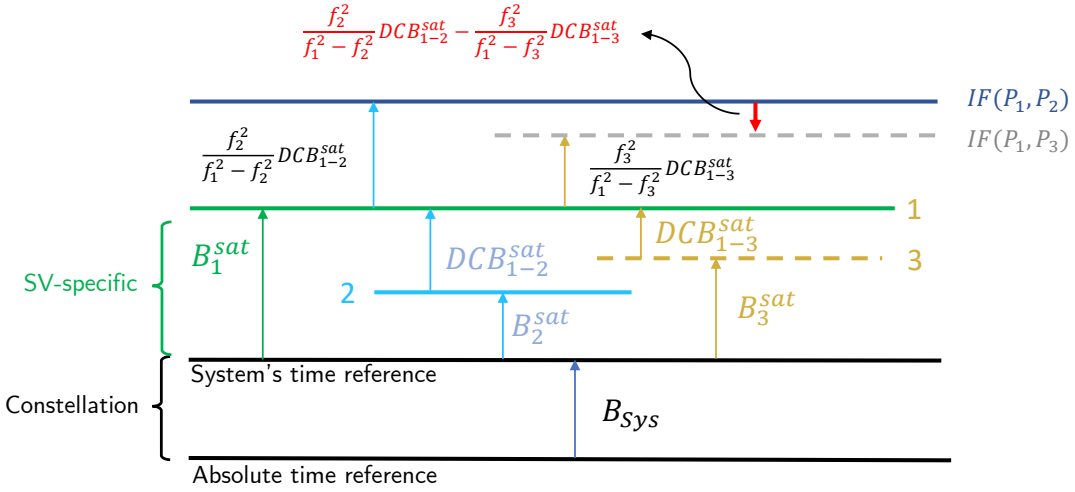

Figure A.1: Schematic representation of the relation between code biases of different code observations. Adapted from [45].

from which, it is possible to obtain the factor that must be removed from the difference $\overline{\delta t}^{sat,(1)}_{IF(P_1,P_2)} - \overline{\delta t}^{sat,(2)}_{IF(P_1,P_3)}$ to obtain the real clock error between source (1) and (2)

$$\epsilon_{clk} = \overline{\delta t}^{sat,(1)}_{IF(P_1,P_2)} - \overline{\delta t}^{sat,(2)}_{IF(P_1,P_3)} + \frac{f_2^2}{f_1^2-f_2^2}DCB_{1-2}^{sat} - \frac{f_3^2}{f_1^2-f_3^2}DCB_{1-3}^{sat}. \tag{A.9}$$

An analogous procedure can be followed for any other combination mix of combination signals. An additional bias has to be taken into account, that corresponds to the reference used by each provider. However, this bias affects equally to all SV of the same constellation. As a consequence, it can be removed by taking the constellation-wise mean of the computed errors. From the user point of view, it would be absorbed by the user clock bias.

Regarding the source of the differential clock biases DCB_{i-j}, the Chinese Academy of Sciences (CAS) provides daily clock biases for all SVs with pico-second accuracy.

Figure A.1 shows a schematic representation of the operations performed. In particular, each of the pseudorange measurements are shown with its correspondent delay with respect to the systems' reference. Then, the identity provided by Eq. (A.6) is applied to obtain the ionospheric combinations of observables 1-2 and 1-3. Finally, the difference between both is the offset that should be removed from the error ϵ_{clk}.

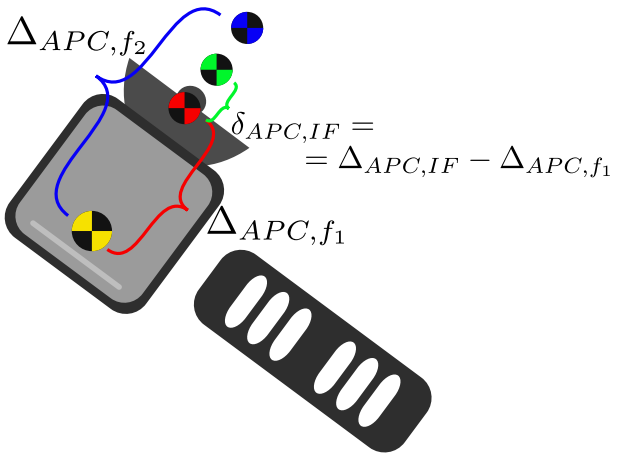

Figure A.2: Scheme of relevant points in the SV-fixed frame of reference for alignment of orbital products.

A.2. Antenna Phase Center Offsets

In general, each orbital position is referred to a specific point in the SV frame of reference, that may not coincide with that of other products. For instance, orbital precise products provided by the Center of Orbit Determination of Europe provides the orbital position of the center of mass of the SV. On the other hand, GPS broadcast ephemerids refer to the antenna phase center (APC) of the L1/L2 ionospheric free combination while Galileo broadcast navigation message refers to the arithmetic mean of the E1, E5 and E6 APCs [37].

In order to perform the appropriate translations, ANTEX files provide the relative position of the APCs of each frequency with respect to the center of mass in a body-fixed frame of reference (IGS frame,[46]). The APC of the ionospheric-free combination of frequencies f_1 and f_2 from the correspondent APC's positions Δ_{APC,f_1} and Δ_{APC,f_2} can be computed using the following relation [37]

$$\Delta_{APC,IF(f_1,f_2)} = \frac{\Delta_{APC,f_1} f_1^2 - \Delta_{APC,f_2} f_2^2}{f_1^2 - f_2^2}. \tag{A.10}$$

When working with precise products, the orbital position of the IF APC is provided by

$$\mathbf{x}_{PP,IF} = \mathbf{x}_{PP,CoM} + \mathbf{R}_B^{ECEF} \Delta_{APC,IF} \tag{A.11}$$

where $\mathbf{R}_B^{ECEF}$ is the rotation matrix from body axes to ECEF. This matrix can be estimated by using the nominal attitude law of the SV which is described in [47] for Galileo

and [48] for GPS. In general it depends on the position of the Earth on ECEF as well as the SV's position.

For Galileo HAS IDD, since the refined orbits $\breve{\mathbf{x}}$ are referred to the single frequency L1/E1 APC, then the orbital position of the IF APC is provided by

$$\breve{\mathbf{x}}_{IF} = \breve{\mathbf{x}}_{L1/E1} + \mathbf{R}_B^{ECEF} \delta_{APC,IF} \tag{A.12}$$

where $\delta_{APC,IF}$ is the distinace between the L1/E1 and the IF APCs, as defined in Figure A.2.

B | Single Point Positioning (SPP) Algorithms description

The aim of this appendix is to provide a general description of the PVT algorithms used for estimating the user position based on a set of ionospheric free pseudorange measurements from Galileo and GPS constellations. In particular, three cases are distinguished based on the source of the orbital and clock bias information: broadcast ephemerides (OS), Galileo HAS IDD (HAS) and precise products (PP).

B.1. Algorithm description

For all cases, a Weighted Least Squares estimator is used, whose state is defined as

$$\mathbf{x} = [x_{rx}, y_{rx}, z_{rx}, \delta t^{rx}_{GPS}, \delta t^{rx}_{Galileo}]^T \tag{B.1}$$

where $[x_{rx}, y_{rx}, z_{rx}]$ is the user's location in ECEF, and $\delta t^{rx}_{GPS}, \delta t^{rx}_{Galileo}$ are the receivers' clock bias with respect to GPS System Time and Galileo System Time, respectively. In the following, a general description of the baseline PVT estimation algorithm is provided.

B.1.1. Satellite position estimation

For each pseudorange measurement available at t_{epoch}, the corresponding constellation index j[1] and Satellite Vehicle ID i are obtained.

Obtaining reception time in Constellation System Time

The receiver time in the constellation j's time reference system is computed as:

$$t^j_{rx} = t_{epoch} - \mathbf{x}(3+j)/c, \tag{B.2}$$

[1] where $j = 1...N_{const}$. For this work, j=1 is GPS and j=2 is Galileo.

where c is the speed of light in m/s.

OUTPUT: Receiver time in Constellation System Time j, t_{rx}^{j}.

Obtaining the geometric transmission delay

The geometric transmission delay is estimated solving iteratively the light-time equation. Firstly, the satellite position $\mathbf{x}_{sat}$ is obtained either from the Broadcast ephemeris, HAS or PP at time t_{rx}^{j}.

Then, the distance between the user and the satellite's IF APC is obtained as

$$d_{rx}^{sat} = |\mathbf{x}(1:3) - \mathbf{x}_{sat}^{BRDC}|. \tag{B.3}$$

and the time taken for the signal to cover that distance is

$$\tau = d_{rx}^{sat}/c. \tag{B.4}$$

OUTPUT: Geometric transmission delay τ.

Relativistic and clock bias corrections

A first guess of the transmission time is obtained as

$$t_{tx} = t_{rx}^{j} - \tau. \tag{B.5}$$

where the superscript for the time reference system has been omitted for simplicity (the time reference corresponding to the pseudorange being processed is always used).

Satellite position $\mathbf{x}_{sat}(t_{tx})$ and velocity $\mathbf{v}_{sat}(t_{tx})$ are obtained from the correspondent source (OS, HAS[2] or PP[3].) at time t_{tx}.

Satellite clock bias is estimated from the broadcast ephemeris using the clock polynomial

$$\delta t_{CB} = a_0 + a_1(t - t_0) + a_2(t - t0)^2, \tag{B.6}$$

where a_i are the coefficients, and t_0 is the reference epoch (i.e. the closest but preceding

[2]Since HAS does not provide velocity corrections, the velocity coincides with that of OS.

[3]Velocity can be obtained as the derivative of the interpolating polynomial that is used to obtained SV's position [11]

epoch at which ephemerides are available). This satellite clock bias is corrected using HAS' clock correction if Galileo HAS is used. For PP, the clocks are estimated using linear interpolation of the provided clock products [11].

On the other hand, the relativistic correction due to orbit eccentricity is computed as

$$\delta t_{rel} = -2\frac{\left(\mathbf{x}_{sat}^{BRDC}\right)^T \mathbf{v}_{sat}^{BRDC}}{c^2}. \tag{B.7}$$

The Δt applied for correcting the SV's clock is now defined as

$$\Delta t = -\delta t_{CB} - \delta t_{rel}. \tag{B.8}$$

As a consequence, the new transmission time is defined as

$$t_{tx}^{corr} = t_{tx} - \tau + \Delta t. \tag{B.9}$$

The satellite position is computed again with the new t_{tx}^{corr} obtaining $\mathbf{x}_{sat}(t_{tx}^{corr})$.

Correction for Earth rotation

For correcting for Earth rotation, the travel time is estimated as

$$t_{travel} = t_{rx}^{j} - t_{tx}^{corr}. \tag{B.10}$$

Then, the correction on the satellite position is obtained as

$$\mathbf{x}_{sat}^{corr} = \begin{pmatrix} \cos\Phi & \sin\Phi & 0 \\ -\sin\Phi & \cos\Phi & 0 \\ 0 & 0 & 1 \end{pmatrix} \mathbf{x}_{sat} \tag{B.11}$$

where $\Phi = \dot{\Omega} t_{travel}$, with $\dot{\Omega} \simeq 7.2921151467E-5$ rad/s.

OUTPUT: Estimated position of the satellite $\mathbf{x}_{sat}^{corr}$.

B.1.2. Tropospheric correction

The tropospheric correction is estimated using the tropospheric delay RTCA model [11]. A specific function is implemented for this purpose.

OUTPUT: Tropospheric delay correction term for the pseudorange, $\delta\rho_{tropo}$.

B.1.3. Compute the corrected pseudorange

Now the corrected pseudorange can be computed as

$$PR_{corr} = PR - c\Delta t - \delta\rho_{rel,path} + \delta\rho_{tropo}. \tag{B.12}$$

OUTPUT: Corrected psudorange for satellite i of constellation j, PR_{corr}.

B.1.4. Solve for the user position

Once the corrected pseudorange measurement is computed for each of the measurements available for the epoch begin solved, then the user position can be corrected using a WLS estimator.

For building the weight matrix, the covariances of the different error contributions must be estimated for each satellite vehicle based on available models, obtaining a vector **w**:

- **Tropospheric error**: σ_{tropo} is estimated as

$$\sigma_{tropo,i} = 0.12 \times 1.001/\sqrt{0.002001 + (\sin EL)^2}, \tag{B.13}$$

  where EL is the elevation of the spacecraft from the a priori user position.

- **Residual error model**: The residual error model for GPS is obtained as follows

$$\sigma_{cmpn,i} = F\sqrt{(0.13 + 0.53\exp(-EL/10))^2 + (0.15 + 0.43\exp(-EL/6.9))^2} \tag{B.14}$$

  where F is computed as

$$F = \sqrt{\frac{f_{L1}^4 + f_{L5}^4}{(f_{L1}^2 + f_{L5}^2)^2}}. \tag{B.15}$$

  begin f_{L1} and f_{L5} the $L1$ and $L5$ frequencies, respectively.

  On the other hand, for Galileo an elevation-dependent multipath and noise value is obtained based on the Milestone Report 3 [3].

- URA_i value is the one obtained from the ARAIM parameters structure. A value of 1 meter is taken as reference for these first tests for both constellations.

The total weight value for each space vehicle is obtained as

$$w_i = URA_i^2 + \sigma_{tropo,i}^2 + \sigma_{cmpn,i}^2. \tag{B.16}$$

The weight matrix is then defined by

$$\mathbf{W} = diag(1/\mathbf{w}). \tag{B.17}$$

The expected pseudorange vector is computed based on the initial user position $\mathbf{x}_0$ and the satellite position estimation $\mathbf{x}_{sat}^{corr}$ for each measurement k as

$$\rho_{0,k} = |\mathbf{x}_0 - \mathbf{x}_{sat,k}^{corr}|. \tag{B.18}$$

and the difference between measured and expected pseudorange can be obtained as

$$\delta\rho_k = PR_{corr} - rho_{0,k} - \mathbf{x}_0(3+j), \tag{B.19}$$

where j is equal to 1 or 2 depending on the constellation associated to measurement k. The last term applies the associated time offset between the receiver clock and the constellation system time, which is included in the state variable set.

Let now $\mathbf{X}, \mathbf{Y}, \mathbf{Z}$ be column vectors with each of the coordinates of the position of the satellites in ECEF reference frame. Let $\mathbf{x}_0(1:3) = [\mathbf{X}_0, \mathbf{Y}_0, \mathbf{Z}_0]^T$ be the a priori guess of the user position. The geometry matrix can be built as

$$G(k,:) = [-(\mathbf{X} - \mathbf{X}_0)/\rho_{0,k}, -(\mathbf{Y} - \mathbf{Y}_0)/\rho_{0,k}, -(\mathbf{Z} - \mathbf{Z}_0)/\rho_{0,k}, A, B] \tag{B.20}$$

where

$$\{A, B\} = \begin{cases} \{1,0\} & \text{if GPS} \\ \{0,1\} & \text{if GAL.} \end{cases} \tag{B.21}$$

Then, the weighted pseudo-inverse is obtained as

$$\mathbf{S} = (\mathbf{G}^T\mathbf{W}\mathbf{G})^{-1}(\mathbf{G}^T\mathbf{W}), \tag{B.22}$$

and $\delta\mathbf{x}$ is obtained as

$$\delta\mathbf{x} = \mathbf{S}\delta\boldsymbol{\rho}. \tag{B.23}$$

Finally, the new estimate of the user position is obtained as

$$\mathbf{x}' = \mathbf{x} + \delta\mathbf{x}. \tag{B.24}$$

OUTPUT: New estimate of user position $\mathbf{x}'$.

Once this is performed, the algorithm can be run iteratively going back to the satellite position estimation algorithm until the variation of the user position between iterations is sufficiently low.

This algorithm should be ran for each epoch where the number of satellites is >= 5 (minimum for solving the problem).

B.2. Pseudocodes

After a general description of the algorithm has been provided, this section presents the pseudocodes that describe the high level implementation of the algorithm. All three cases require as input

- PR_{vec}: N-dimensional Vector of ionospheric free pseudoranges obtained for the epoch at which the navigation solution is computed.
- *eph*: Matrix containing the broadcast ephemeris data for each SV.
- gps_{SOW}: GPS second of week of the estimation epoch.
- gps_{WN}: GPS week number for the estimation epoch.
- *svid*: 2xN that contains constellation and PRN associated with each of the pseudoranges.

Algorithm B.1 describes the implementation of the estimation using broadcast ephemerids. Each iteration consists on a estimation of the SV's position and pseudoranges corrections, and then the WLS is solved. When the norm of the user position variation between two iterations is below 1E-6, the final solution is obtained. For the case of HAS, algorithm B.2 has the changes made with respect to OS marked in red. HAS corrections are applied as explained in the corresponding ICD [24] to the clocks and orbit computed from the navigation message.

Finally, for the PP, no ephemeris are used at all, as the solution is obtained directly from the SP3 and CLK files. The `getSatPosVelPP` function already performs the required

APC translations. Algorithm B.3 describes the implementation with the changes with respect to OS marked in red.

Algorithm B.1 User position computation - OS case

Require: $PR_{vec}, eph, gps_{SOW}, gps_{WN}$, svid
  $n_{iter} \leftarrow 0$
  $x_{usr} \leftarrow zeros(3.1)$
  $x_{usr,old} \leftarrow zeros(3.1)$
  while $(|x_{usr} - x_{usr,old}| > 1E-6$ && $n_{iter} < N_{iter,max})$ **do**
    for PR in PR_{vec} **do** ▷ Iterate over all the available pseudoranges.
      $t_{tx} \leftarrow gps_{SOW} - x(3+j)/c$ ▷ j is 1 for GPS PR and 2 for GAL PR.
      $\tau \leftarrow$ findGeometricDelay$(t_{rx}, eph, svid, gps_{SOW}, x_{usr})$
      $t_{tx} \leftarrow t_{rx} - \tau$ ▷ First guess of TX time.
      clockBias $\leftarrow$ getClockBiasEph$(t_{tx}, eph, svid)$ ▷ Sat. clock bias from ephemerides.
      $[x_{sat}, v_{sat}] \leftarrow$ getSatPosVel$(t_{tx}, eph, svid)$
      $\delta_{rel} \leftarrow$ getDeltaRelEcc(x_{sat}, v_{sat}) ▷ Get the rel. delay due to orbit eccentricity.
      clockBias $\leftarrow$ clockBias $+ \delta_{rel}$ ▷ Lump δ_{rel} in the clockBias for next iter.
      $\Phi \leftarrow \dot{\Omega}(t_{tx} - t_{rx})$ ▷ Earth rotation angle during $t_{rx} - t_{tx}$.
      $x_{sat} \leftarrow$ correctEarthRotation(Φ, x_{sat})
      $\delta_{tropo} \leftarrow$ tropoRTCA$(gps_{DOY}, x_{sat}, x_{usr})$
      $PR^{corr} \leftarrow PR +$ clockBias$c + \delta_{rel}c - \delta_{rel,path} + \delta_{tropo}$ ▷ Corrected pseudorange.
    end for
    $x_{usr}^{new} \leftarrow x_{usr}$ ▷ Buffer user position.
    $W \leftarrow$ eye(3) ▷ Allocate weight matrix.
    for $i = 1:30$ **do**
      if $i > 1$ **then**
        $el \leftarrow$ getElevation(x_{usr}^{new}, x_{sat}) ▷ Elevation vector for each SV.
        $[w, b] \leftarrow$ findSigmaErrorModel$(el, svid, URA)$ ▷ Get σ^2 and biases per SV.
        $W \leftarrow (\text{diag}(w))^{-1}$ ▷ Weight matrix.
      end if
      $[x_{usr}^{new}, \delta_x] \leftarrow$ solveWLS$(PR^{corr}, x_{usr}^{new}, x_{sat}, W)$ ▷ δ_x is the correction provided by WLS.
      if $\delta_x < 1E-6$ && $i > 1$ **then** ▷ Convergence condition
        break
      end if
      $n_{iter} \leftarrow n_{iter} + 1$
    end for
  end while

Algorithm B.2 User position computation - OS case

Require: $PR_{vec}, eph, gps_{SOW}, gps_{WN}$, svid
  $n_{iter} \leftarrow 0$
  $x_{usr} \leftarrow zeros(3.1)$
  $x_{usr,old} \leftarrow zeros(3.1)$
  while $(|x_{usr} - x_{usr,old}| > 1E-6$ && $n_{iter} < N_{iter,max})$ **do**
    for PR in PR_{vec} **do** ▷ Iterate over all the available pseudoranges.
      $t_{tx} \leftarrow gps_{SOW} - x(3+j)/c$ ▷ j is 1 for GPS PR and 2 for GAL PR.
      $\tau \leftarrow$ findGeometricDelay$(t_{rx}, eph, svid, gps_{SOW}, x_{usr})$
      $t_{tx} \leftarrow t_{rx} - \tau$ ▷ First guess of TX time.
      clockBias $\leftarrow$ getClockBiasEph$(t_{tx}, eph, svid)$ ▷ Sat. clock bias from ephemerides.
      $[x_{sat}, v_{sat}] \leftarrow$ getSatPosVel$(t_{tx}, eph, svid)$
      $[x_{sat}, \text{clockBias}] \leftarrow$ applyHAS$(t_{tx}, x_{sat}, v_{sat})$ ▷ Apply HAS corrections.
      $\delta_{rel} \leftarrow$ getDeltaRelEcc(x_{sat}, v_{sat}) ▷ Get the rel. delay due to orbit eccentricity.
      clockBias $\leftarrow$ clockBias $+ \delta_{rel}$ ▷ Lump δ_{rel} in the clockBias for next iter.
      $\Phi \leftarrow \dot{\Omega}(t_{tx} - t_{rx})$ ▷ Earth rotation angle during $t_{rx} - t_{tx}$.
      $x_{sat} \leftarrow$ correctEarthRotation(Φ, x_{sat})
      $\delta_{tropo} \leftarrow$ tropoRTCA$(gps_{DOY}, x_{sat}, x_{usr})$
      $PR^{corr} \leftarrow PR +$ clockBias$c + \delta_{rel}c - \delta_{rel,path} + \delta_{tropo}$ ▷ Corrected pseudorange.
    end for
    $x_{usr}^{new} \leftarrow x_{usr}$ ▷ Buffer user position.
    $W \leftarrow$ eye(3) ▷ Allocate weight matrix.
    for $i = 1:30$ **do**
      if $i > 1$ **then**
        $el \leftarrow$ getElevation(x_{usr}^{new}, x_{sat}) ▷ Elevation vector for each SV.
        $[w, b] \leftarrow$ findSigmaErrorModel$(el, svid, URA)$ ▷ Get σ^2 and biases per SV.
        $W \leftarrow (\text{diag}(w))^{-1}$ ▷ Weight matrix.
      end if
      $[x_{usr}^{new}, \delta_x] \leftarrow$ solveWLS$(PR^{corr}, x_{usr}^{new}, x_{sat}, W)$ ▷ δ_x is the correction provided by WLS.
      if $\delta_x < 1E-6$ && $i > 1$ **then** ▷ Convergence condition
        break
      end if
      $n_{iter} \leftarrow n_{iter} + 1$
    end for
  end while

Algorithm B.3 User position computation - PP case

Require: $PR_{vec}, eph, gps_{SOW}, gps_{WN}$, svid
  $n_{iter} \leftarrow 0$
  $x_{usr} \leftarrow zeros(3,1)$
  $x_{usr,old} \leftarrow zeros(3,1)$
  while $(|x_{usr} - x_{usr,old}| > 1E-6$ && $n_{iter} < N_{iter,max})$ **do**
    for PR in PR_{vec} **do** ▷ Iterate over all the available pseudoranges.
      $t_{tx} \leftarrow gps_{SOW} - x(3+j)/c$ ▷ j is 1 for GPS PR and 2 for GAL PR.
      $\tau \leftarrow$ findGeometricDelay$(t_{rx}, eph, svid, gps_{SOW}, x_{usr})$
      $t_{tx} \leftarrow t_{rx} - \tau$ ▷ TX time.
      clockBias $\leftarrow$ getClockBiasPP$(t_{tx}, gps_{WN}, svid)$ ▷ Sat. clock bias from PP.
      $[x_{sat}, v_{sat}] \leftarrow$ getSatPosVelPP$(t_{tx}, gps_{WN}, svid)$ ▷ Get position and velocity from PP.
      $\delta_{rel} \leftarrow$ getDeltaRelEcc(x_{sat}, v_{sat}) ▷ Get the rel. delay due to orbit eccentricity.
      clockBias $\leftarrow$ clockBias $+ \delta_{rel}$ ▷ Lump δ_{rel} in the clockBias for next iter.
      $\Phi \leftarrow \dot{\Omega}(t_{tx} - t_{rx})$ ▷ Earth rotation angle during $t_{rx} - t_{tx}$.
      $x_{sat} \leftarrow$ correctEarthRotation(Φ, x_{sat})
      $\delta_{tropo} \leftarrow$ tropoRTCA$(gps_{DOY}, x_{sat}, x_{usr})$
      $PR^{corr} \leftarrow PR +$ clockBias$c + \delta_{rel}c - \delta_{rel,path} + \delta_{tropo}$ ▷ Corrected pseudorange.
    end for
    $x_{usr}^{new} \leftarrow x_{usr}$ ▷ Buffer user position.
    $W \leftarrow$ eye(3) ▷ Allocate weight matrix.
    for $i = 1:30$ **do**
      if $i > 1$ **then**
        $el \leftarrow$ getElevation(x_{usr}^{new}, x_{sat}) ▷ Elevation vector for each SV.
        $[w, b] \leftarrow$ findSigmaErrorModel$(el, svid, URA)$ ▷ Get σ^2 and biases per SV.
        $W \leftarrow (\text{diag}(w))^{-1}$ ▷ Weight matrix.
      end if
      $[x_{usr}^{new}, \delta_x] \leftarrow$ solveWLS$(PR^{corr}, x_{usr}^{new}, x_{sat}, W)$ ▷ δ_x is the correction provided by WLS.
      if $\delta_x < 1E-6$ && $i > 1$ **then** ▷ Convergence condition
        break
      end if
      $n_{iter} \leftarrow n_{iter} + 1$
    end for
  end while

List of Figures

List of Tables

List of Acronyms

Acronym	Description
GNSS	Global Navigation Satellite System
GPS	Global Positioning System
SV	Space Vehicle
PR	Pseudorange
URE	User Range Error
URA	User Range Accuracy
RAIM	Receiver Autonomous Integrity Monitoring
ARAIM	Advanced Receiver Autonomous Integrity Monitoring
HAS	High Accuracy Service
HADG	High Accuracy Data Generator
GCS	Ground Control Segment
SS	Space Segment
IDD	Internet Data Distribution
SIS	Signal-In-Space
ULS	Up-Link Station
GSS	Galileo Sensing Station
SDD	Service Definition Document
ICD	Interface Control Document
SIS	Signal-In-Space
IDD	Internet Data Distribution
EUSPA	EU Agency for the Space Program
ESA	European Space Agency
IGS	International GNSS Service
ECEF	Earth-Centered Earth-Fixed
CODE	Center of Orbit Determination of Europe

Acronym	Description
CAS	Chinese Academy of Sciences
SOW	Seconds of Week
TOW	Time of Week
ICAO	International Civil Aviation Organization
NAGU	Notice Advisory for Galileo Users

Acknowledgements

First, I would like to express my deepest gratitude to my supervisor at DLR, Omar García Crespillo, for providing me with the opportunity to work on this project and guiding my way during the development of this thesis. Your advice and support are an essential part of this work. In addition, I would like to thank Florian Rößl for the countless meetings and Skype calls, as well as your understanding. Thanks for always being available for me.

I would also like to thank my other colleagues from the Integrated Navigation Systems Integrity Group at DLR: Anja, Ana and Samuel. They made everyday life in the (home) office very pleasant.

Finally, I would like to thank my supervisor at Politecnico, Prof. Lorenzo Luini, for his availability, which allowed me to develop my work at DLR.

Este trabajo pone punto y final a una etapa que comenzó en septiembre de 2018 y que me ha llevado a vivir en Sevilla, Milán y Múnich. Estos han sido los años más exigentes y fructíferos hasta la fecha en todos los ámbitos.

En primer lugar, me gustaría hacer referencia a mis padres: nunca podré agradecer lo suficiente todo el esfuerzo que habéis realizado para brindarnos las mejores oportunidades, el apoyo que habéis dado a mis hermanos y a mí y la motivación que me dais siempre para convertirme en una mejor versión de mí mismo. Gracias también a mis hermanos Adolfo y Nacho por vuestros consejos, enseñanzas y apoyo.

También quiero dar las gracias a Laura por ser mi apoyo, refugio y guía. Gracias por celebrar conmigo mis metas y éxitos, y por orientarme cuando surgen dudas y falta confianza. Sin ti, el resultado habría sido diferente. Gracias por todo.

Por último, me gustaría acordarme de Pablo. Te fuiste de manera inesperada, dejándonos a tu grupo de siempre huérfanos. Gracias a Adrián, Alfonso, Diego, Javier y Jaime por permanecer unidos y seguir siendo un apoyo pese a la distancia y las circunstancias.